

AD-A021 736

ELECTRET TAPE TRANSDUCER

G. Kirby Miller

GTE Sylvania, Incorporated

Prepared for:

Rome Air Development Center

February 1976

DISTRIBUTED BY:

NTIS

National Technical Information Service
U. S. DEPARTMENT OF COMMERCE

REPRODUCED BY
**NATIONAL TECHNICAL
INFORMATION SERVICE**
U. S. DEPARTMENT OF COMMERCE
SPRINGFIELD, VA. 22161

REPORT DOCUMENTATION PAGE		READ INSTRUCTIONS BEFORE COMPLETING FORM
1. REPORT NUMBER RADC-TR-76-22	2. GOVT ACCESSION NO.	3. RECIPIENT'S CATALOG NUMBER
4. TITLE (and Subtitle) ELECTRET TAPE TRANSDUCER		5. TYPE OF REPORT & PERIOD COVERED Final Technical Report March 1975 - September 1975
		6. PERFORMING ORG. REPORT NUMBER N/A
7. AUTHOR(s) Dr. G. Kirby Miller		8. CONTRACT OR GRANT NUMBER(s) F30602-75-C-0075
9. PERFORMING ORGANIZATION NAME AND ADDRESS GTE Sylvania Incorporated P. O. Box 188 Mountain View CA 94040		10. PROGRAM ELEMENT, PROJECT, TASK AREA & WORK UNIT NUMBERS 62702F 65151328
11. CONTROLLING OFFICE NAME AND ADDRESS Rome Air Development Center (OCDS) Griffiss AFB NY 13441		12. REPORT DATE February 1976
		13. NUMBER OF PAGES 132
14. MONITORING AGENCY NAME & ADDRESS (if different from Controlling Office) Same		15. SECURITY CLASS. (of this report) UNCLASSIFIED
		15a. DECLASSIFICATION/DOWNGRADING SCHEDULE N/A
16. DISTRIBUTION STATEMENT (of this Report) Approved for public release; distribution unlimited.		
17. DISTRIBUTION STATEMENT (of the abstract entered in Block 20, if different from Report) Same		
18. SUPPLEMENTARY NOTES RADC Project Engineer: William F. Gavin, Jr. (OCDS)		
19. KEY WORDS (Continue on reverse side if necessary and identify by block number) Electrets Transducer Ultrasonics Sensors		
20. ABSTRACT (Continue on reverse side if necessary and identify by block number) This report covers an initial program to establish the feasibility of a new line transducer based on an active ultrasonic electret tape concept. It des- cribes a theoretical model based on a lumped-element harmonic electromechanical analysis and was programmed for a high speed digital computer to allow the assessment of the effects of fourteen transducer parameters. It also describes the method used for charging the electret layer, the techniques developed for fabricating samples of the transducer, the test procedures required to evaluate		

UNCLASSIFIED

SECURITY CLASSIFICATION OF THIS PAGE(When Data Entered)

the active and passive performance characteristics of the samples, and refinements to the fabrication process necessary to develop long samples.

J UNCLASSIFIED

SECURITY CLASSIFICATION OF THIS PAGE(When Data Entered)

SUMMARY

This report covers the initial program to establish the feasibility of a new line intrusion detection concept based on an active ultrasonic electret tape transducer. The idea is to electrically drive a long multi-layered tape transducer having an electret layer and elastically coupled (moving) layers at an ultrasonic frequency so that it radiates a narrow beam of ultrasound all along its length. An object moving into the ensonified region reflects some of the energy back to the tape transducer. The reflected signal is picked up by the tape transducer acting as a microphone and is separated from the driving signal by a special hybrid electronic package that utilizes the Doppler shift in the reflected signal. A processor then operates on the received signal to generate the appropriate alarm. This study was aimed primarily at electret transducer development rather than at the total detection system.

The approach included both analytical and experimental tasks. First, a theoretical model based on a lumped-element harmonic electromechanical analysis was derived and programmed for a high speed digital computer so that the effects of 14 transducer parameters on its performance both as a radiator and as a receiver could be assessed (Sec. 2). In the laboratory a "liquid contact" method was developed for charging the FEP films used in the transducer as the electret layer (Sec. 3.2). Then methods were developed for fabricating short samples of the electret tape transducer (Sec. 3.4) that were designed on the basis of the computer modeling results, additional analytical work (Sec. 3.3) and material availability. After fabricating four small samples, test procedures were developed and implemented to evaluate the active and passive performance characteristics of the transducers (Sec. 3.5). Methods for making longer samples were then developed and four longer samples (.12 to .5 m) were constructed. Two of these were used to demonstrate the intrusion detection capability of the transducers by comparing the target-reflected signal from the receiving transducer with the signal used to drive the radiating transducer. The primary conclusions of this program are:

1. The ultrasonic doppler detection concept appears to be sound and the electret tape developed appears to be an adequate source and receiver for such a system.
2. Construction techniques are available for fabricating short tape transducers (0.5 m so far) that have open circuit sensitivities of at least -69 dB re 1 V/Pa

and radiation efficiencies of at least 0.01%. Since this performance level was achieved on our fourth sample, it is felt that significant improvements will be made in subsequent samples.

3. A computer implemented model of the transducer has been developed for use in assessing its performance as a radiator, receiver and in a detection system. Discrepancies between the predictions of the model and the measurements in the lab appear to be due to non-uniformities in the hand-made transducers.
4. An adequate liquid contact charging technique has been developed that produces effective surface charge densities on 50 μm FEP of at least 0.1 m C/m^2 even after four months. The typical decay rate is observed to be about 1 dB/time doubling after the first ten days.
5. The internal mechanical damping is very large in the current transducers (~ 50 to 70 times the characteristic impedance of air). This makes for lower efficiency but allows for fairly broad band operation so that the detection system can be operated over a frequency range of at least half an octave.

TABLE OF CONTENTS

<u>Section</u>	<u>Title</u>	<u>Page</u>
	SUMMARY	ii
1	INTRODUCTION	1-1
	1.1 Electret Tape Intrusion Detection Concept	1-1
	1.1.1 Potential Advantages	1-1
	1.2 Scope and Organization of Investigation	1-2
2	TRANSDUCER ANALYSIS	2-1
	2.1 Model Derivation	2-1
	2.1.1 Radiation Efficiency	2-5
	2.1.2 Receiving Sensitivity	2-6
	2.1.3 Directivity	2-7
	2.1.4 Target Simulation	2-7
	2.2 Computer Implementation	2-8
	2.3 Results and Discussion	2-9
	2.3.1 Tape Length and Width	2-11
	2.3.2 Frequency	2-12
	2.3.3 Mechanical Damping Constant	2-12
	2.3.4 Air Gap Thickness	2-14
	2.3.5 Conductor Thickness	2-14
	2.3.6 Electret Thickness and Surface Charge Density	2-18
	2.4 Summary and Discussion	2-21
3	EXPERIMENTAL INVESTIGATION	3-1
	3.1 General Procedure	3-1
	3.2 Electret Preparation	3-1
	3.2.1 Background	3-1
	3.2.2 The Charging Procedure	3-2
	3.2.3 Charge Measurement	3-4
	3.2.4 Results	3-7
	3.2.4.1 Electret Thickness and Applied Voltage Effects	3-7
	3.2.4.2 Annealing and Longevity	3-10

TABLE OF CONTENTS
(Continued)

<u>Section</u>	<u>Title</u>	<u>Page</u>
3	3.2.4.3 Charging Summary	3-13
	3.3 Design Aids	3-15
	3.3.1 Transduction Coefficient	3-15
	3.3.2 Tape Width Effects	3-15
	3.3.3 Frequency	3-19
	3.4 Transducer Construction	3-19
	3.4.1 General Procedure and Discussion	3-25
	3.4.2 Early Design	3-27
	3.4.3 Later Design	3-28
	3.5 Measuring Performance	3-31
	3.5.1 Capacitance	3-31
	3.5.2 Sensitivity	3-31
	3.5.2.1 Instrumentation	3-31
	3.5.2.2 Results	3-32
	3.5.3 Radiation	3-38
	3.5.3.1 Instrumentation	3-38
	3.5.3.2 Directivity	3-40
	3.5.3.3 Efficiency	3-43
4	DEMONSTRATION AND CONCLUSIONS	4-1
	4.1 Two-Tape Detection System Demonstration	4-1
	4.2 Conclusions	4-1
5	RECOMMENDATIONS	5-1
Appendix A	TAPE TRANSDUCER ANALYSIS	A-1
	1.0 Background	A-1
	2.0 Electrical Considerations	A-1
	3.0 Mechanical Considerations	A-3
	4.0 Input Impedance and Mechanical Resonance	A-7

TABLE OF CONTENTS
(Continued)

<u>Section</u>	<u>Title</u>	<u>Page</u>
5.0	Radiation Efficiency	A-7
6.0	Axial Pressure and Directivity Index	A-8
7.0	Receiving Sensitivity	A-10
8.0	Conjugate Impedance Matching	A-10
9.0	Beam Width	A-11
Appendix B	COMPUTER PROGRAM FOR MODEL OF ELECTRET- TAPE TRANSDUCER PERFORMANCE	B-1
1.0	Fortran Coding	B-1
1.1.1	Ultrasonic Electret Tape Detector Model	B-1
2.0	Program Variable Dictionary	B-10
Appendix C	RADIATION IMPEDANCE OF A BAFFLED INFINITE STRIP	C-1
Appendix D	OTHER COMPUTER MODEL PLOTS	D-1

LIST OF ILLUSTRATIONS

<u>Figure</u>	<u>Title</u>	<u>Page</u>
2-1	Tape Cross Section	2-2
2-2	Flow Diagram of Computer Model	2-10
2-3	Open Circuit Sensitivity vs. Frequency	2-13
2-4	Resonance Frequency vs. Air Gap	2-15
2-5	Open Circuit Sensitivity vs. Air Gap at $f = f_0$	2-16
2-6	Transfer Impedance vs. Air Gap	2-17
2-7	Transfer Impedance vs. Electret Thickness	2-19
2-8	Effect of $\sigma_e \sqrt{d}$ on Open Circuit Sensitivity	2-20
2-9	Effect of $\sigma_e \sqrt{d}$ on Transfer Impedance	2-22
3-1a.	Short Tape Liquid Contact Charging Apparatus	3-3
3-1b	Long Tape Charging Apparatus	3-3
3-2a	Electret Surface Potential Measurement Apparatus	3-6
3-2b	Long Tape Electret Strength Measurement Apparatus	3-6
3-3	Relating Surface Potential to Charge Density for FEP Electrets	3-8
3-4	Effects of Charging Voltage and Film Thickness on Electret Strength after Three Days	3-9
3-5	Effect of Charging Voltage and Sample Thickness on Surface Potential After 40 days	3-11
3-6	Electret Strength History after Three Samples	3-12
3-7	Average Electret Decay	3-14
3-8	Effects of Layer Thicknesses on Transduction Constant	3-16
3-9	Resistance per unit Length of Thin Aluminum Strip	3-17
3-10	Frequency vs. kw for Various Tape Widths	3-18
3-11	Tape Radiation Directivity Patterns	3-20
3-12	Tape Radiation Directivity Patterns	3-21
3-13	Directional Radiation Characteristics of Long Tape Radiator	3-22

LIST OF ILLUSTRATIONS (Cont'd)

<u>Figure</u>	<u>Title</u>	<u>Page</u>
3-14	Directivity Index vs. Acoustical Width Parameter	3-23
3-15	Effects of Air Gap and Moving Mass on Mechanical Resonance	3-24
3-16	Electret Tape Cross Section	3-26
3-17a	Material Layers for Early Samples	3-29
3-17b	Transducer Samples D2, D3 and D4	3-29
3-18	Material Layers for Longer Samples	3-30
3-19	Instrumentation for Sensitivity Determinations in Anechoic Chamber	3-33
3-20	Open Circuit Sensitivity vs. Frequency	3-34
3-21	Open Circuit Sensitivity vs. Damping	3-36
3-22	Standard Source Output as Measured by Three Receivers	3-37
3-23	Instrumentation Used in Determining Radiation Efficiency	3-39
3-24	Effective Inductance Factor for Real Inductances	3-41
3-25	Measured Directivity Pattern for Sample D4	3-42
4-1	Instrumentation for Two Tape Detection Demonstration	4-2
4-2	Transducers for Two Tape Detection Demonstration	4-3
A-1	Electrically Important Cross Section	A-1
C-1	Radiation Impedance of Baffled Vibrating Strip of Infinite Length	C-5
D-1	Z_T vs. Frequency for Sample D1	D-2
D-2	Efficiency vs. Frequency for Sample D1	D-3
D-3	Driving Current vs. Frequency	D-4
D-4	Diaphragm Displacement vs. Frequency	D-5
D-5	Matching Source Resistance vs. Frequency	D-6
D-6	Source Inductance for Conjugate Impedance Matching vs. Frequency	D-7

LIST OF ILLUSTRATIONS (Cont'd)

<u>Figure</u>	<u>Title</u>	<u>Page</u>
D-7	Beamwidth vs. Frequency for Sample D1	D-8
D-8	Drive Current vs. Mechanical Damping Constant	D-9
D-9	Matching Source Resistance vs. Mechanical Damping Constant	D-10

<u>Table</u>	<u>Title</u>	<u>Page</u>
2-1	Parameter Effects Summary	2-23
C-1	Thickness of Effective Mass Load at Low Frequencies	C-4

EVALUATION

The objective of this effort was to determine the feasibility of a new line transducer based on an active ultrasonic electret tape concept. It consists of a long multi-layered tape transducer having an electret layer which is driven at an ultrasonic frequency. A moving layer radiates this frequency all along the length of the transducer. An object entering the field reflects some of the energy back to the transducer which is detected, separated from the transmitted signal, and processed as an alarm.

In this effort, the major problems that were solved included: charging the electret, bonding and laminating the various layers and the development of suitable test procedures to evaluate the tape. The success obtained in this phase of the effort now allows the design and fabrication of a hybrid electronics unit and extending the transducer to long lengths.

The next phase of this development will result in the fabrication of a model of a complete sensor suitable for limited field testing. The work documented in this report was accomplished under RADC Technical Planning Objective 7.

William F. Gavin, Jr.

WILLIAM F. GAVIN, Jr.
Project Engineer

ELECTRET TAPE TRANSDUCER

1.0 Introduction

This final report records the details of a six-month investigation funded by RADC, Contract No. F30602-75-C-0075 and performed March - September, 1975, by the Security Systems Department of GTE Sylvania's Mountain View, California, facility. The purpose of this effort was to examine a new perimeter intrusion detection concept to determine its feasibility and to develop laboratory test models for its demonstration.

1.1 Electret Tape Intrusion Detection Concept

Sylvania's Security System Department (SSD), having been active in the security system area for over fourteen years, has been aware of the need for reliable perimeter intrusion detection systems for both government and commercial applications. In particular, there has been no such system that is rapidly deployable. To meet this need, the electret tape concept was developed.

The Active Ultrasonic Tape Intrusion Detection or ACUTID system is based on an active ultrasonic doppler detection scheme using a long, thin multi-layered tape (containing an electret layer) as the radiating and receiving transducer. This transducer is essentially an elongated electret microphone with configuration, materials and dimensions engineered to make it a good radiator as well. The highly directional ultrasonic CW beam radiated by the tape uniformly all along its length illuminates any object crossing it. This action causes a reflected doppler-shifted ultrasonic signal that is received by the tape and separated from the driving signal by special hybrid electronic circuitry. A special processor then operates on the received signal and generates the appropriate alarm.

1.1.1 Potential Advantages

Such an intrusion detector has a number of distinct advantages when compared with existing perimeter protection systems.

1. Since it does not require burial or special supports (such as a fence), it can be quickly rolled into place around a nearly arbitrary perimeter to be protected.

1.1.1 (Continued)

2. It can be manufactured with an adhesive on the non-radiating side so that it can be installed very quickly on reasonably smooth walls or ceilings.
3. Because of its mechanical flexibility, it can be fastened to irregular surfaces and go around corners.
4. Being active, it can be used even in very noisy environments where passive devices would be inoperable.
5. The very low volume of material per unit length coupled with current techniques for automatically making uniform laminated tapes in great lengths allow the likely cost for the transducer to be so low that expendable transducer systems may be practical.
6. Unlike most other perimeter protection systems, the ultrasonic electret tape system would not have stringent alignment or installation requirements.
7. Being acoustic, its operation does not provide an electromagnetic signal that could be used for terminal guidance of a hostile missile. Nor will it produce radiation that could interfere with the operation of SIGINT or ELINT collection equipment.

1.2 Scope and Organization of Investigation

This effort is concerned primarily with the transducer portion of the ACUTID system-- it being felt that this is the key requirement for the successful development of the system. Because of the exploratory nature of the investigation of a new concept, it was impossible to reliably predict how much progress would be made in a six month effort. However, a general course of action was developed and followed. First, the theoretical feasibility of the transducer portion of the concept was examined by use of an electromechanical mathematical model derived for the simplest of possible tape transducer configurations. This lumped parameter model takes into account the radiation loading of the medium and the effects of the driving source impedance as well as the dimensions and characteristics of the materials used in the layers. The model was then programmed for digital computer and used to examine the effects of the various parameters on the performance of the modeled transducer as a radiator, as a receiver and as a radiator-receiver system over reasonable ranges of each parameter. This information was plotted to form a rational basis for transducer design. After investigating the characteristics of available materials in light of the results of the model study, several designs were

1.2 (Continued)

developed. Materials were then assembled and methods developed for fabricating the designs. Several short samples were then fabricated and their radiation and receiving performance characteristics were evaluated. After an adequate transducer was developed in this manner, the detection concept was demonstrated in the lab.

In this report we present descriptions of the above tasks in roughly the order of performance under the general heading: Transducer Analysis and Experimental Investigations. In the final sections we describe a detection system demonstration and then draw together the significant conclusions and make the logical recommendations for continued development of the ACUTID system.

2.0 Transducer Analysis

In order to understand the performance characteristics of the proposed tape transducer and thus to aid in its design, a mathematical model believed to simulate its steady-state small-signal operation in all important respects was derived from basic principles using the lumped-element electromechanical analysis after F. V. Hunt¹. The details of this derivation are presented in Appendix A. The analysis develops a set of coupled algebraic equations in the phasor surface charge density and the phasor diaphragm displacement with complex constants derivable from fourteen transducer parameters and from four target related parameters. From the simultaneous solutions of these equations can be calculated the important performance characteristics of the transducer as a receiver, as a radiator, and as a target detector.

These operations were programmed for computer in a format that would allow convenient variations of the many parameters either singly or in combinations. This program then became the tool for studying the effects on the transducer performance produced by each parameter when varied over a range considered reasonable for that parameter. A flexible computer plotting routine was developed to allow rapid visual evaluation of the enormous amount of data generated in this way. Appendix D contains a sampling of these plots.

2.1 Model Derivation

In this section we list the assumptions and outline the equations involved in the electromechanical model of the electret tape transducer. A detailed derivation is given in Appendix A.

Consider the multi-layered tape shown in Figure 2-1. This is the simplest electret transducer configuration. The driving amplifier is modeled by an ideal sinusoidal voltage source (E_s) in series with a complex source impedance (Z_s). The incident steady-state acoustic pressure field, p , is assumed uniform over the tape's surface. The outer-most layer is a protective insulating plastic

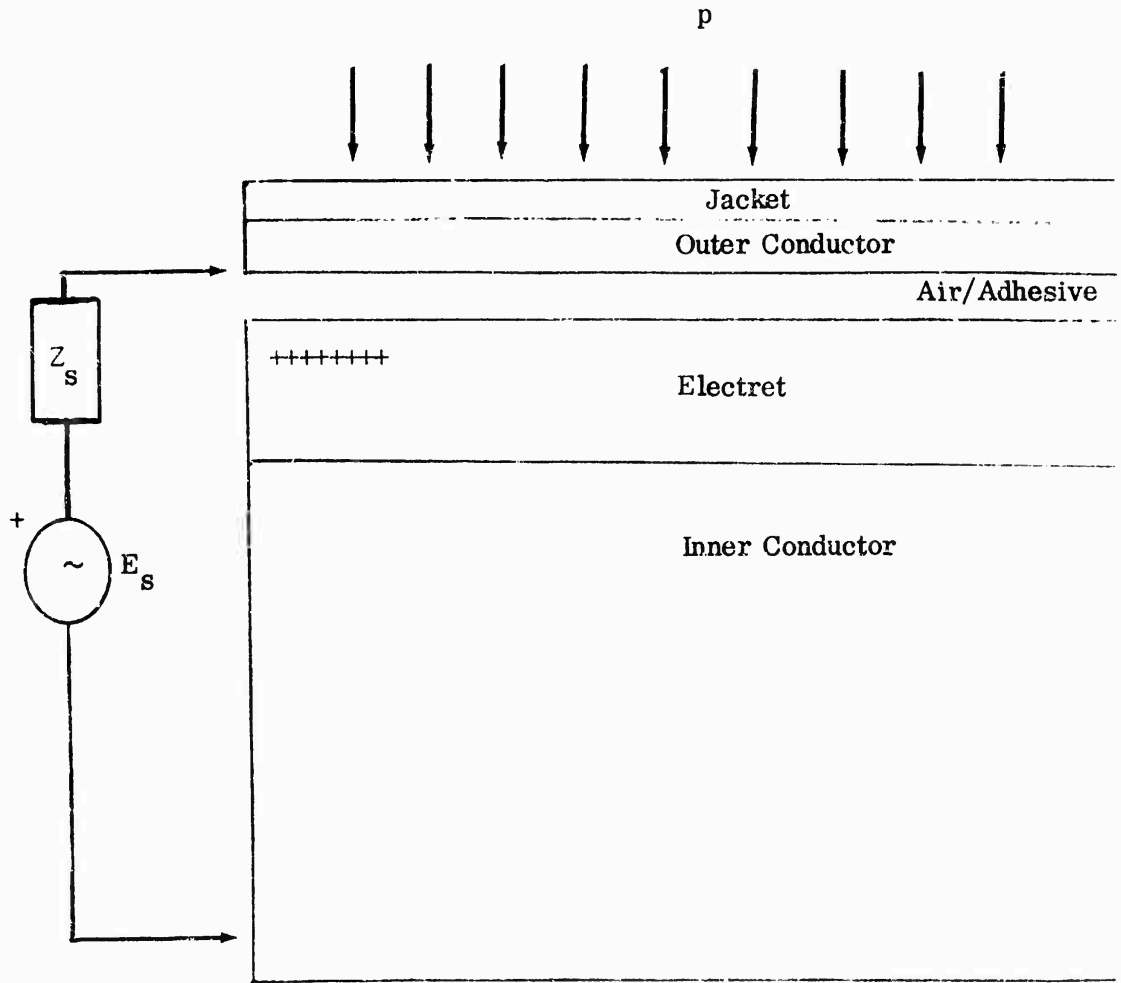


Fig. 2-1 Tape Cross Section

2.1 (Continued)

jacket. This is rigidly bonded to the outer conductor which is likely to be of aluminum for lightness. Only these two outer layers are assumed to move (either due to the incident pressure or to the electric current from the driving amplifier). The charge stored in the electret is assumed to be equivalent to a uniform surface charge density, σ_e and the electret is assumed to be bonded rigidly to the inner conductor layer. If C_e is the capacitance per unit area of the electret and "a" is the thickness of the air gap/adhesive layer between the electret and the outer (moving) conductor, the differential equation relating surface charge density, σ , on the outer conductor to the applied voltage and air gap is:

$$\dot{\sigma} Z_s S + \frac{\sigma a}{\epsilon_a} + \frac{\sigma}{C_e} = E_s - \frac{\sigma_e}{C_e} \quad 2-1$$

where S is the total surface area of the sample, $S = w\ell$
and ϵ_a is the effective permittivity of the air gap/adhesive layer

Note that only E_s , σ , and a are functions of time in this equation.

Now consider the mechanical aspects of the transducer. We wish to write an equation expressing the equilibrium of forces per unit area acting on the diaphragm. Aside from the incident acoustic pressure field, p, mentioned before, we have an electrostatic pressure on the outer conductor equal to $\sigma^2/2\epsilon_a$. The reaction pressure due to the acceleration of the moving layers is $M\ddot{x}$, where M is the total moving mass/unit area. That due to internal friction and heat loss is assumed proportional to the velocity of the moving layers with constant of proportionality (damping constant per unit area), D.

Another reaction pressure proportional to the velocity is that of the radiation load presented by the surrounding medium. This pressure depends on the specific acoustic radiation impedance of the tape, Z_A . The remaining reaction pressure is Kx where $K (= \frac{\gamma P_0}{a}$ for air) is the effective spring constant/unit area of the

2.1 (Continued)

air/adhesive layer ($\gamma = 1.4$ for air and $P_0 =$ atmospheric pressure). Taking the displacement, x , to be positive in the outward direction, we can write the equilibrium pressure equation as

$$M\ddot{x} + D\dot{x} + Kx + Z_A \dot{x} + \frac{\sigma^2}{2\epsilon_a} + p = 0 \quad 2-2$$

Equations 2-1 and 2-2 form a mildly non-linear set in σ and x . We can linearize these equations by expanding the time varying quantities in the first few terms of a Fourier series.

$$\text{Letting } x = x_0 + \frac{x}{2} e^{j\omega t}, \quad a = a_0 + x, \quad \sigma = \sigma_0 + \frac{\sigma}{2} e^{j\omega t}$$

$$p = \frac{p}{2} e^{j\omega t} \quad \text{and} \quad E_s = \frac{E}{2} e^{j\omega t},$$

the zeroth order terms can be collected to form

$$\frac{a_0 + x_0}{\epsilon_a} + \frac{l}{C_e} + \frac{\sigma_0}{\sigma_0 C_e} = 0 \quad 2-3$$

$$\frac{\gamma P_0 a_0}{(x_0 + a_0)^2} + \frac{\sigma_0^2}{2\epsilon_a} = 0 \quad 2-4$$

These can be solved simultaneously for x_0 , the static displacement of the diaphragm caused by the electret, and σ_0 , the static surface charge density the electret induces on the conductor.

The first order terms, those having harmonic time dependence at the driving radian frequency, ω , can be collected to form

$$\left. \begin{aligned} \sigma Z_e + x T &= E \\ \sigma T + x Z_m &= -p \end{aligned} \right\} \quad 2-5$$

where

$$Z_e = \frac{l}{C_0} + j\omega S Z_s = \frac{l}{C_0} - \omega S X_s + j\omega S R_s$$

C_0 is the static capacitance/unit area of the electret device (with $p = E = 0$)

$T = \frac{J_0}{\epsilon_a}$ is the transduction coefficient

2.1 (Continued)

$$Z_m \equiv -\omega^2 M - \omega X_A + K + j(D + R_A) = R_m + jX_m$$

The simultaneous solution of 2-5 for the phasors x and σ yields

$$\sigma = \frac{pT + E Z_m}{Z_e Z_m - T^2} \quad 2-6$$

$$x = \frac{-pZ_e - ET}{Z_e Z_m - T^2} \quad 2-7$$

When the transducer is used as a receiver, $E = 0$, and when it is used as a radiator, $p = 0$.

2.1.1 Radiation Efficiency

From these basic solutions can be derived most of the important performance characteristics of the tape transducers. One of the more critical performance characteristics is the radiation efficiency defined as

$$\eta = \frac{\text{Acoustic Power Radiated}}{\text{Total Electrical Power Required}}$$

This takes on the simple form

$$\eta = \frac{1}{\left(1 + \frac{R_s}{R_{in}}\right) \left(1 + \frac{D}{R_A}\right)} \quad 2-8$$

where $R_{in} = \frac{X_m T^2}{\omega S |Z_m|^2}$ is the real part of the

input impedance of the transducer (derived in Appendix A). Equation 2-8 shows clearly that for greatest radiation efficiency the source resistance should be made small with respect to the input resistance of the transducer and that the internal damping should be kept below the real part of the acoustic radiation impedance. If the source resistance is made to match R_{in} then

$$\eta_{\text{matched}} = \frac{0.5}{1 + D/R_A} \quad 2-9$$

2.1 (Continued)

If the frequency, ω_o , at which $R_m = 0$ is used, then the efficiency becomes

$$\eta_{\omega_o} = \frac{1}{\left(1 + \frac{D}{R_A}\right) \left[\left(1 + \frac{D}{R_A}\right) \left(\omega_o^2 S R_S R_A\right) + 1 \right]} \quad 2-10$$

2.1.2 Receiving Sensitivity

Since it was hoped to use the same transducer as receiver and radiator, the receiving sensitivity is another important quantity. If S_p is the area of tape exposed to incident acoustics pressure, p , the voltage, v , developed across the load impedance Z_s , (corresponding to the source impedance with the ideal voltage source shorted) is $j \omega \sigma Z_s$; so using 2-6

$$\left| \frac{v}{p} \right| = \frac{\omega S_p T}{|Z_e Z_m - T^2|} |Z_s| \quad 2-11$$

While this sensitivity measure does give the actual voltage-to-pressure ratio to be expected in practice, a more common sensitivity parameter is the open circuit sensitivity, defined as the magnitude of the ratio of the voltage to the acoustic pressure producing it when the voltage is taken across an open circuit at the transducer's terminals. This turns out to be

$$\left| \frac{v}{p} \right|_{oc} = \frac{S_p T}{S |Z_m|} = \frac{T S_p / S}{\sqrt{(K - \omega^2 M - \omega X_A)^2 + \omega^2 (D + R_A)^2}} \quad 2-12$$

At the frequency $\omega = \omega_o$ where $R_m = 0$ this becomes simply

$$\left| \frac{v}{p} \right|_{oc} = \frac{S_p T}{S \omega_o (D + R_A)} \quad 2-13$$

2.1.3 Directivity

One of the performance characteristics of interest is the directivity, a measure of the ability of the transducer to restrict its radiation energy to a narrow beam. Consider the pressure distribution in a plane perpendicular to the tape. The pressure at a point defined by the cylindrical coordinates r, θ in the plane is given by²

$$p(r, \theta) = \frac{\sin(kw \sin \theta)}{kw \sin \theta} p_x(r) = d(\theta) p_x(r) \quad 2-14$$

where $p_x(r)$ is the pressure on the perpendicular to the tape surface measured at a range r from the tape

θ is the angle measured from the perpendicular to the tape surface

w is the tape width

k = the wave number = 2π frequency/speed of sound in medium

In our case, we know the velocity of the tape (from the derivative of 2-7) and the radiation impedance Z_A , so we can calculate the total radiated power, P . The far field axial pressure is then given by

$$p_x(r) = \sqrt{\frac{\rho c P}{2l r \int_0^{\pi/2} d^2(\theta) d\theta}} \quad 2-15$$

Although the directivity is best displayed by a polar plot of the pressure field at different angles from the perpendicular to the tape surface (the directivity pattern), the directivity index is a useful number which summarizes the directionality of the source. If \bar{P}_x is the power that would be radiated by a semicylindrically radiating source with far field pressure $p_x(r)$, then the directivity index is

$$D.I. = 10 \log_{10} (\bar{P}_x/P) = 10 \log_{10} \left(\frac{2}{\pi} \int_0^{\pi/2} d^2(\theta) d\theta \right) \quad 2-16$$

The greater the D.I. the more concentrated the acoustic radiation is about the perpendicular to the tape surface. A D.I. of zero indicates a radiation completely uniform in all directions, ie., no directivity.

2.1.4 Target Simulation

So far we have considered only performance characteristics associated either with radiation or receiving. However, we want to use these characteristics simultaneously for the detector application. To connect them we need to simulate a target--something

2.1.4 (Continued)

that reflects some radiated energy back to the tape for reception. For this purpose, we assume the existence of a square plate of width l_t with a pressure reflectivity r_t located a perpendicular distance d_t above the tape and parallel to it. The average radiation pressure on the target is approximated by $p_x(r)$ for

$$r = \sqrt{d_t^2 + l_t^2/16} \quad \text{where } p_x \text{ is given by 2-15.}$$

Assuming specular reflection from the target (which is many wavelengths in width), the additional spreading loss suffered by the reflected disturbance will decrease its value by a factor of $\sqrt{2}$ compared to the average value reflected by the target. In addition to the spreading loss, the pressure is decreased by a factor of r_t due to the absorption of some of the energy by the target and another factor of the form³

$$e^{-2(af^2 + b \log_{10} f - c)d_t} \quad (2-17)$$

due to the attenuation of sound during its propagation caused by heat conduction, friction, and molecular absorption. Thus, the received pressure using 2-15 and 2-17 is approximated by

$$p = \sqrt{\frac{\rho c P}{2l \int_0^{l/2} d^2(\theta) d\theta \sqrt{d_t^2 + l_t^2/16}}} e^{-\left[21.2f^2 + .072 \ln f - .663\right] 2d_t} \quad (2-18)$$

In our model this input pressure was assumed to be sensed only by a tape segment l_t in length for purposes of deriving performance characteristics of the detector. One such characteristic is Z_T the transfer impedance defined as the receiver voltage output across the external load divided by the input current supplied by the driving amplifier. This is a detection system figure of merit; since for constant input voltage, it is an estimate of how much useful output can be expected for a given input.

2.2 Computer Implementation

A Fortran IV code was written for SSD's Nova computer implementing the relevant mathematical expressions developed in the previous section (along with many

2.2 (Continued)

others). The code was designed to provide a user with a flexible and convenient tool for examining the effects of numerous tape-associated variables on the transducer's performance.

The flow diagram of Fig. 2-2 shows the general procedure used. A listing of the program and a dictionary of variables are included along with a more detailed discussion of the program in Appendix B. Most of the program is straight forward. An exception is the calculation of the radiation impedance of the infinite strip. It is believed that the code for this complex quantity is unique to the current program. This is shown and discussed in Appendix C.

2.3 Results and Discussion

Once the computer coding for the transducer simulation was debugged, the examination of the effects of the parameters began. The procedure devised for this task was to postulate a standard parameter set and then vary each parameter by itself over a range believed to cover that practical for the parameter. The important performance characteristics were then plotted as functions of each varied parameter. Over 360 such plots were generated during this study. As more experience was gained, new standard sets of parameters were tried from which the individual parameters were varied. Most of the results of this section are based on Standard #3 which has the parameters:

Tape Width	2 cm
Tape Length	10 m
Cuter Jacket Thickness	15 μm
Cuter Jacket Density	1700 kg/m^3
Moving Conductor Thickness	10 μm
Moving Conductor Density	2700 kg/m^3
Adhesive/Air Gap Thickness	20 μm
Adhesive/Air Gap Density	1.18 kg/m^3
Adhesive/Air Gap Permittivity	$8.854 \times 10^{-12} \text{ F}/\text{m}$
Dielectric Thickness	100 μm
Dielectric Permittivity	$2.1 \epsilon_0 \text{ F}/\text{m}$
Internal Mechanical Damping Constant	1000 $\text{Pa}\cdot\text{s}/\text{m}$

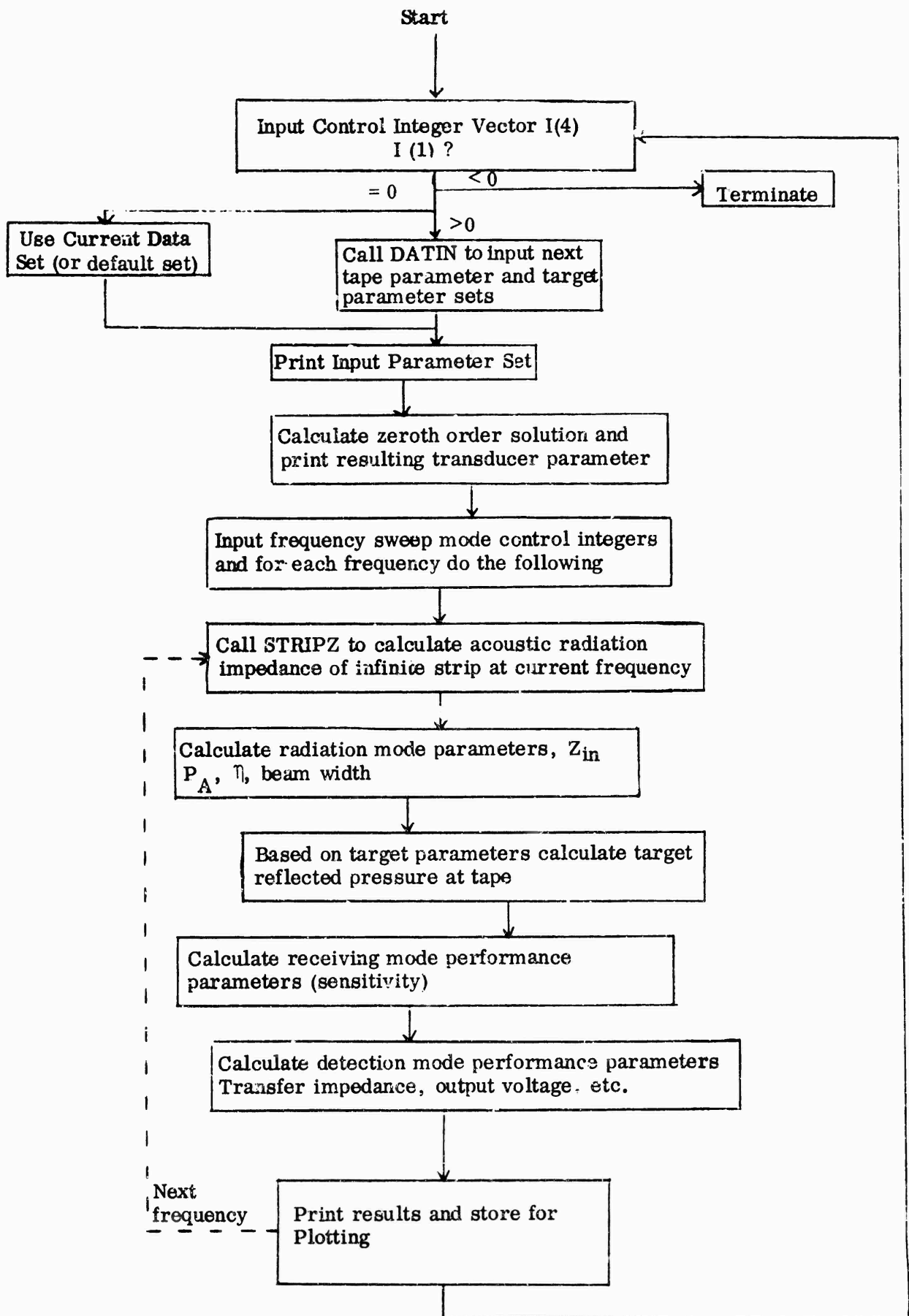


Figure-2-2 Flow Diagram of Computer Model

2.3 (Continued)

Electret Surface Charge Density	100 $\mu\text{C}/\text{m}^2$
Target Cross Dimension	0.4 m
Target Distance from Tape	1 m
Target Pressure Reflection Coefficient	0.5

The mechanical resonance frequency, f_0 , for this set of parameters was found to be 58.6 kHz.

In the following subsections we examine the effects of the most important transducer parameters on the several performance characteristics. Unless otherwise stated, the frequency is f_0 , that at mechanical resonance and the source impedance conjugate matched to the transducer. Also the input voltage is held constant at 10 V.

2.3.1 Tape Length and Width

To study the effects of length and width we varied the former over the range .1 to 100 m and the latter over the range 5 to 40 mm. As expected, the radiation efficiency, η , at mechanical resonance f_0 , was completely independent of length. However, a slight dependence on width was found because the real part of the specific acoustic radiation impedance is a function of kw . Since kw never got below 5, R_A never got far from ρc (see Fig. C-1, Appendix C), so the dependence was slight.

The frequency of resonance is also independent of length and only slightly affected by width because the contribution to the moving mass from X_A (which depends on kw) is insignificant for these frequencies and moving mass materials.

The value of source impedance required to conjugate match the input impedance of the transducer is exactly inversely proportional to the surface area of the tape. Thus, the greater the tape width and/or length, the smaller the required input resistance and series inductance. However, since the sensitivity is proportional to the magnitude of this impedance, the sensitivity is also inversely proportional to tape surface area. This was not true of course of the open circuit sensitivity (S_{OC}), which was found independent of length and width as long as the entire area was exposed to the sound. When a fixed length l_p is assumed exposed to pressure (as for the target simulation), the effective open circuit sensitivity is inversely proportional to l .

2.3.1 (Continued)

The transfer impedance Z_T is proportional to l^{-2} . This indicates that for every order of magnitude increase in length we must supply 100 times as much current to maintain the same output signal caused by a target reflection. This is reasonable since a factor of 10 is required first to excite the layer area to the same amplitude, and the other factor of 10 is required to make up the l_p/l loss in effective sensitivity due to l_p being fixed.

2.3.2 Frequency

When varied over the range 10-100 kHz, the frequency of excitation is found to have a major effect on most of the performance characteristics. The efficiency is one exception being affected only slightly (through the dependence of R_A on kw where $k \equiv 2\pi f/c$). The open circuit sensitivity (Fig. 2-3) displays a resonance-like peak near the frequency of mechanical resonance, f_o . It appears to level off at low frequencies and roll-off above resonance. The conjugate-matching input resistance has a nearly identical dependence on frequency. In fact, only near the peak is the resistance found to be high enough to be practical. As might be expected, the sharpness of this resonance peak is found to be strongly dependent on the mechanical damping constant D ; the greater the D , the broader the peak and the lower the frequency at which it occurs. The transfer impedance is found to decrease gradually ($\sim 1/f$) with total disregard for the resonance frequency region (as long as $Z_s = Z_{in}^*$ at each frequency). However, unless R_s is large enough to be practically realizable at frequencies below resonance, the fact that the system figure of merit (Z_T) improves as frequency is decreased, is only of academic interest.

2.3.3 Mechanical Damping Constant

Of all the parameters used in the model, the mechanical damping constant, D , is least understood. Not only do we not know of the mathematical relations between it and the physical parameters of the transducer on which it depends, but we also do not even know the approximate range of values which should be considered typical. We started by assigning it values in the range of ρc on the assumption that the internal mechanical losses might be on the same order as the losses due to radiation. Since $\rho c = 410$, $D = 1000$ seemed reasonable. This gives a potential radiation efficiency of about 15% for $R_s = R_{in}$. Since this is much greater than other workers expected and D is the only parameter that could produce the difference, we

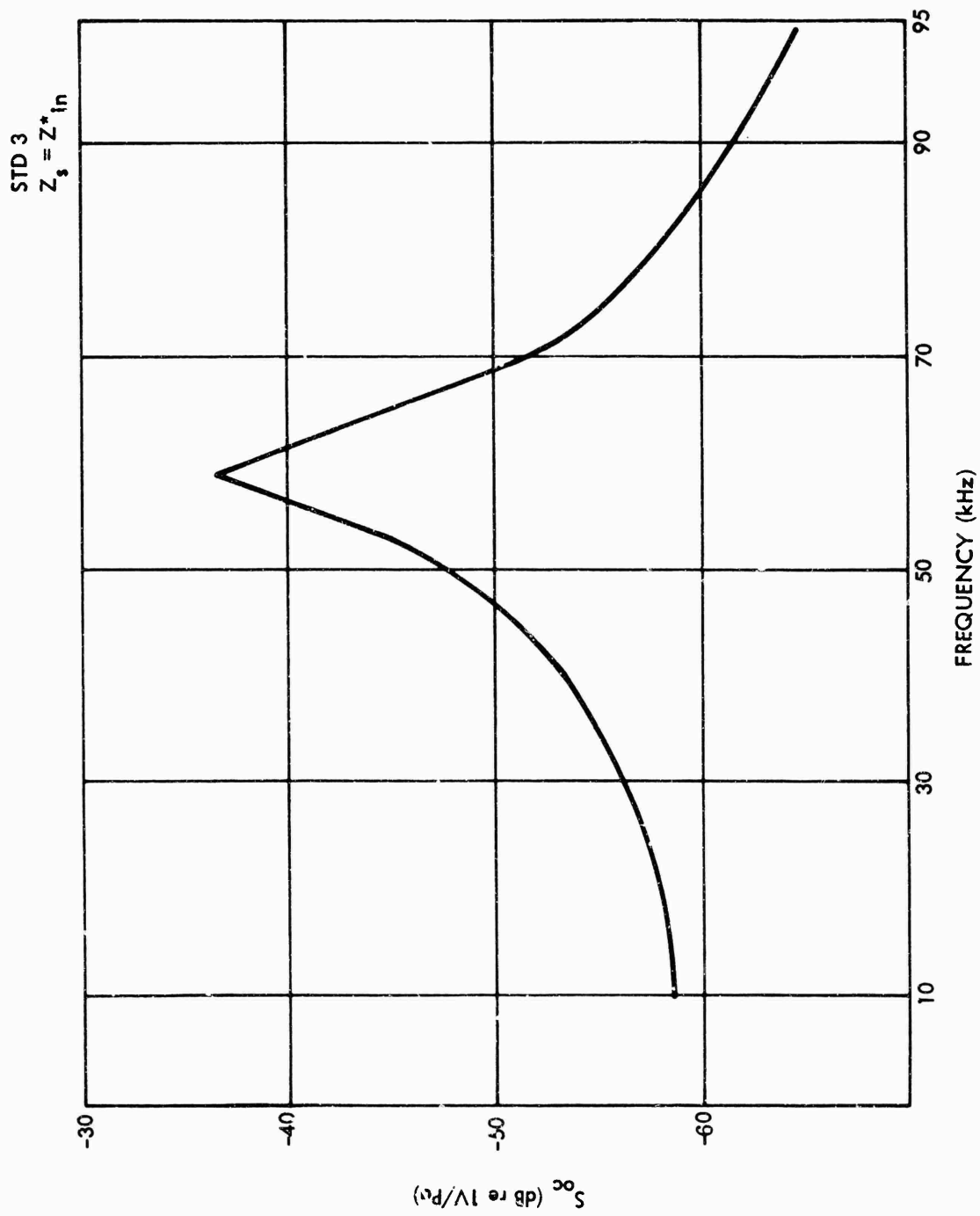


Figure 2-3. Open Circuit Sensitivity vs Frequency

2.3.3 (Continued)

later tried much greater values for D . For most of this study we varied D from 50 to 5000 Pa-s/m.

As expected from Eq. 2-9, for $D \gg R_A$ the efficiency varies like D^{-1} . Thus, D is the determining factor for radiation efficiency. The open circuit sensitivity is also adversely affected by increasing D . The dependence is like D^{-1} for $D \gg R_A$. This is also true for the transfer impedance and for $R_s (=R_{in})$. The source inductance, however, is independent of the damping as are the particle displacement and the sensitivity. Obviously, it is desirable to keep the damping as small as possible unless broad band operation is considered important.

2.3.4 Air Gap Thickness

The air gap was varied over the range 0.5 to 500 μm . Since it is the controlling factor in the mechanical compliance, as it decreases the mechanical resonance is expected to rise. This is the observed phenomenon, see Fig. 2-4. Because of this resonance frequency dependence, the performance characteristics as functions of air gap are studied at the resonance frequency corresponding to the current value of air gap. For $f = f_0$ the radiation efficiency is found to be independent of air gap except for the slight variations caused by the dependence of R_A on frequency. The open circuit sensitivity, Fig. 2-5, as well as the source resistance go through a maximum as a function of air gap (at about 50 μm). This is interesting since it indicates that by increasing the 20 μm used in Standard #3 by a factor of 5, we should achieve a slight increase in open circuit sensitivity.

Fig. 2-6 also indicates that we should increase the air gap to achieve improved system performance, as indicated by the transfer impedance, Z_T .

2.3.5 Conductor Thickness

We varied this quantity over the range .05 to 50 μm . The thickness of the outer conductor is the controlling factor in the moving mass/unit area, and would be expected (like the air gap) to have an effect on the mechanical resonance frequency. As expected, f_0 decreases with increasing conductor thickness. At $f = f_0$ efficiency, sensitivity and particle displacement are found to be independent of conductor thickness. However, Z_T and S_{oc} are found to increase with increasing conductor thickness, again apparently due to the reduction in frequency it causes. The source resistance

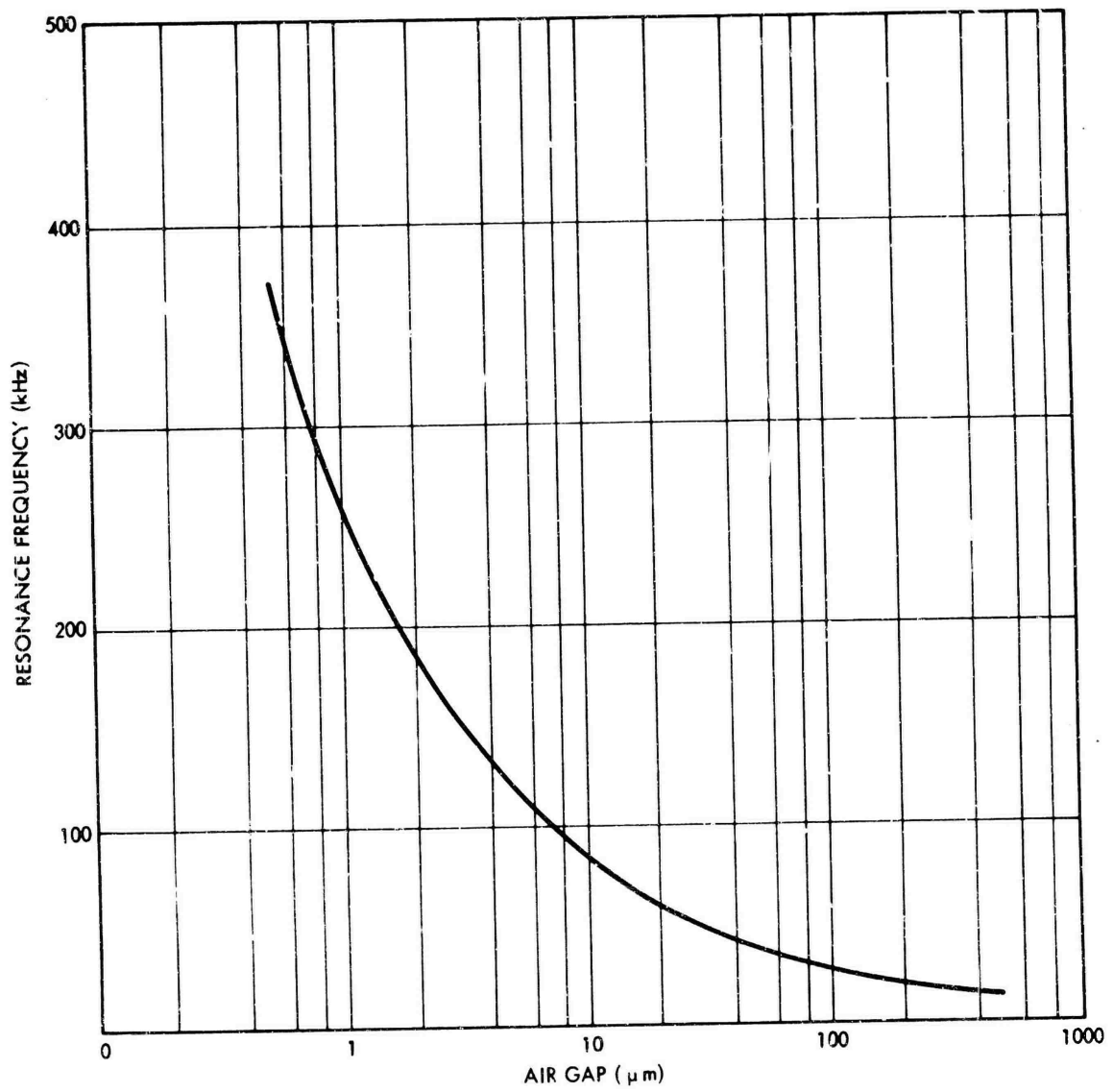


Figure 2-4. Resonance Frequency versus Air Gap

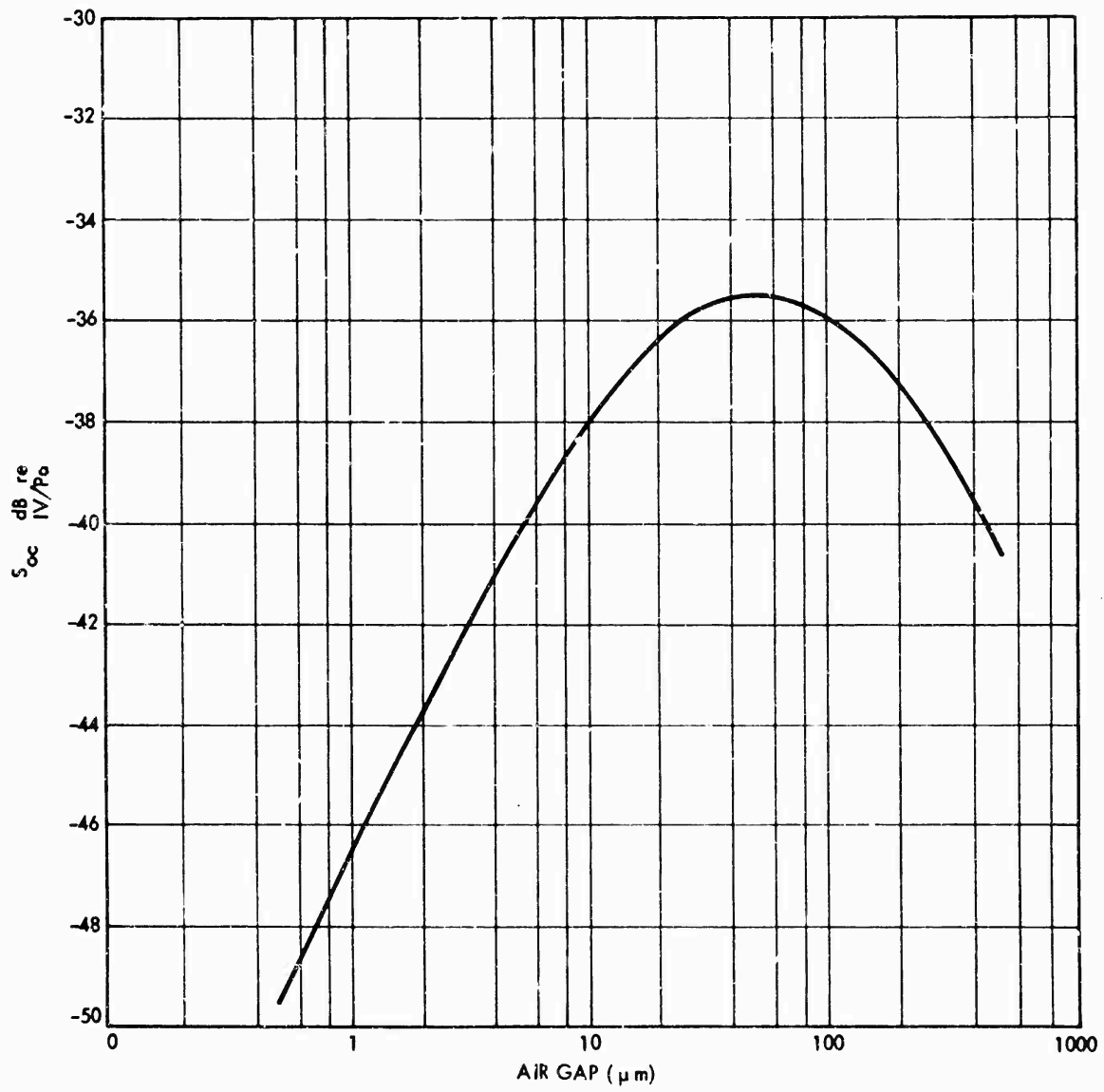


Figure 2-5. Open Circuit Sensitivity versus Air Gap at $f = f_0$

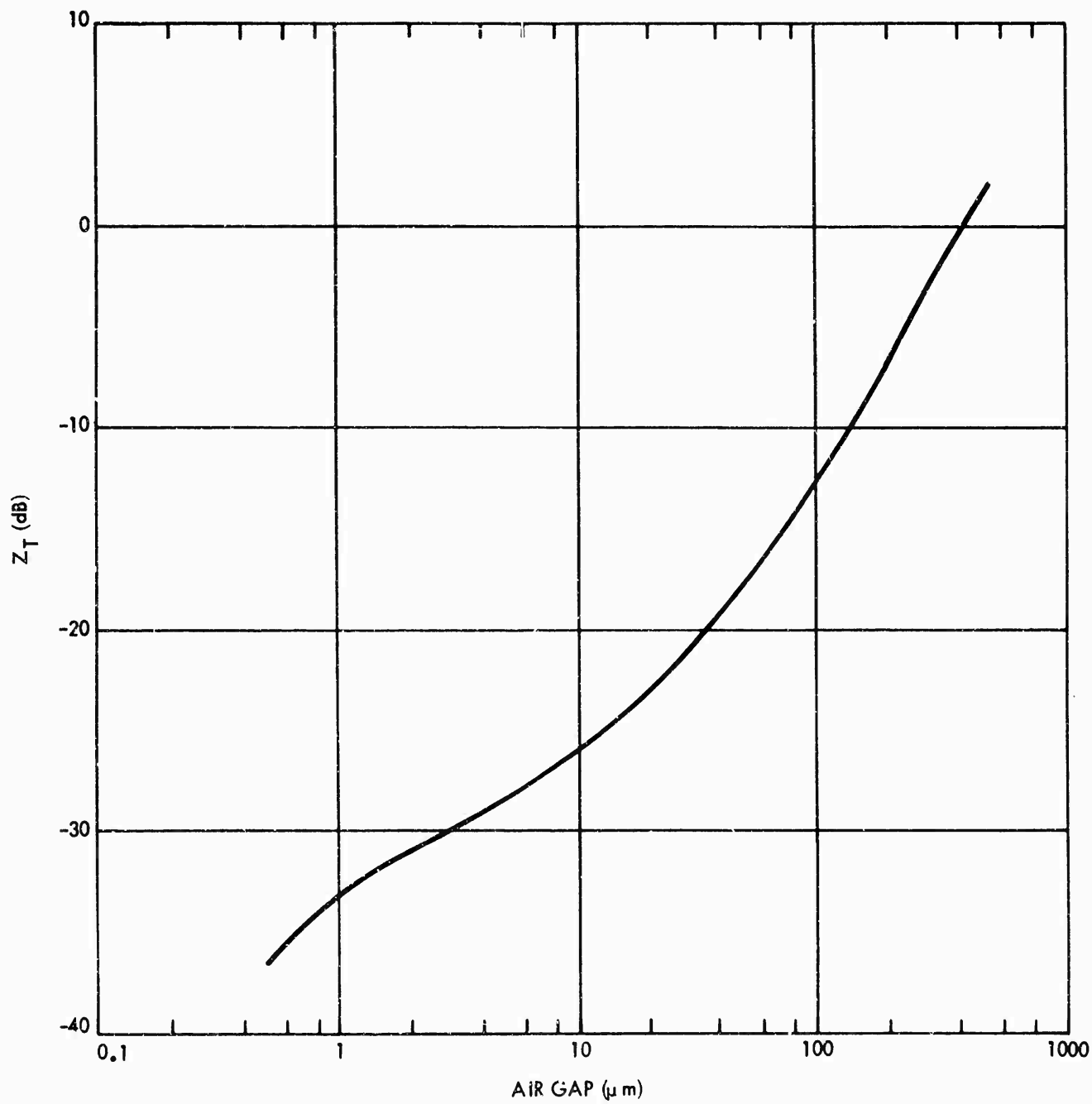


Figure 2-6. Transfer Impedance vs. Air Gap
2-17

2.3.5 (Continued)

and inductance increase monotonically with conductor thickness (like Z_T and S_{oc}) over the limits examined.

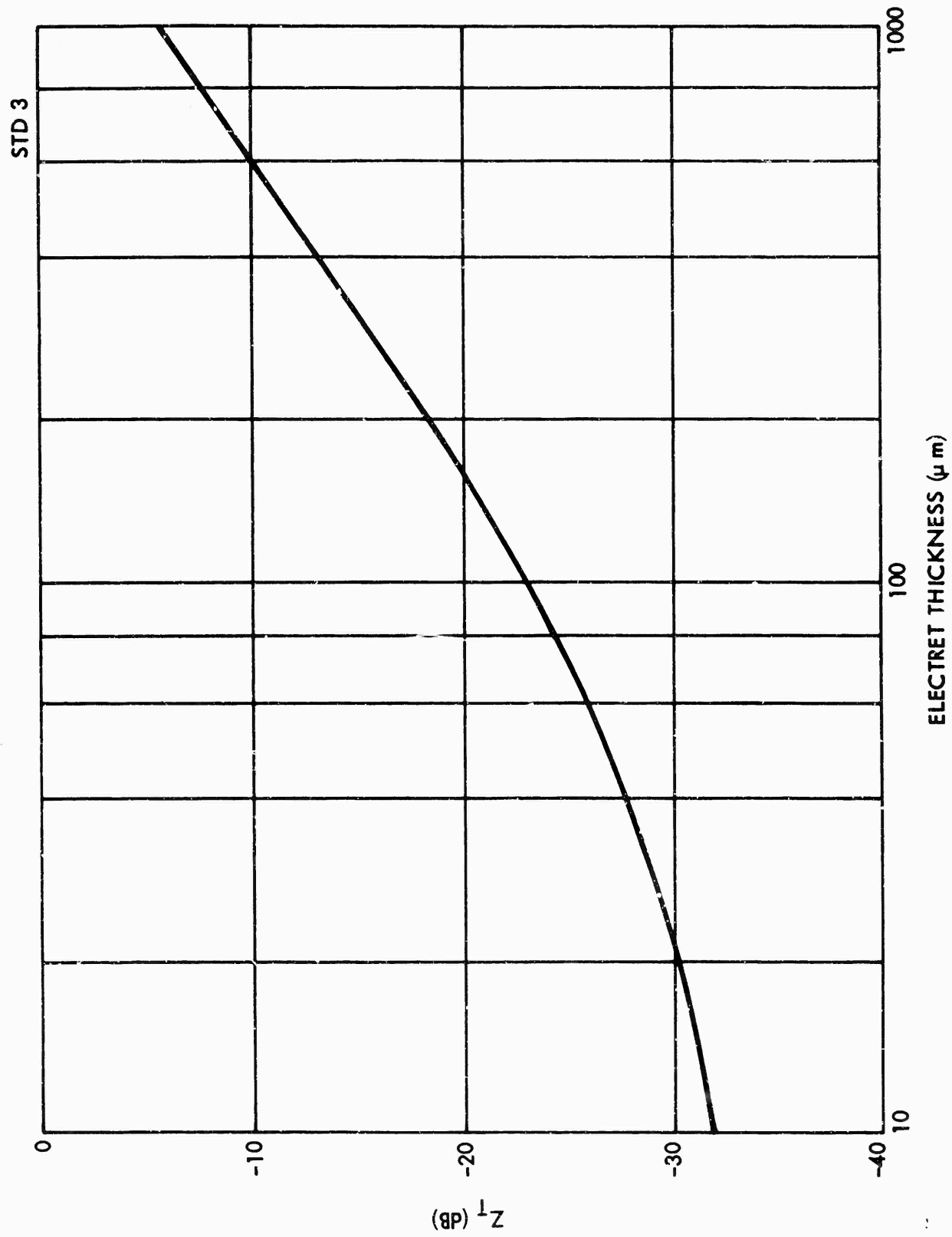
2.3.6 Electret Thickness and Surface Charge Density

The electret thickness, d , was varied over the range 10-1000 μm . Since mechanical resonance is independent of d , all the data refers to $f_o = 58.6$ kHz. The efficiency of radiation is the only parameter found to be independent of d . The open circuit sensitivity increases with d but especially rapidly for $d < 50$ μm . For $d \geq 500$ μm the increase in S_{oc} with d appears to be leveling off. Z_T (Fig. 2-7) and R_s also increase monotonically with d , so it would appear desirable to use a very thick electret layer if possible.

However, it must be remembered that this analysis varies only a single parameter at a time. So as we increase the electret thickness, d , we are assuming a constant surface charge density. Yet, as will be shown in Fig. 3-3 of the following chapter, the surface potential of the electret must increase directly with d to maintain a given surface charge density. In our experiments with various thicknesses of electret, we found that the surface potential varies no more rapidly than with the square root of the thickness. This means that to be realistic we should decrease the electret surface charge density as d is allowed to increase.

Surface charge density, σ_e , was varied over the range 1 to 10,000 $\mu\text{C}/\text{m}^2$. As expected, the efficiency is unaffected by σ_e . Interestingly, above 1 mC/m^2 the charge density was found to have a marked effect on the frequency of mechanical resonance. This is believed due to the increased stiffness resulting from the reduction in air gap caused by the electrostatic pressure (which goes as σ_e^2) on the moving conductor. The open circuit sensitivity, R_s , and Z_T all go through maxima in the range $\sigma_e = 1-2$ mC/m^2 . Curiously, the particle displacement is nearly proportional to σ_e^{-1} in the range examined. This is apparently due to the reduction in current drive as R_s increases with σ_e . However, above $\sigma_e \sim 1$, it is due to the increased stiffness as the air gap is reduced as described above.

In keeping with the experimental finding that the electret surface potential varied as the square root of the film thickness, we ran the case $\sigma_e \sqrt{d} = \text{const.}$ for $\text{const.} = \sqrt{10^{-11}}$, $\sqrt{10^{-12}}$, and $\sqrt{10^{-13}}$ $\text{C-m}^{-3/2}$. When plotted against σ_e , see Fig. 2-8, S_{oc} still goes through a broad maximum for each case. These maxima imply optimum electret thicknesses of 33, 35, and 40 μm for the respective cases as



2-19

Figure 2-7. Transfer Impedance vs Electret Thickness

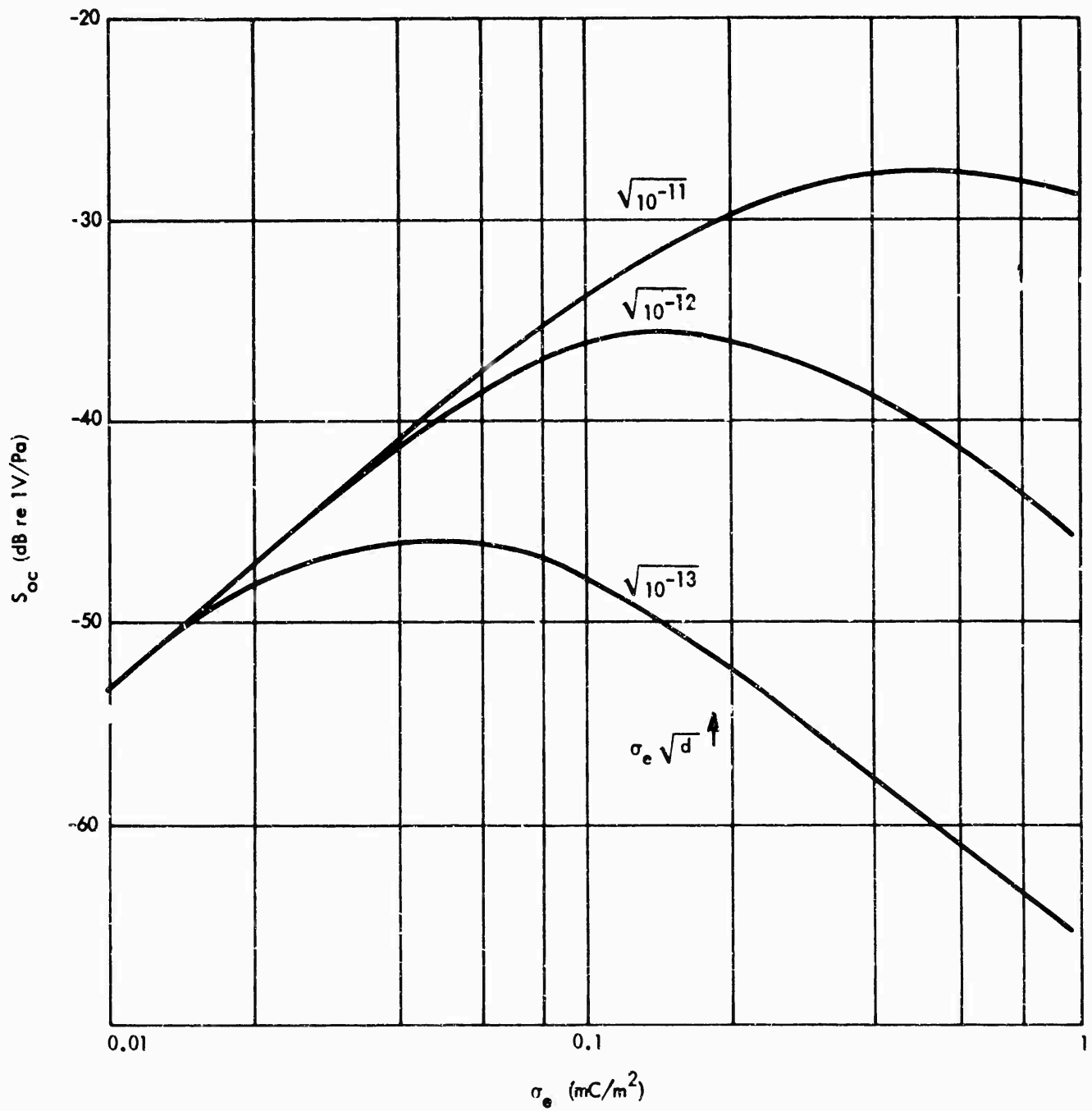


Figure 2-8. Effect of $\sigma_e \sqrt{d}$ on Open Circuit Sensitivity

2.3.6 (Continued)

$\sigma_e = .4, .13$ and $.05 \text{ mC/m}^2$. The transfer impedance plotted against σ_e low appears quite different--Fig. 2-9 shows a decreasing Z_T with small σ_e ($\sigma_e \sqrt{d} = \text{const.}$) but leveling out for $\sigma_e \gtrsim 0.1 \text{ mC/m}^2$. These curves can be summarized by the statement that for achievable σ_e ($\sim 0.2 \text{ mC/m}^2$ or less), we should make $\sigma_e \sqrt{d}$ large by making d large.

The later experimental finding, that eventually $\sigma_e d = \text{const.}$ seems to be a more accurate description, was not discovered in time to investigate with the model.

2.4 Summary and Discussion

Table 2-1 briefly summarizes the approximate effects that nine transducer parameters have on three performance characteristics as presented in the preceding section. In general, it appears the designer is left with adequate freedom to develop a transducer emphasizing any desired aspect of performance. For example, transducer parameters can be found which effect efficiency but not open circuit sensitivity and also vice versa.

In general, the results are encouraging. The radiation efficiencies are higher than expected and the open circuit sensitivities are adequate. Not all of the results are well understood, for example the peak found in the S_{oc} vs σ_e curve. It is not clear why further increases in surface charge density should reduce the sensitivity above the value 2 mC/m^2 . It is due to the ω^{-1} factor in the expression for S_{oc} but is still curious. Since this is above the values of σ_e we achieved with our electrets, it will not be a factor in our designs. Another related outcome is that working at low frequencies seems to be desirable for both receiving sensitivity and system performance (Z_T).

One of the facts emerging from this modeling analysis is that achieving good performance may require a source resistance lower than practical with typical amplifiers. This is especially true when it is considered that making $Z_s = Z_{in}^*$ requires a series inductor as part of Z_s . Inductors are notorious for being difficult to obtain in low DC resistance values in the ultrasonic range, especially for large values of inductance. Thus, it may be necessary in practice to use solid state electronic devices which can be designed to have large inductive reactances but with low effective resistances.

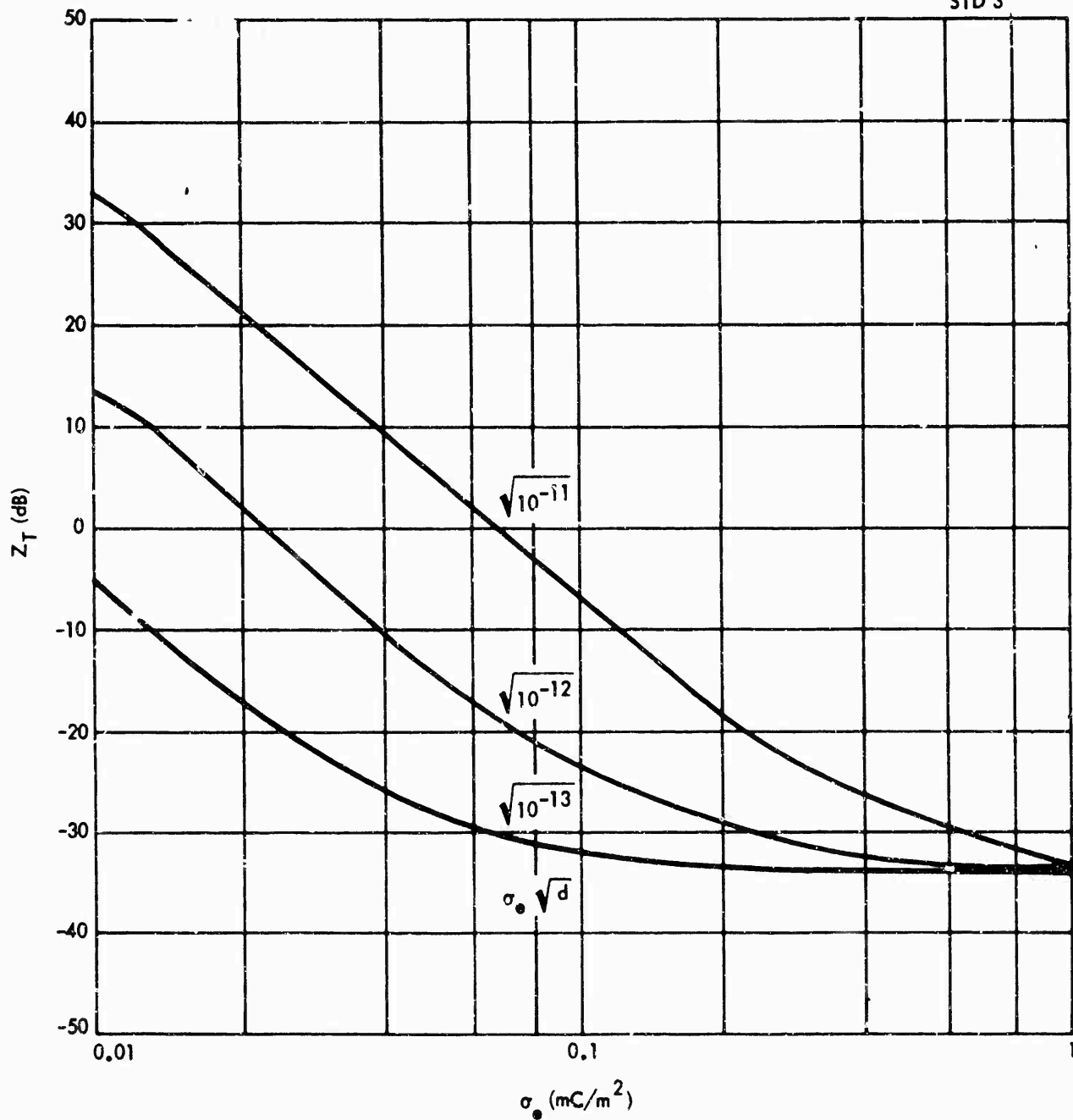










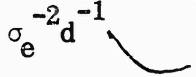


Figure 2-9. Effect of $\sigma_e \sqrt{d}$ on Transfer Impedance

For $Z_s = Z_{in}^*$ and $f = f_o$	Efficiency	Open Circuit Sensitivity	Transfer Impedance
Frequency	$\sim 0^*$		$\sim f^{-1}$ to $f^{-1/2}$
Length	0	l^{-1}	l^{-2}
Width	$\sim 0^*$	0	0
Damping	D^{-1}	D^{-1}	D^{-1}
Air Gap Thickness	$\sim 0^*$	\sqrt{a} 	
Moving Conductor Thickness	$\sim 0^*$		
Electret Thickness	0		
Surface Charge Density	0	σ_e 	
$\sigma_e d = \text{const.}$	0		$\sigma_e^{-2} d^{-1}$ 

* Dependence comes through R_A (kw)

Table 2-1. Parameter Effects Summary

2.4 (Continued)

In a limited analysis effort such as this, it is always necessary to limit the investigation to fit the project plan, leaving undone numerous tasks which present themselves as the analysis goes on. For example, in the present case it would appear desirable to examine the effects of not matching the conjugate input impedance with the source impedance. Also, the effects of operating at frequencies in the vicinity but not exactly at the resonance frequency warrant examination. Additional standard parameter sets should also be simulated to ascertain that the above results are not unique to Standard #3. In view of the long term experimental findings, it now appears desirable to treat $\sigma_e d = \text{const.}$ as a parameter and examine its effects on the performance characteristics.

3.0 Experimental Investigation

While the theoretical analysis and computer simulation produced a degree of confidence that an electret tape transducer was feasible, the experimental phase of this program provided the proof. In this section we trace the laboratory program through its various phases: preparation of electret materials, design of experimental samples, fabrication of sample transducers, and transducer performance evaluation.

3.1 General Procedure

So that the various discussions will be properly connected to the effort as a whole, we first trace the general procedure. First, we developed a technique for charging the teflon tape. This was necessary because the originally intended source was no longer making charged electret films. The method used (called the liquid-contact electrification method) was found described in the recent literature.^{4,5} Since the development of an improved charging method was not within the scope of this effort, we only did enough experimental work to provide confidence that adequate electrets could be produced. We did, however, do some limited testing to determine the effects of polymer thickness and applied voltage on surface charge density and longevity.

As soon as we felt that an adequate procedure for charging was available, we concentrated on designing fabricatable samples. This was based somewhat on the availability of materials as well as the modeling analysis (described previously). Several design aids and plots were derived and used to come up with a design for fabrication.

Because the construction of this sort of design did not exist, we had to develop the techniques for putting it together. This involved achieving excellent adhesive bonds between a variety of film materials, determining the best time to charge the teflon layer, eliminating air between some layers and producing a uniformly compliant layer.

Finally, in order to evaluate and improve the designs, measurement techniques were developed for these transducers. In addition to normal capacitance and resistance measurements, we determined radiation efficiency and open circuit sensitivity. These were greatly facilitated by SSD's anechoic chamber.

3.2 Electret Preparation

3.2.1 Background

When it was discovered that the source used for the proposal quotation (October 1973)

3.2.1 (Continued)

was no longer making electrets, we recognized that the success of the entire program would depend on our ability to find an alternative source or to make adequate electrets ourselves. After unsuccessfully trying to locate another source for electrets, we began to look into published methods of charging that might be suitable for the tape configuration. Two methods seemed appropriate. One, the corona discharge method, is used by most Japanese electret microphone manufacturers. In this method the film is rolled over a cylinder at a high potential with respect to a knife edge positioned parallel to the cylinder's axis and separated from the film by a controlled distance.

In the other method (liquid contact), the film to be charged is slowly pulled over a flat conducting surface while being lightly pushed against it by the edge of a fluid-saturated sponge that extends across the desired width. The fluid is held at a high potential with respect to the conducting subsurface. Because of its simplicity, this method was tried first; and because it proved adequate, no others were attempted.

3.2.2 The Charging Procedure

The only material charged in this study was FEP teflon film of various thickness. First the film is bonded to a copper substrate of the desired size so that air bubbles are eliminated. Any bubbles allowed to remain produce low-charge areas. This multi-layer slab is then placed in a special charging jig such as those shown in the photographs of Fig. 3-1. Here the sample is shown being pulled beneath a sponge saturated with ethyl alcohol which is at a high potential (4 kV is typical) with respect to the copper substrate. Ideally, the alcohol wets the surface of the teflon uniformly as the sample is pulled by and rapidly evaporates afterwards. Although alcohol is a poor electrical conductor, enough charges migrate under the influence of the electric field to leave a high effective surface charge density on the electret. Care must be exercised to prevent any sparking in this procedure, since alcohol is a much better fuel than a conductor. (Numerous sponges became fine pyrotechnic displays during the development of a spark-free technique.) The sample was pulled manually (as shown in Fig. 3-1) using a long, light, non-conducting cord to avoid shock hazard to the operator.

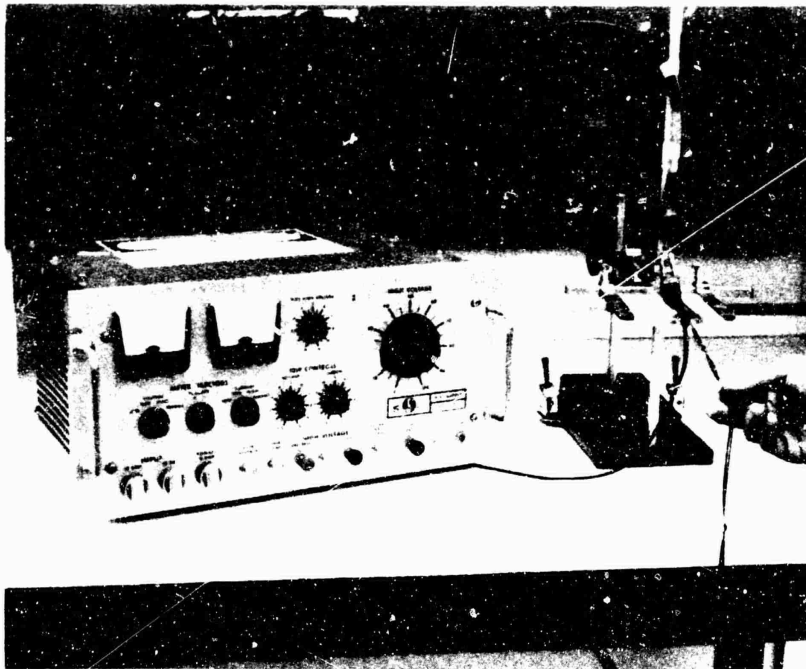


Figure 3-1a. Short Tape Liquid Contact Charging Apparatus

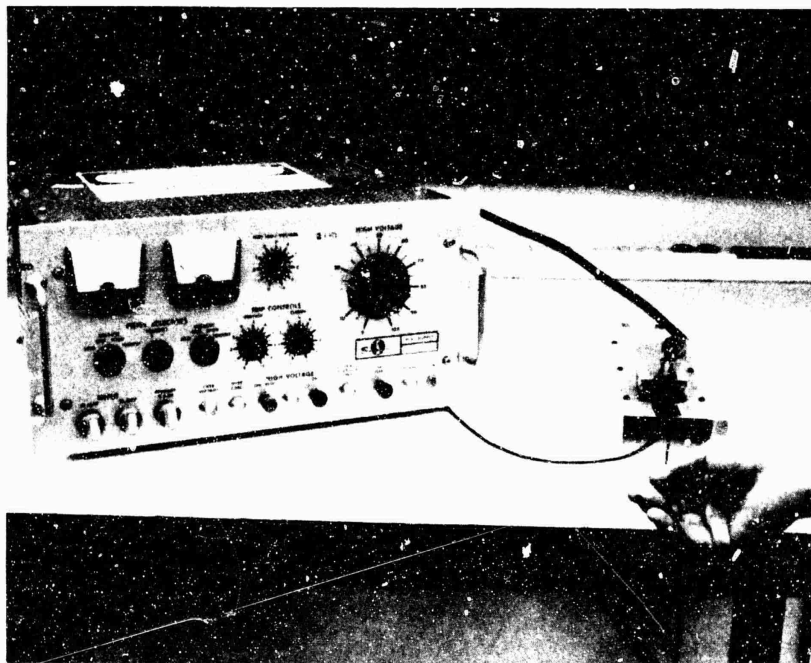


Figure 3-1b. Long Tape Charging Apparatus

3.2.2 (Continued)

In the early apparatus (Fig. 3-1a), the sample was held in position during pulling by a set of "U" tracks which fit over opposite edges of the sample assembly. The length of samples that could be charged with this apparatus was limited to several inches--adequate for learning purposes. The later apparatus (Fig. 3-1b) can accommodate a very long sample (not shown). In this case the "U" tracks are replaced with straight guide surfaces, and vertical motion is not constrained except by the sponge pressure. If the pulling is done gently, there is no significant vertical motion anyway. The pulling is done slowly enough to allow charges to flow until self-limited--about 1 cm/s. The most critical factor in the process seems to be the uniformity of the liquid contact. Any area not wetted or an area in which a drop forms will result in non-uniform charge distribution. The sponge was much better in achieving uniformity than the initially-used rag wick.

The surface of the teflon film must be very clean. We used acetone and a degreasing agent to eliminate any extraneous film and dust. In addition, the electret was kept shielded with a copper cover when possible after charging to avoid depoling caused by charged particles latching onto the electret. During measurement of the electret strength, the electret was handled at a laminar flow bench where filtered air is continually moving upward past the specimen.

The sponge torch problem was eventually solved by coating the sponge sides with light silicone grease so the fluid's vapor was not able to come out there. It was also found to be beneficial to use a blower to dissipate the alcohol vapor. Silicone grease was also spread along the edges of the sample to contain the liquid better and to prevent a liquid shorting path around the edge.

Both freon (degreasing agent) and acetone were used instead of ethyl alcohol as the charging liquid with excellent results. Although we standardized on ethyl alcohol, it appears that at least these two (and probably other) fluids could be used as well. However, too few samples were tried to warrant making any more than this qualitative statement concerning the charging liquid.

3.2.3 Charge Measurement

In order to study the effects of treatment parameters and sample characteristics on the size and uniformity of the charge produced, a standard method of measuring it was developed using Sylvania's Monroe 144S-4 electrostatic volt meter. The measurement

3.2.3 (Continued)

set-up is shown in the photographs of Fig. 3-2. In each foreground is the electrostatic probe being used to measure the surface potential at a point on the electret sample facing it on the left. Both sample and probe can be precisely controlled in position so that the probe can scan the surface of the sample as desired. The Monroe probe is designed to measure the surface potential on a small spot directly in front of the 30 mil diameter observation hole in the probe structure with respect to the user-supplied ground. In our case the copper layer immediately beneath the teflon film is grounded to the meter, and the probe is positioned about 5 mils from the sample being measured. To avoid the problem of charged dust particles contaminating the probe's sensitive aperture and thus making the measurements inaccurate, a stream of filtered air is continually pumped out of the hole. The surface potential can be read directly from the meter on the instrument, or using the meter output terminal it can be recorded on a continuous chart (as shown in Fig. 3-2).

For purposes of making comparisons we scanned the length of the sample along three parallel lines: one in the middle and one on each side, half-way from the middle to the edge (referred to as Top, Middle, and Bottom traces). During each scan the output of the meter is plotted on the chart recorder. In a later version of the apparatus designed for long samples, Fig. 3-2b, the scanning is done by manually pulling the sample past the probe three times for the three traces.

The three traces are converted to average surface potentials by using a planimeter to measure the area between the trace and the zero potential (or ground) line, measuring the length of the trace, and using a calibrated voltage to determine the relation between the chart scale and meter voltage. The three average surface potentials for a sample are then averaged to arrive at a single number believed to be directly proportional to the average surface charge density of the sample. The actual relation between the average measured surface potential V_s and the effective average surface charge is easily calculated using the same kind of analysis as that in Appendix A (Section 2). Since the probe head is held at the potential it is measuring, we get

$$V_s = \frac{\sigma_{e1}}{C_e} + \frac{\sigma_{e2} + \sigma_{e1}}{C_a} \quad 3-1$$

$$\text{or } V_s = \frac{\sigma_e}{C_e} = \frac{\sigma_e d}{\epsilon_e} \quad \text{where } \sigma_{e1} = -\sigma_{e2} \equiv \sigma_e \quad 3-2$$

3-5

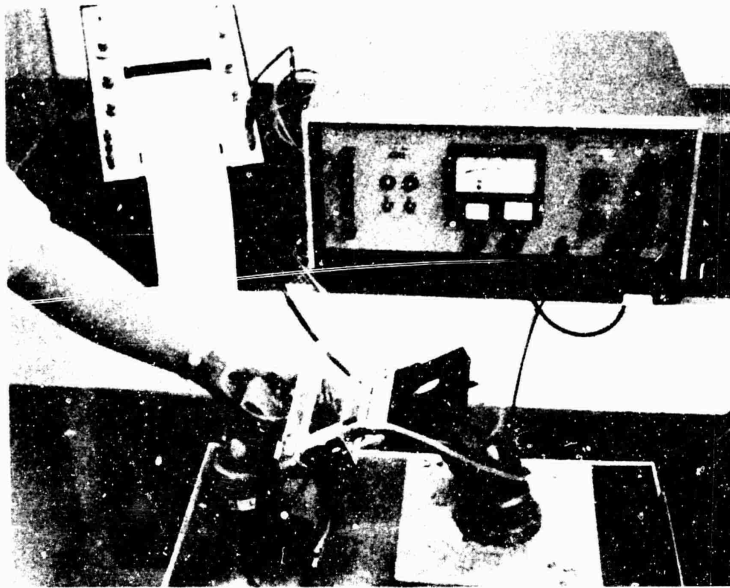


Figure 3-2a. Electret Surface Potential Measurement Apparatus

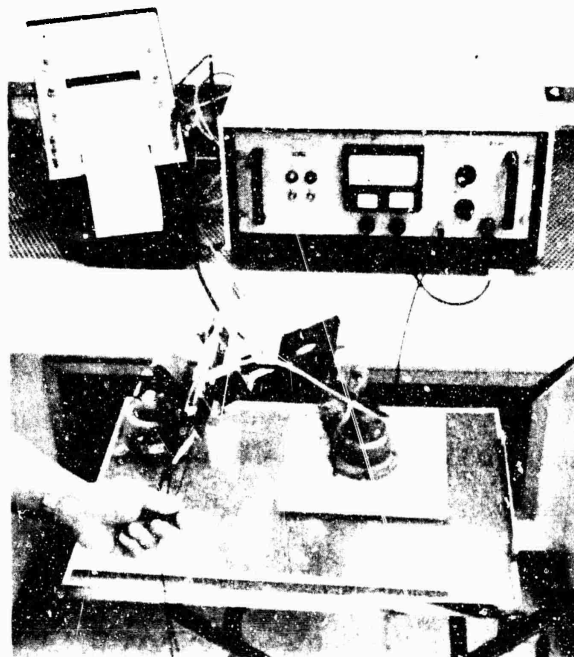


Figure 3-2b. Long Tape Electret Strength Measurement Apparatus

3.2.3 (Continued)

Fig. 3-3 is a plot of this relation between the measured surface potential and the surface charged density for eight different thickness of FEP electrets. This shows that for thicker electrets, it takes a higher surface potential to achieve a given surface charge density.

3.2.4 Results

In developing the charging (and bonding) techniques, 79 small samples were prepared and charged by the method just described. Measurements made on these were used to answer the questions concerning the effects of the treatment voltage, electret thickness, and time on the effective surface charge density.

3.2.4.1 Electret Thickness and Applied Voltage Effects

It was noticed quite early that the surface potential for the thick electret samples was in general much greater than that measured on the thin electrets for a given applied voltage. However, from Fig. 3-3 we knew that to achieve the same charge density, the surface potential would need to be much greater for the thicker electret. Fig. 3-4 shows data for 50 μm thick samples (lower trace) and 500 μm thick samples (upper trace). The average surface potentials 3 days after charging are plotted as functions of the negative applied charging voltage. (Negative voltages were always used following the initial discovery that the FEP teflon we used has a built-in negative surface potential bias.) Each point on the figure represents an average of two samples. 10 kV was the highest applied voltage that could be used with the 50 μm thick samples without causing breakdown.

There are at least two noteworthy conclusions to be drawn from these data. The increase in surface potential with applied voltage is nearly a straight line (at least for the 50 μm case). The relation is thus an exponential one and very nearly (for both voltages in kV)

$$V_s = .31 (-E_{DC})^{.31} \quad 3-3$$

In the case of the 500 μm thickness, an even smaller exponent appears appropriate. Thus, we see that the return for increases in applied DC charging voltage is meager. This helped us conclude that, since its value is not very critical, we should use an applied voltage only as large as convenient to handle (no greater than about 5 kV).

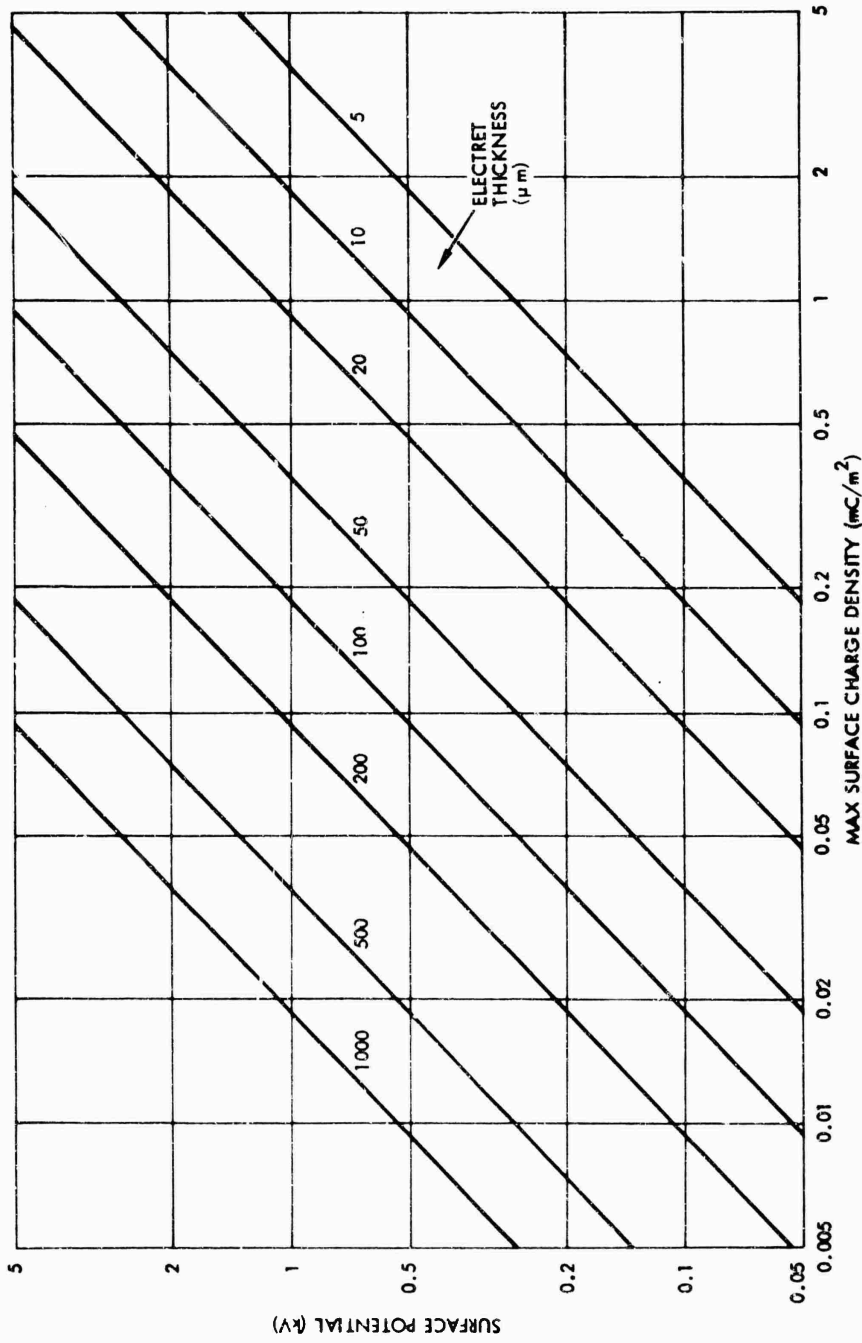


Figure 3-3. Relating Surface Potential to Charge Density for FEP Electrets

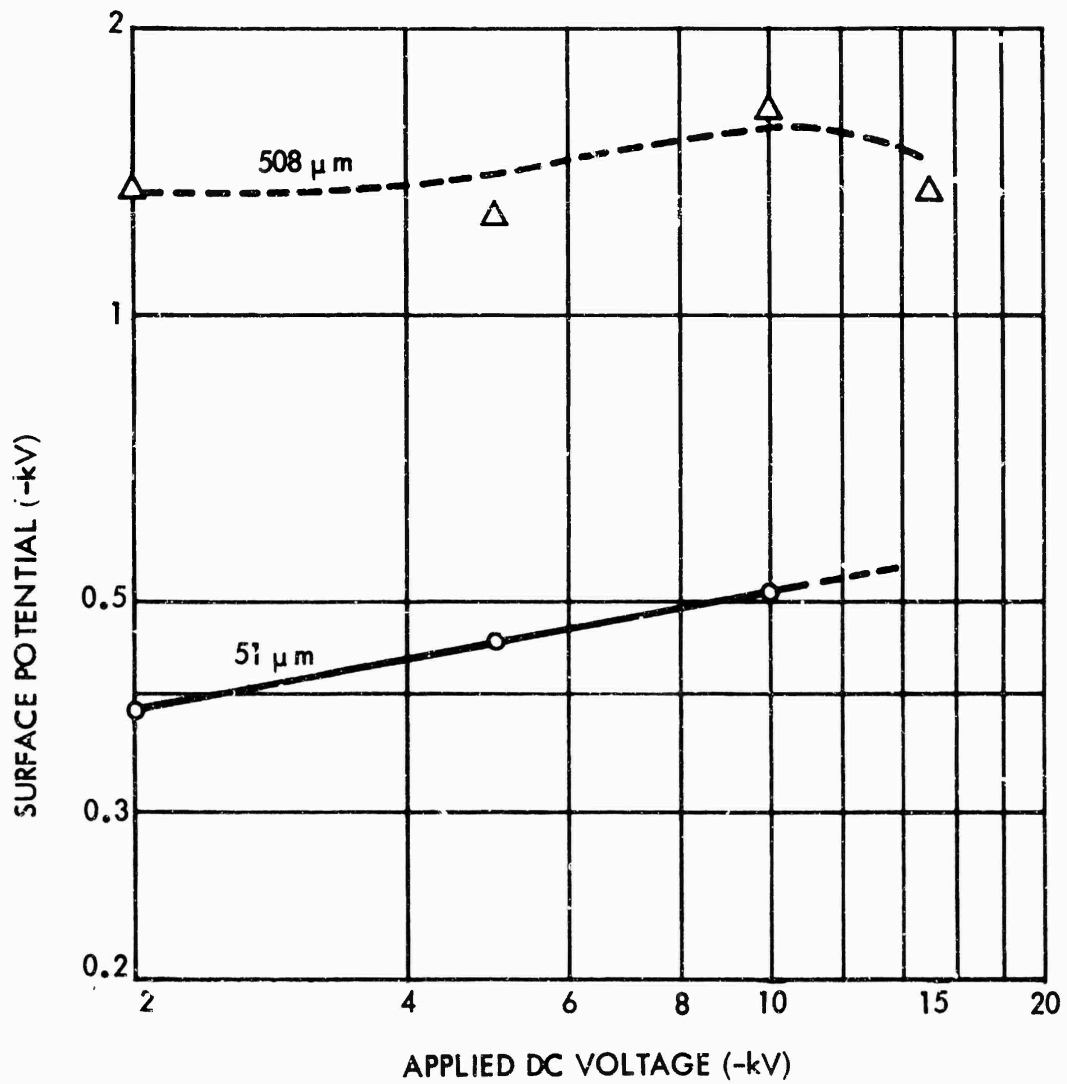


Figure 3-4. Effects of Charging Voltage and Film Thickness on Electret Strength After Three Days

3.2.4.1 (Continued)

The other interesting feature of Fig. 3-4 is the comparison between the effects due to the two thicknesses of electret. The ratios of the average surface potentials for the two thicknesses are 3.6 at 2 kV, 3.1 at 5kV and 3.2 at 10 kV. Since these average 3.3 which is pretty close to $\sqrt{10}$ (the ratio of the thickness is 10), it is tempting to conclude that the electret surface potential for the liquid contact method of charging depends on the square root of the sample thickness. While the data is too meager to warrant making that conclusion with confidence, it is a reasonable assumption to make and had an impact on the modeling task.

Ten other plots like Fig. 3-4, but corresponding to measurements made at different periods after charging (out to 118 days), were made to see if the same trends remained with time. Fig. 3-5 shows the situation at 40 days after charging. Each plotted point represents the average surface potential (using the three trace planimeter method) measured for a different sample of either 50 or 500 μm thickness. This gives an idea of the sample-to-sample spread. The trends are similar to those found on the 3rd day after charging. However, a significant decrease in the charge density for the high voltage thicker electrets is observed when compared with that for the thin samples or with the values for the thicker samples at earlier determinations. This is further shown by measurements at later times.

By 96 days after charging, there is no significant difference between the surface potential of the 50 and 500 μm samples regardless of the original applied charging voltage used. Both averaged about 300 V at that time. This represents a 14 dB drop for the thicker film compared with its 3-day potential but only about 3 dB drop for the thinner film. Thus, we conclude that the thin film achieves a more stable charge and eventually maintains a surface charge density advantage (Fig. 3-3) of about 10 to 1 compared with the thicker film. This compares with its initial advantage of about 3 to 1. The reasons for this phenomenon are not at all clear.

3.2.4.2 Annealing and Longevity

In some cases after charging a sample, we would anneal it by exposing it to high temperatures for a short period. The effect of annealing is apparently to speed up the normal charge decay past the initially rapid-loss period. Fig. 3-6 shows the effects of initial charging, annealing and subsequent normal decay on the average

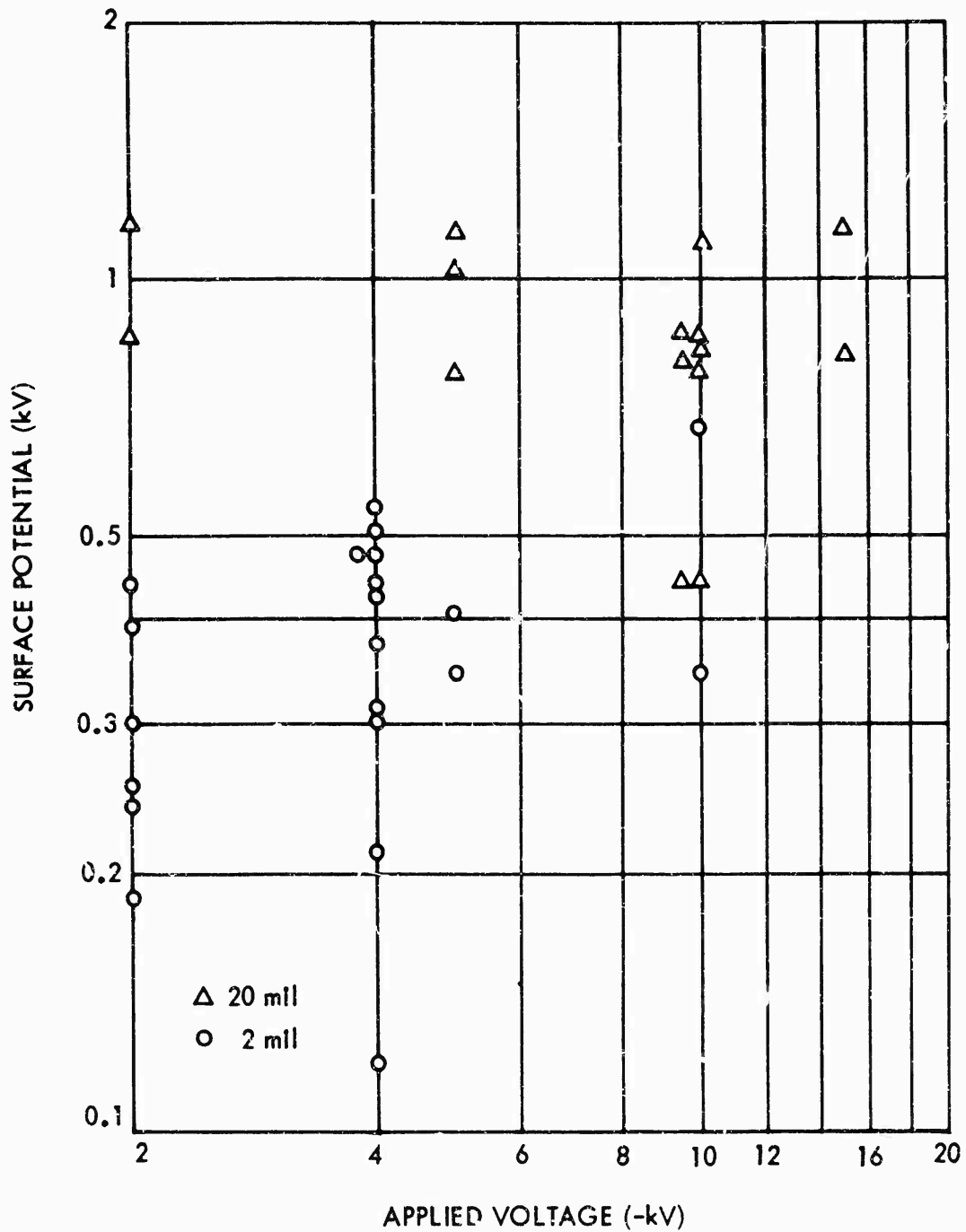


Figure 3-5. Effect of Charging Voltage and Sample Thickness on Surface Potential After 40 Days

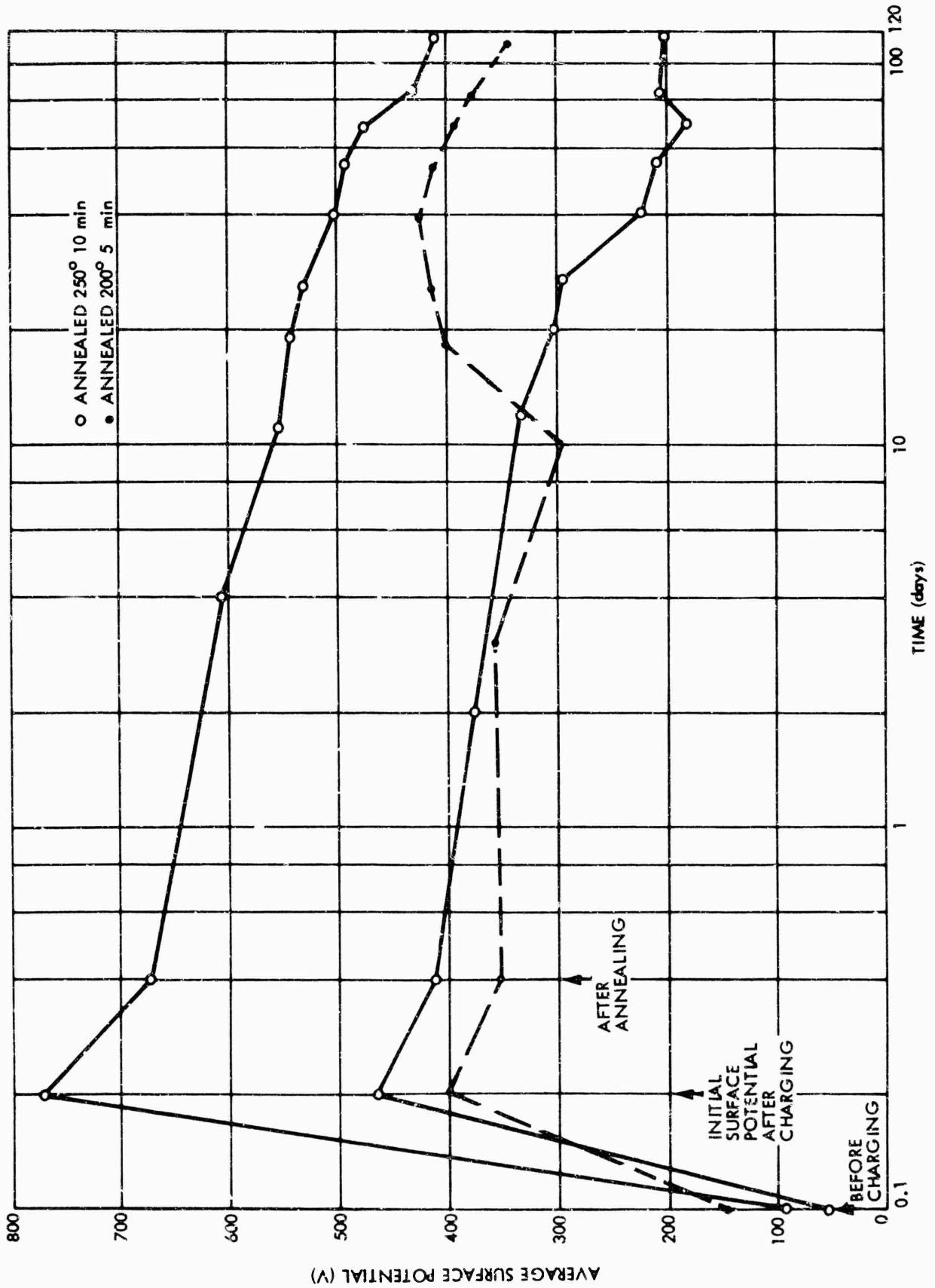


Figure 3-6. Electret Strength History for Three Samples

3.2.4.2 (Continued)

measured surface potential for nine 50 μm thick samples. The dotted curve is for three samples annealed at 200°C for 5 minutes. The other two curves are each for three samples annealed at 250°C for 10 minutes. The annealing quickly reduces the surface potential by 10 to 15%. Why the three samples of upper curve should be so much better charged is not known nor is the reason for the apparent discontinuity in the dotted curve at 10 days. However, Fig. 3-7, showing the average surface potential of all 9 samples in dB relative to their average surface potentials after annealing as a function of linear time, gives an idea of the average decay rate. The curve in this figure is a decay rate corresponding to 1 dB/doubling of time after 10 days following charging. Discounting measurements within the first 10 days, this rate appears to fit the data reasonably well at least for the first four months (the period of our measurements).

3.2.4.3 Charging Summary

Fortunately for the rest of this study, the results of this short excursion into the subject of charging electret films were mostly positive. We found that:

1. A liquid contact charging technique produces good quality electrets when applied to FEP films of 50 to 500 μm thicknesses.
2. The value of the applied DC charging voltage is not very critical if above 2 kV, the resulting surface potential being proportional to no more than the cube root of the charging voltage (even less for the thicker films).
3. The initial surface potential achieved with this method appears to vary with the square root of the film thickness. However, after about 100 days the surface potential is substantially independent of the film thickness--being about -300 V then.
4. The average decay rate for the thin (50 μm) electret films is on the order of 1 dB/time doubling after the first 10 days following charging.

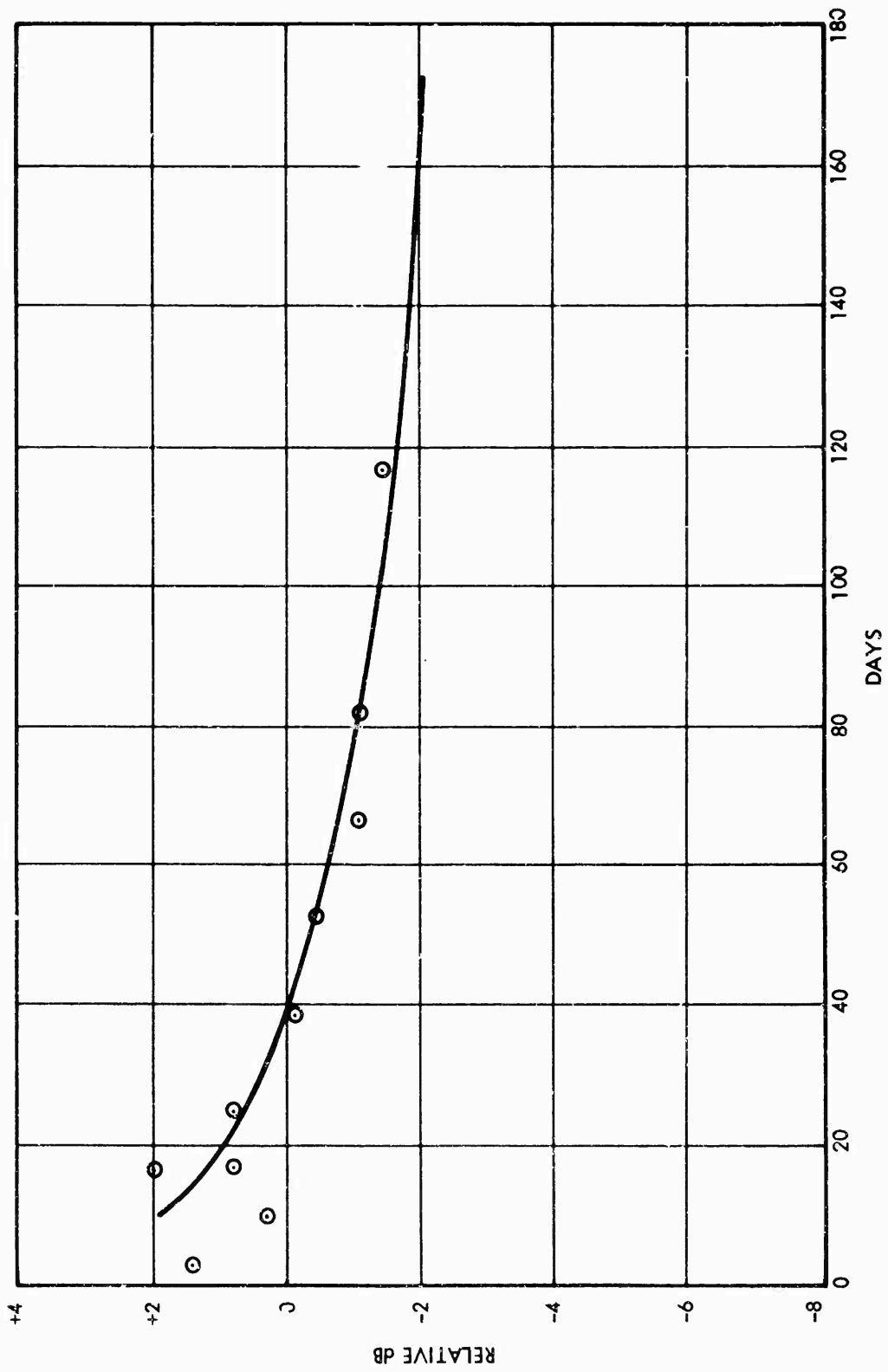


Figure 3-7. Average Electret Decay

3.3 Design Aids

While the results of the computer modeling (Sec. 2) provided general guidelines for design, there are a number of other guidelines and aids that should be mentioned.

3.3.1 Transduction Coefficient

Even before the computer model was implemented, a number of calculations were made to attempt to clarify the relations among some of the many transducer parameters. Since it was believed that the transduction coefficient, T , (a measure of the coupling between the electrical and mechanical systems) would be a key parameter, its dependence on σ_e , a , and d was examined. Fig 3-8 shows the result--the transduction coefficient per unit electret surface charge density plotted as a function of the ratio of thicknesses of the air gap and electret. The roll-off characteristic for $a \geq 0.2d$ indicates the desirability of keeping $d \geq 5a$ to get the best coupling for a given electret strength.

3.3.2 Tape Width Effects

A quick perusal of the summary table, Table 2-1, serves to indicate that the tape width does not have a major effect on any of the important performance characteristics shown. Does this mean that the width can be chosen arbitrarily? Certainly not. The width must be considered in the light of several practical transducer considerations.

For one thing we have assumed in the analysis that the transducer performance is independent of the point of disturbance. If, however, the moving conductor layer is made very light by reducing its thickness, might not the resistance become sufficiently high as to produce significant driving voltage drop from one end of the tape to the other? To answer this question, Fig. 3-9 was plotted. Here is shown the electrical resistance per unit length of an aluminum strip versus its thickness for various values of strip widths. This indicates that a 100 m length of a 1" wide strip 1 μm thick and of aluminum will only have slightly more than 11 Ω of resistance. Note that for copper the ordinate should be multiplied by ~ 0.6 .

The other major effects of width have to do with the directional characteristics of the radiated ultrasonic pressure field. Since these are best understood in terms of the dimensionless product kw (also called dimensionless width or acoustic size parameter) a useful set of curves, Fig. 3-10, shows just how various widths relate frequency to kw . For example a 20 mm wide tape operating at 30 kHz is found to have

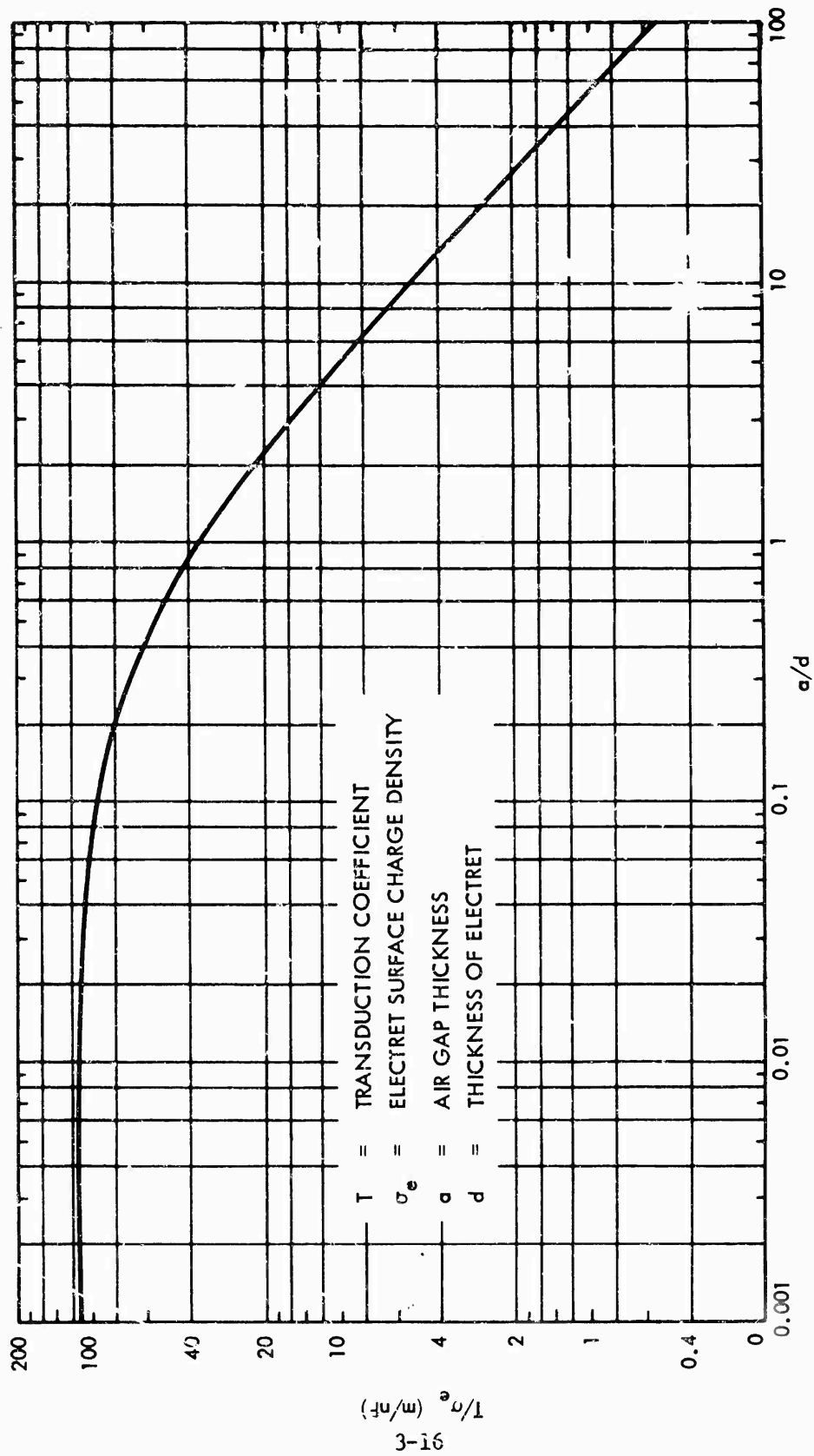


Figure 3-8. Effects of Layer Thicknesses on Transduction Constant

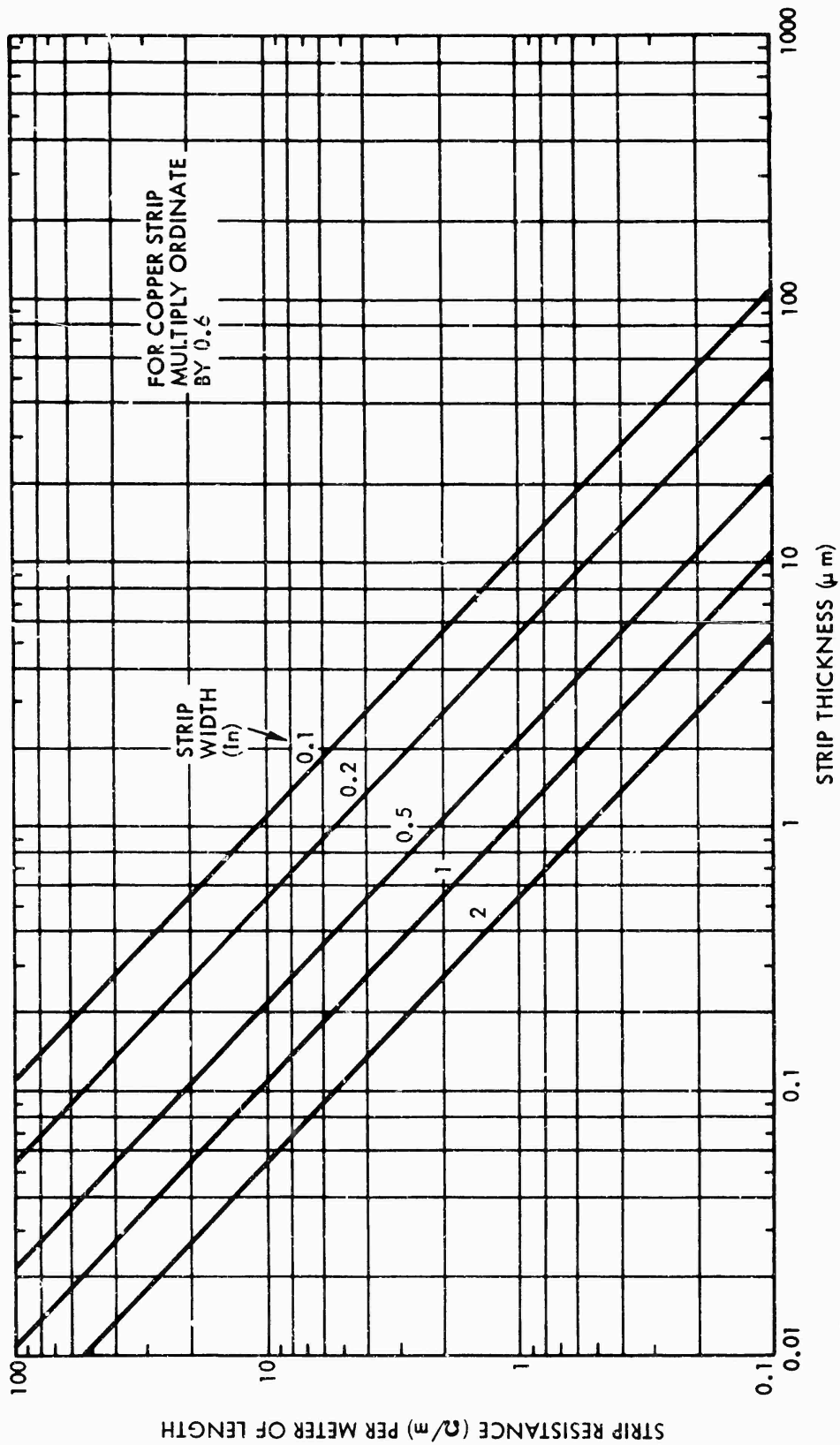


Figure 3-9. Resistance per unit Length of Thin Aluminum Strip

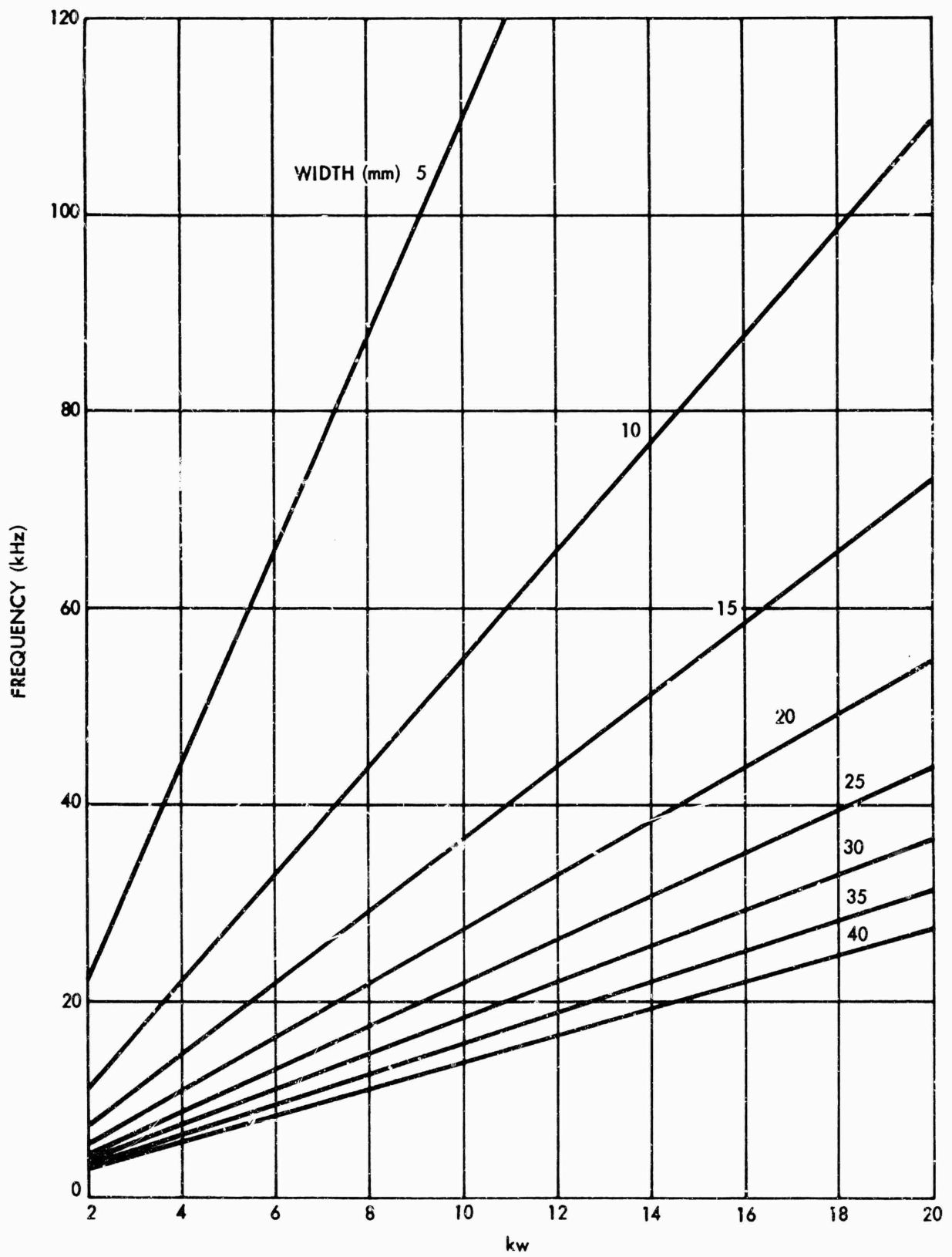


Figure 3-10. Frequency vs kw for Various Tape Widths
3-18

3.3.2 (Continued)

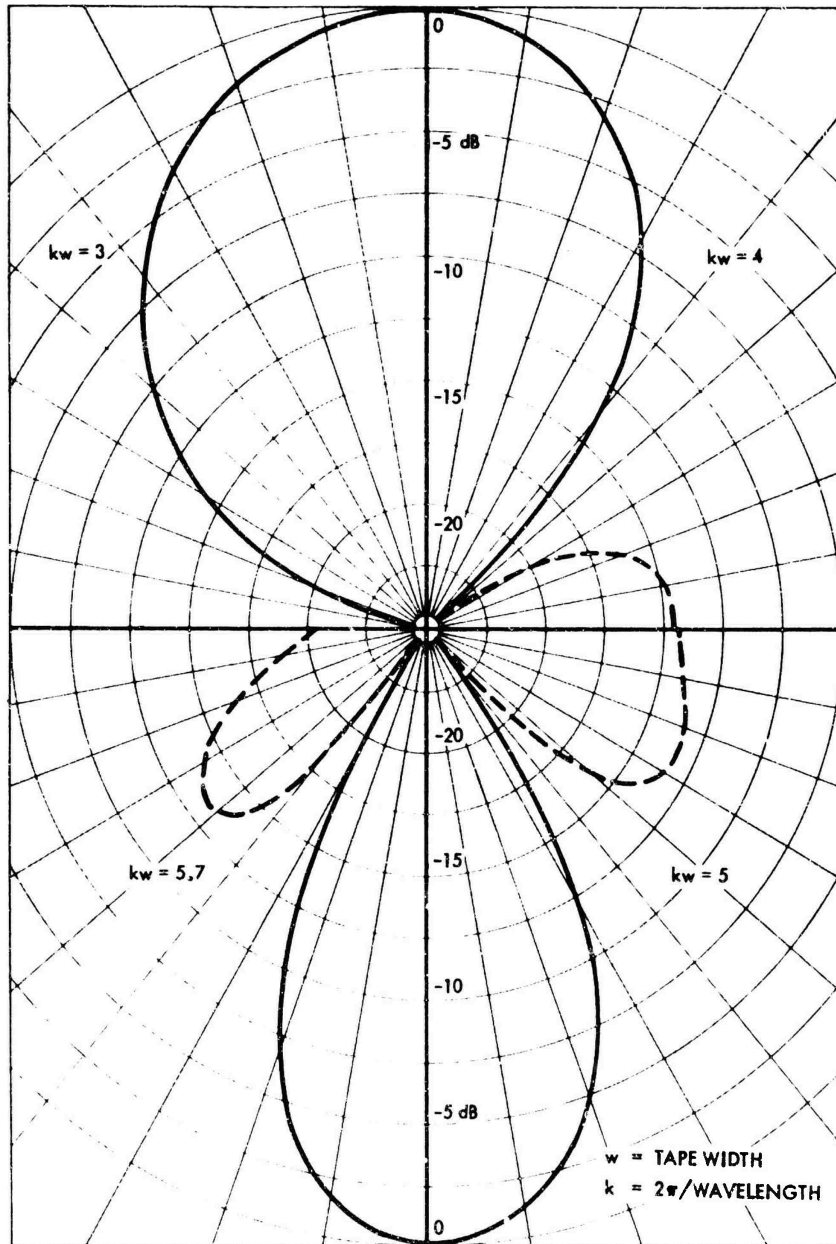
a kw of 11. The significance of knowing kw is shown in Figs. 3-11 to 3-14. Here, in the first two figures, are plotted 8 different far-field directivity patterns for kw = 3, 4, 5, 5.7, 6.5, 8, 9 and 10 (in clockwise order on each figure starting from the upper left). Each quarter of the figure represents a 90° portion of the directivity pattern. This is sufficient because of symmetry and the baffling assumption. Note that adjacent lobes are out of phase (minus signs). Fig. 3-13 shows the half power beam-width of the major lobe and the angles at which the first several minor lobes occur as continuous functions of kw. Fig. 3-14 shows the single figure measure of the concentration of the radiation, the directivity index (DI), as a function of kw. All of these directivity related plots are useful design aids in assessing the degree of spread in the ultrasonic energy radiated from the tape. Probably we would want to maintain at least as much directivity as that corresponding to kw = 3 (a 56 degree major beam width and a DI of about 4.8 dB).

3.3.3 Frequency

The modeling results indicate that it may be desirable to work in the frequency range at the lower end of the ultrasonic range. Thus, it is desirable to be able to place the mechanical resonance frequency by design. Fig. 3-15 was developed to provide just such a design aid. Here the frequency of mechanical resonance (for small vibrations) is plotted versus the thickness of the air gap for various values of moving mass/unit area. Thus, knowing the moving mass of the available materials (0.95 kg/m^2 is typical) allows the designer to specify the air gap thickness that will result in the desired resonance frequency.

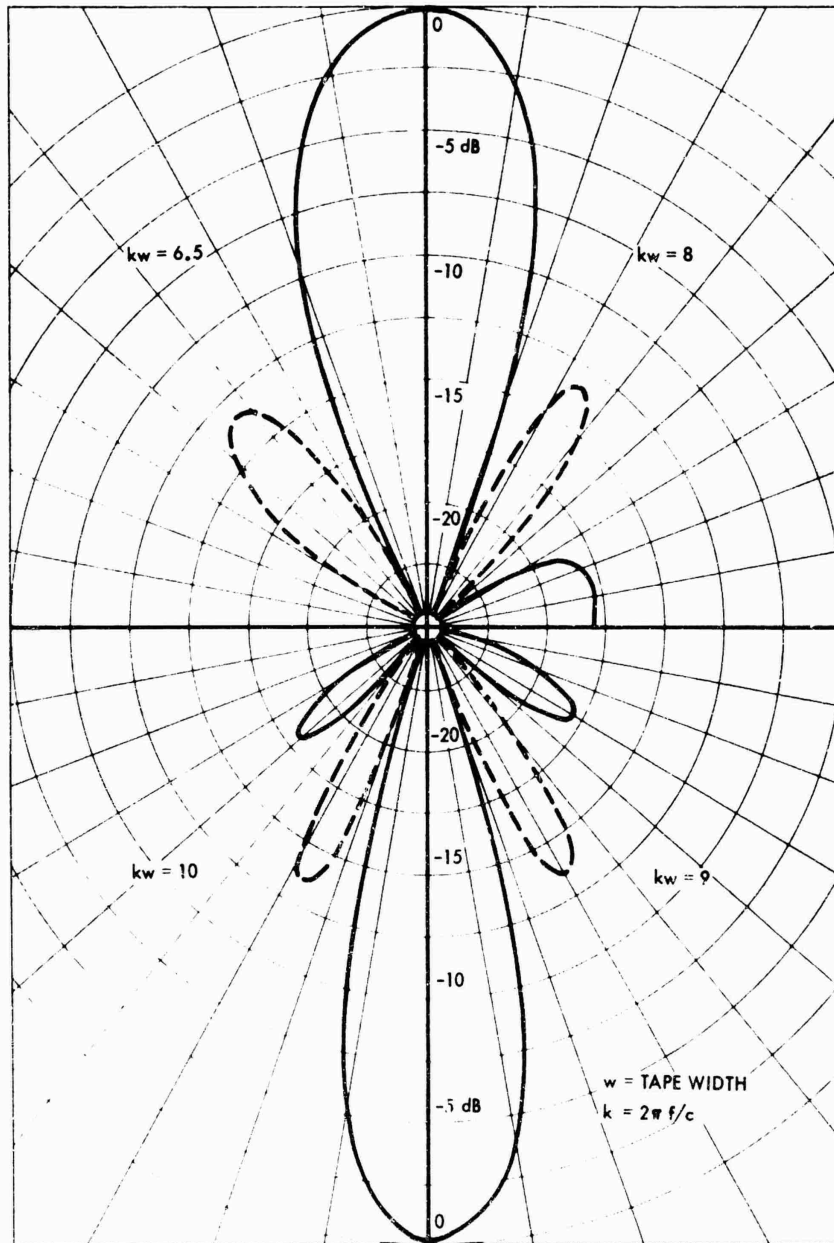
3.4 Transducer Construction

After obtaining promising results from the computer model, developing a method for making adequate electrets and designing a sample transducer based on the model, the design aids of the last section and the constraints of material availability, we were in need of procedures for fabricating the samples. While outwardly appearing to be a simple task, the development of these required techniques turned out to be time consuming and often frustrating. Not only did bonding well and uniformly to the FEP electret layer cause problems (as expected), but even bonding copper to copper-coated FEP turned out to be a challenge at one point.



EDL-F900

Figure 3-11. Tape Radiation Directivity Patterns



EDL-F900

Figure 3-12. Tape Radiation Directivity Patterns

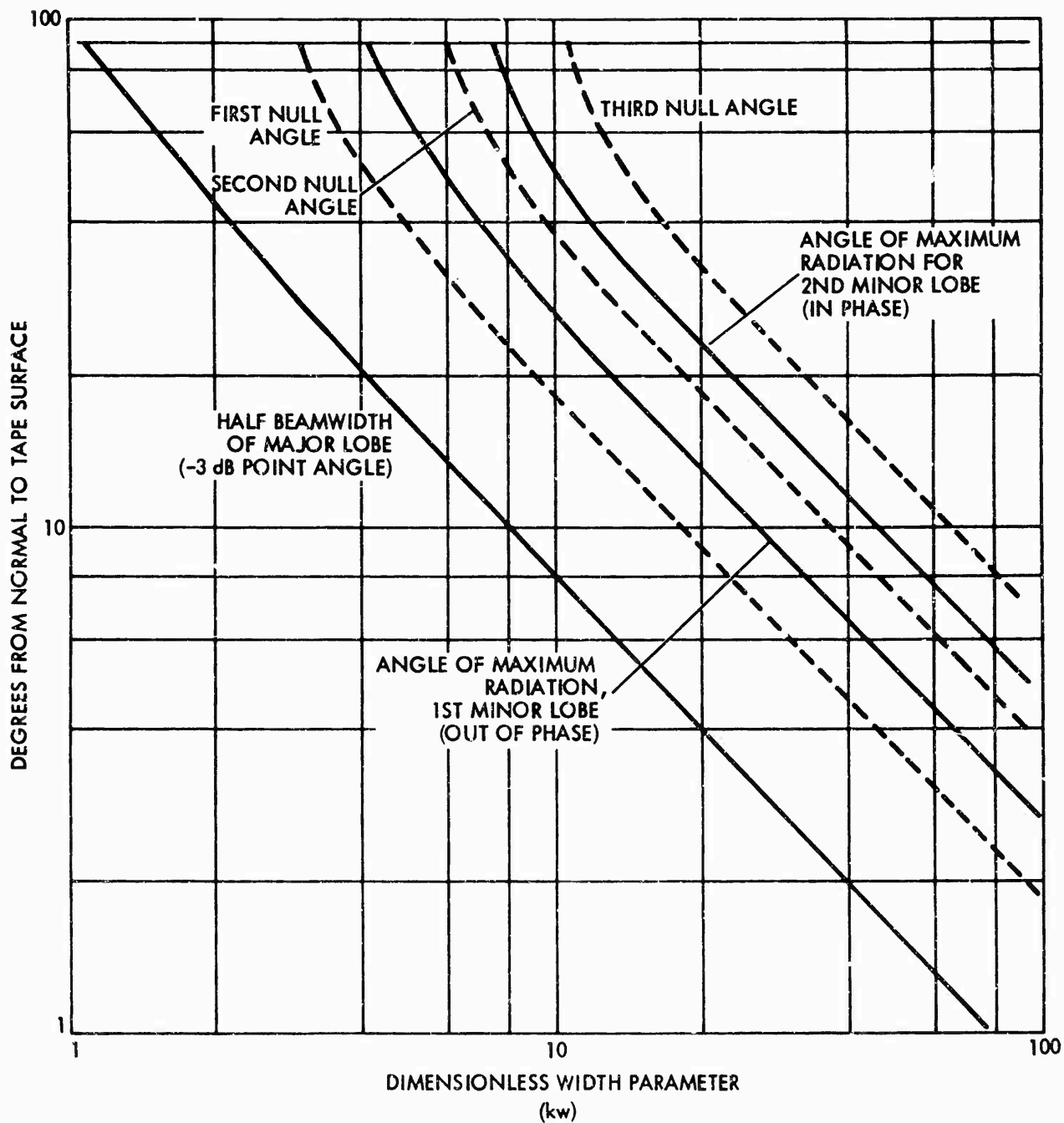


Figure 3-13. Directional Radiation Characteristics of Long Tape Radiator

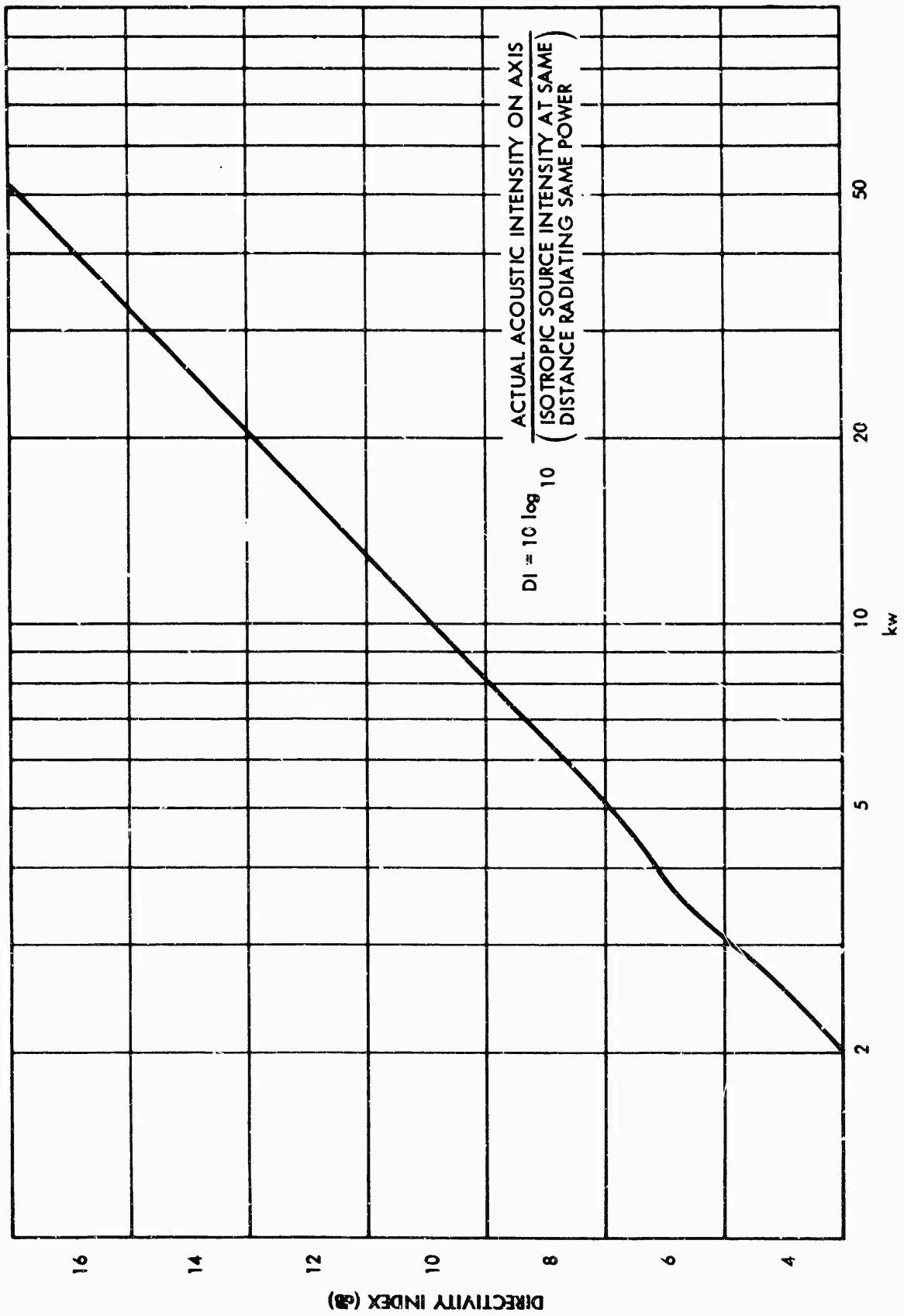


Figure 3-14. Directivity Index vs Acoustical Width Parameter

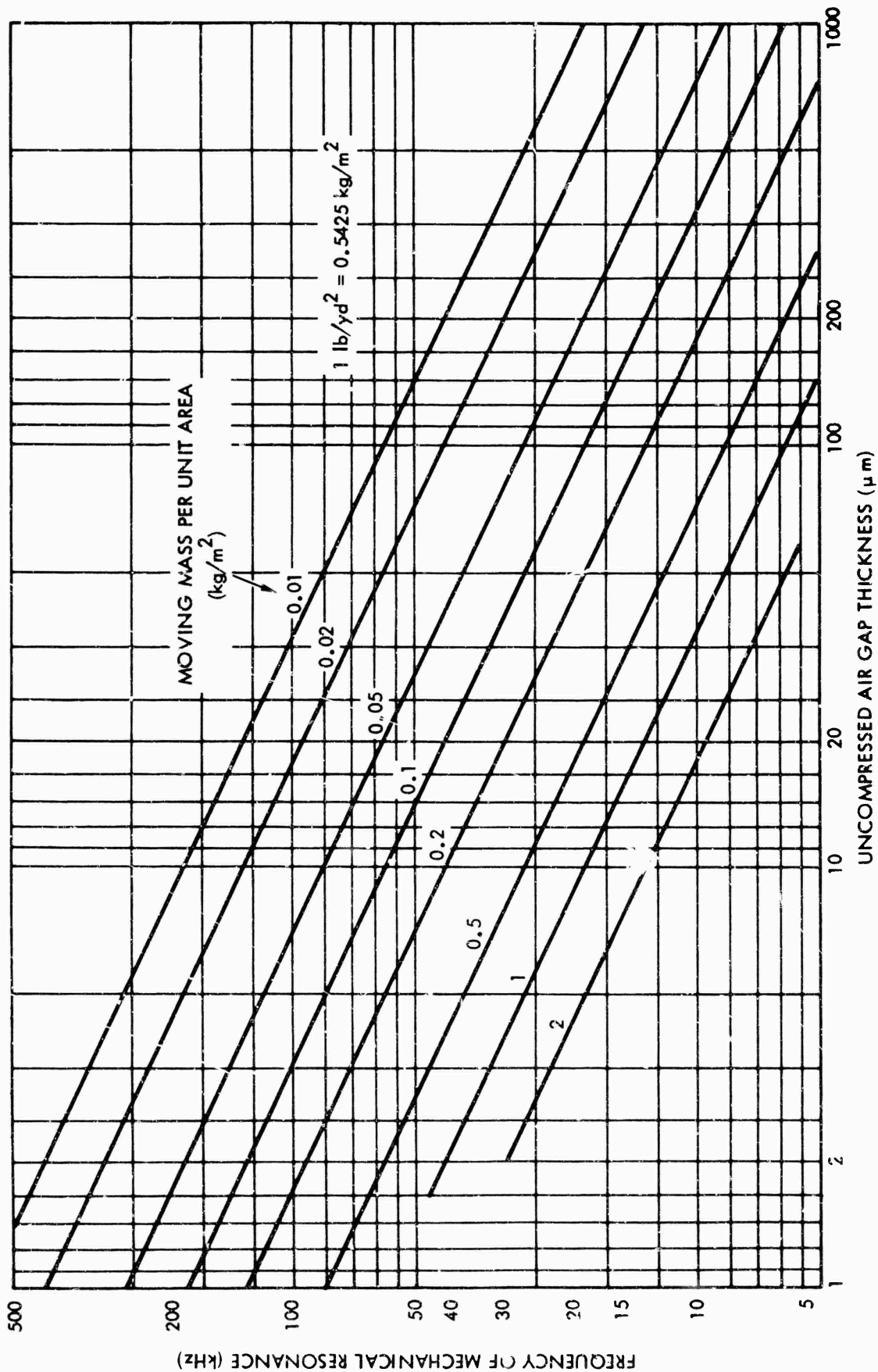


Figure 3-15. Effects of Air Gap and Moving Mass on Mechanical Resonance

3.4.1 General Procedure and Discussion

The basic transducer configuration is shown in Fig. 3-16. Notice that for this simplest shielded and insulated case, there are seven material layers. Some adjacent layers may be purchased already bonded or fused together, e. g., the Mylar coated aluminum expected to be used for the moving (outer two) layers. For the early models, no commercially available FEP-copper laminate was available, so this critical bond had to be perfected in the lab (along with several other less critical and simpler bonds). For ease of handling in the early models, we used copper-clad epoxy board material for at least two of the layers beneath the electret layer. Although it was generally thicker and stiffer than needed, it provided a convenient and stable platform for developing fabrication skills.

In developing bonding techniques we tried using 3M Scotchweld 2216, 3M 1838 structural adhesive, 3M Scotchcoat 8, Eastman 910, Hysol epoxi-patch and solder as bonding agents; and freon, tetra-etch, punice rubbing, printed circuit board etchant, trichloroethylene, acetone, and hydrochloric acid solution as surface preparers. In addition we tried applying various combinations of heat and pressure to improve the resulting bonds. In every case we eventually found a combination of bonding agent and treatment that produced satisfactory bonds.

Referring to the figure, the general steps of construction are as follows:

1. The FEP teflon film to be used (layer 3) is cut to size, etched on one side with Tetra-etch, and bonded on that side to a solid copper layer (#4).
2. If the bond is satisfactory (free of air bubbles and tight), the teflon is charged using the liquid contact method.
3. If the charge is considered adequate in magnitude and uniformity, the free copper surface is bonded to the epoxy side of a copper-clad epoxy board (layers 5 and 6) of the appropriate size.
4. After this bond dries and is found adequate, the aluminum coated Mylar laminate (layers 1 and 2) is bonded to the free surface of the electret only around the periphery. Air is expelled from the interface as desired by rolling the surface repeatedly. However, one of the as yet unsolved construction problems is to find a way to leave the remaining air of uniform thickness.
5. The final step of bonding an insulating layer (#7) to the copper side of the copper-clad epoxy board is the least critical and probably could be eliminated in many cases. It provides electrical isolation.

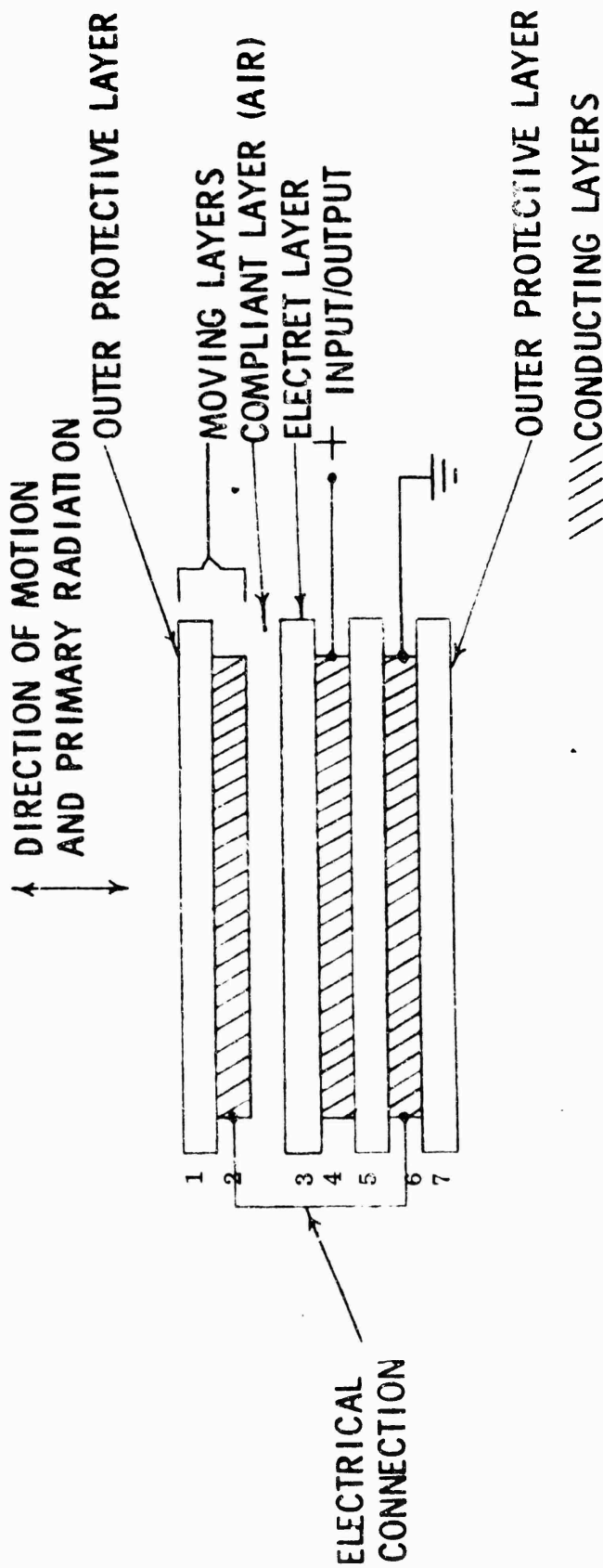


Figure 3-16. Electret Tape Cross Section

3.4.1 (Continued)

As mentioned previously, the most critical bond is considered to be that between the electret (layer 3) and the inner conductor (layer 4). The reason for this stems from the fact that the electrostatic forces produced in the active mode occur between layers 2 and 3 across the air gap. These forces push downward on the electret (and its supporting layers) just as hard as they push up on the moving conductor (layer 2). Since we wish to maximize the radiation and hence the motion of the outer layers, we need to design the mechanical impedance for the outer layers to be much smaller than that for the electret and its support layers. This is done by making the electret stiff and massive relative to the stiffness and inertia of the moving layers. One way to do this is to work at the frequency of mechanical resonance. Another way to do this for a wide range of frequencies is to make the thickness of the electret layer much greater than that of the moving layer. This aim is made less constraining on the electret if it is rigidly bonded to the inner conducting layer #4. Since copper is at least four times as dense as teflon, it does not take a very thick layer of copper to provide a substantial inertia relative to that of the moving layer.

However, if any tiny air pockets remain at the interface, all bets are off. This allows the electret layer to move with relative ease and will absorb some of the energy that would otherwise have been usefully radiated by the outer layers. This is especially true for thin electret layers but should be kept in mind in all cases. It was mainly to avoid this potential problem that we fabricated the later transducer models using an electret layer that was purchased fuse-bonded to a copper layer. Unfortunately, this copper layer was only available (without special order, expenses and delays) in relatively thin coatings. For this reason it was felt necessary to bond it to an additional thicker copper layer. Previous experience had indicated that a copper-to-copper bond is relatively simple, so we were quite unprepared for the difficulties we had in bonding the copper-coated teflon to a thicker copper layer. Many bonding treatments worked fine for the solid copper but would not stick to the copper side of the teflon-copper laminate--much to the manufacturer's surprise. A method based on using a torch and solder turned out to be the best solution. In the future we will wait for the special order.

3.4.2 Early Design

Our experimental philosophy with respect to construction of samples was to first make devices that were easy to make, handle and evaluate even though not necessarily optimal in anticipated performance. Then as we felt we understood our

3.4.2 (Continued)

measurements, we would make more realistic samples. The first four samples, designated D1 through D4, were thus all small and incorporated a thick, rigid base of phenolic. All of these early samples used 508 μm thick FEP electret layers, and all used the same aluminized Mylar ($\sim .044 \text{ kg/m}^2$) for the moving layers. In D1 the total length and width are 40 mm and 14 mm while in the rest the length and width are 51 and 25 mm, respectively.

Fig. 3-17 shows photographs of samples D2-D4 and also of the material layers used to fabricate them. The FEP layer, even though 508 μm thick, is clear and barely discernible in these photos. Fig. 3-17a shows the layers from top to bottom. Beneath both the aluminized Mylar and the electret is a 508 μm thick copper layer which is in turn bonded to the epoxy side of a copper-clad epoxy board (a total of 750 μm thick). The total thickness of all these layers is a bit over 2 mm when the adhesive and air gap layers are included. This is then mounted on the 1 cm thick phenolic board for convenience in handling. As shown in Fig. 3-17b copper foil tabs are inserted during the construction to allow convenient electrical access to the inner and outer conducting layers.

3.4.3 Later Design

After successfully measuring the performance characteristics of these early samples, it was decided to attempt to construct some longer, more flexible samples. For this purpose we constructed the new charging apparatus and another apparatus for measuring electret strength of the longer samples, already shown. Fig. 3-18 shows the layers in order from top to bottom for this configuration. These samples used the same moving layers of aluminized Mylar ($.045 \text{ kg/m}^2$) as before; but in an attempt to make the air layer more uniform, they were rolled repeatedly while the adhesive (3M Scotchcoat 8) was setting up on the edges. The electret layer was 127 μm thick FEP fuse-bonded to "3 oz. copper" that is in turn soldered to a solid copper layer 580 μm thick. This bond is achieved by heating up the solid copper layer with a torch, tinning its surface with solder, laying on the FEP copper laminate and then applying uniform pressure over the entire area. This squeezes out any excess solder and produces a thin but rigid copper-to-copper bond (when nothing else was able to). A 508 μm thick layer of FEP (not charged--just an insulating layer) was bonded (Eastman 910) to the solid copper on one side and to a 76 μm thick layer copper (adhesive tape) on the other. The total thickness of this arrangement is only about 1.5 mm. Samples using this basic design were constructed at lengths of 13 cm, 36 cm and 51 cm in that order.



Figure 3-17a. Material Layers for Early Samples

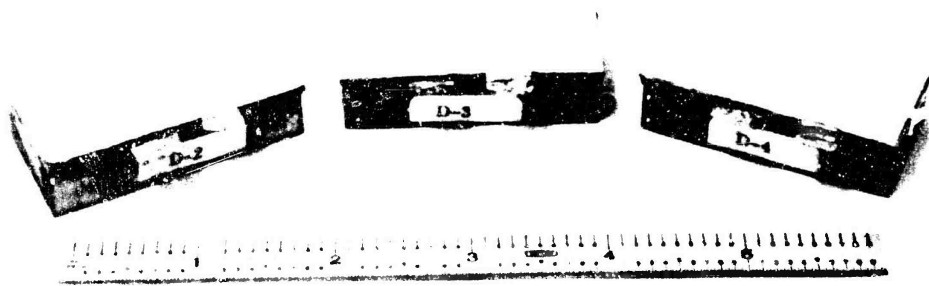


Figure 3-17b. Transducer Samples D2, D3 and D4



Figure 3-18. Material Layers for Longer Samples

3.5 Measuring Performance

After going through the design, charging and construction tasks described so far, we were most eager to evaluate the capabilities of the transducer samples as measured in the laboratory. The basic measurements were electrical capacitance, receiving acoustic sensitivity and radiation efficiency and directivity.

3.5.1 Capacitance

Although it is very easy to specify a 100 μm air gap thickness, it is not so easy to fabricate it with reliability. In fact, this quantity is also difficult to ascertain after fabrication is complete. Direct methods based on thickness measurements with a micrometer are inaccurate due to the extreme compressibility of the air layer and also due to the expected variability from point to point (the average thickness is desired). The capacitance method is based on the formula:

$$a = \epsilon_a \left(\frac{w\ell}{C_T} - \frac{d}{\epsilon_e} \right) \quad 3-4$$

where C_T is the total measured capacitance of the sample for which

$w\ell$ is the area and

d is the thickness of the dielectric with permittivity ϵ_e .

There are problems with this method too. For small samples it is difficult to make accurate capacitance measurements (in the ~ 10 pF range); yet, since we are differencing quantities that may be in the same ball park to form the air gap thickness, accuracy is required. In addition, the effects of the portion (especially significant in the early samples) of the moving layer bonded to the electrode are difficult to accurately account for.

Although the measured data indicate a wider spread, we believe our air gaps have a 20 to 200 μm average thickness with the smaller figure applying to the later samples. 100 μm was the design specification.

3.5.2 Sensitivity

3.5.2.1 Instrumentation

Early acoustic measurements (sensitivity, radiation efficiency, directivity) were hampered by lack of an anechoic facility. We first used the outdoor environment

3.5.2.1 (Continued)

and then a Sylvania microwave anechoic chamber for making acoustic measurements. Although these proved to be much better than laboratory bench measurements (except when the wind was high outdoors), they were also of limited quality. After our acoustic anechoic chamber arrived and was set up, the quality (and quantity) of data picked up noticeably. This chamber is made by Eckels Corporation. It is shock mounted, has a 250 Hz lower frequency limit (for 99% absorption), and a three-foot cube of free-field working space.

At first, a Bagno magnetostrictive ultrasonic source radiating at 19.2 kHz was used for the sensitivity measurements. This was soon replaced with a JBL 075-105 dynamic super tweeter that is easily controlled in frequency, amplitude and even waveform. Also available for measuring the acoustic pressure fields were two B & K condenser microphones, (the 4133 1/2" and the 4135 1/4"), their associated preamp (2615) and power supply (2801).

The instrumentation for measuring sensitivity is very straight forward. A source is allowed to illuminate the test sample (mounted in its baffle) in the anechoic chamber, and its output level following a known amount of amplification is recorded. Then the process is repeated with the only change being that the test sample is replaced by a lab standard microphone of known sensitivity. By comparing output levels, the sensitivity of the test sample may be directly compared to that of the calibrated microphone.

The specific instrumentation for measuring sensitivity is shown in Fig. 3-19. The drive for the JBL tweeter is supplied by a Crown DC-300 amplifier being fed by a variable frequency signal generator. The test sample is interfaced to the Aquadyne, Inc., AQ-125 preamp which has 25 dB of voltage gain and an input impedance exceeding 500 M Ω . The amplified signal is then band-passed (Krohnkite 3550) to eliminate noise away from the driving frequency and recorded (rms VTVM and scope) along with the gains used. The standard microphone preamp was followed by a 20/40 dB HP voltage amplifier and then the same band pass filter, meter and scope.

3.5.2.2 Results

The early sensitivity measurements for sample D1 varied from -73 to -83 dB re 1 V/Pa for four different determinations at 19.2 kHz with an average of about -75 dB. For comparison the computer model was used to simulate D1 with the result shown in Fig. 3-20. The sensitivity at 19.2 kHz is seen to be about -52.7 dB re 1 V/Pa for the

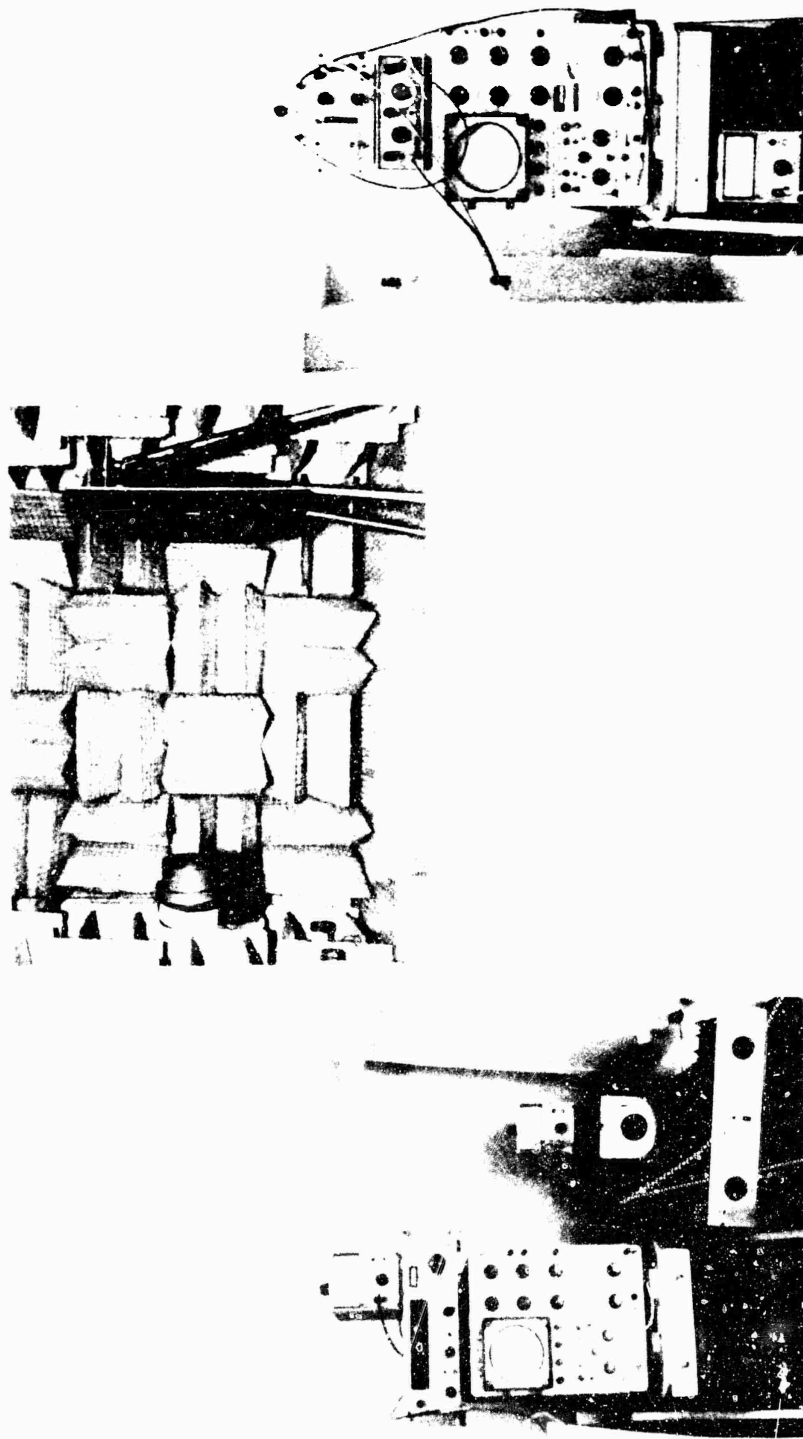


Figure 3-19. Instrumentation for Sensitivity Determinations in Anechoic Chamber

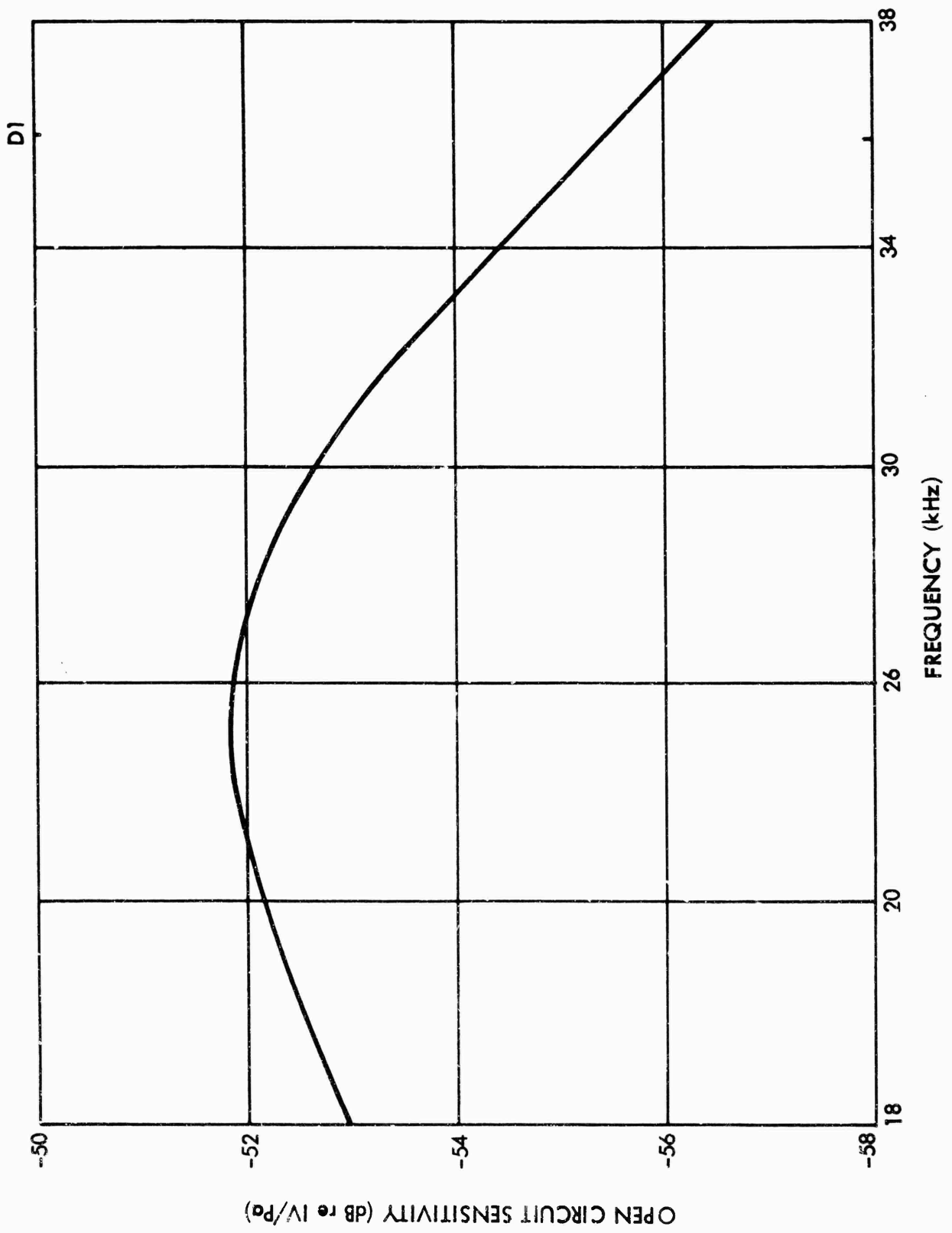


Figure 3-20. Open Circuit Sensitivity vs Frequency

3.5.2.2 (Continued)

damping constant used in the model, 5 kPa-s/m, and without taking into account the capacitance divider effect of the shielding layers required in the fabrication (but not in the model). The latter amounts to 5.6 dB for D1. When this correction is made (-58.3 dB) the model result is still at least 14 dB below the best measured values. To see if this discrepancy could be caused by a poor choice of the damping constant in the model, we generated the data plotted in Fig. 3-21. This shows the effects of the damping constant on open circuit sensitivity. It indicates that increasing the damping constant from 5 to nearly 30 kPa-s/m could indeed account for an additional 15 dB decrease in open circuit sensitivity for D1. From this it appears likely that the internal damping of our sample is on the order of 30 kPa-s/m--much greater than the values assumed for most of the modeling work. (The maximum radiation efficiency for conjugate impedance matching using $D = 30$ kPa-s/m is about 0.7%. This should still be acceptable).

Sensitivity measurements (4) on samples D2-D4 varied from -67 to -88 dB for D4. This last sample is only 10.5 dB below the predicted value using the low damping constant (5 kPa-s/m). To decrease sensitivity by this much would take a damping constant of a little less than 20 kPa-s/m (see Fig. 3-21).

Since it seemed to be the best, sample D4 was used for additional sensitivity (and radiation) measurements in the anechoic chamber using the JBL source. Sensitivity calculations were made at 11 kHz and 25 kHz with -68 and -71.1 dB re 1 V/Pa results respectively (averaging the results using the two B & K microphones). Fig. 3-22 shows the amplitude vs frequency response of the JBL source as measured by the two B & K microphones and sample D4 between 10 and 40 kHz. The main features track well, but there is an obvious tendency for fill-in at low levels for D4. This is believed due to the fact that the JBL produces an appreciable electrostatic field as well as radiating ultrasonically. At the 1/2 m spacing used and for the high input impedance preamp used, the small tape sample can act as an electrostatic signal receiver as well. This problem is hard to eradicate since it is at the frequency of interest. Better shielding around the edges of the sample is required. In view of this interpretation of Fig. 3-22, we believe that the acoustic frequency response of the tape sample is quite flat--at least up to about 30 kHz. This would agree with the expected model results for $D = 20$ to 30 kPa-s/m.

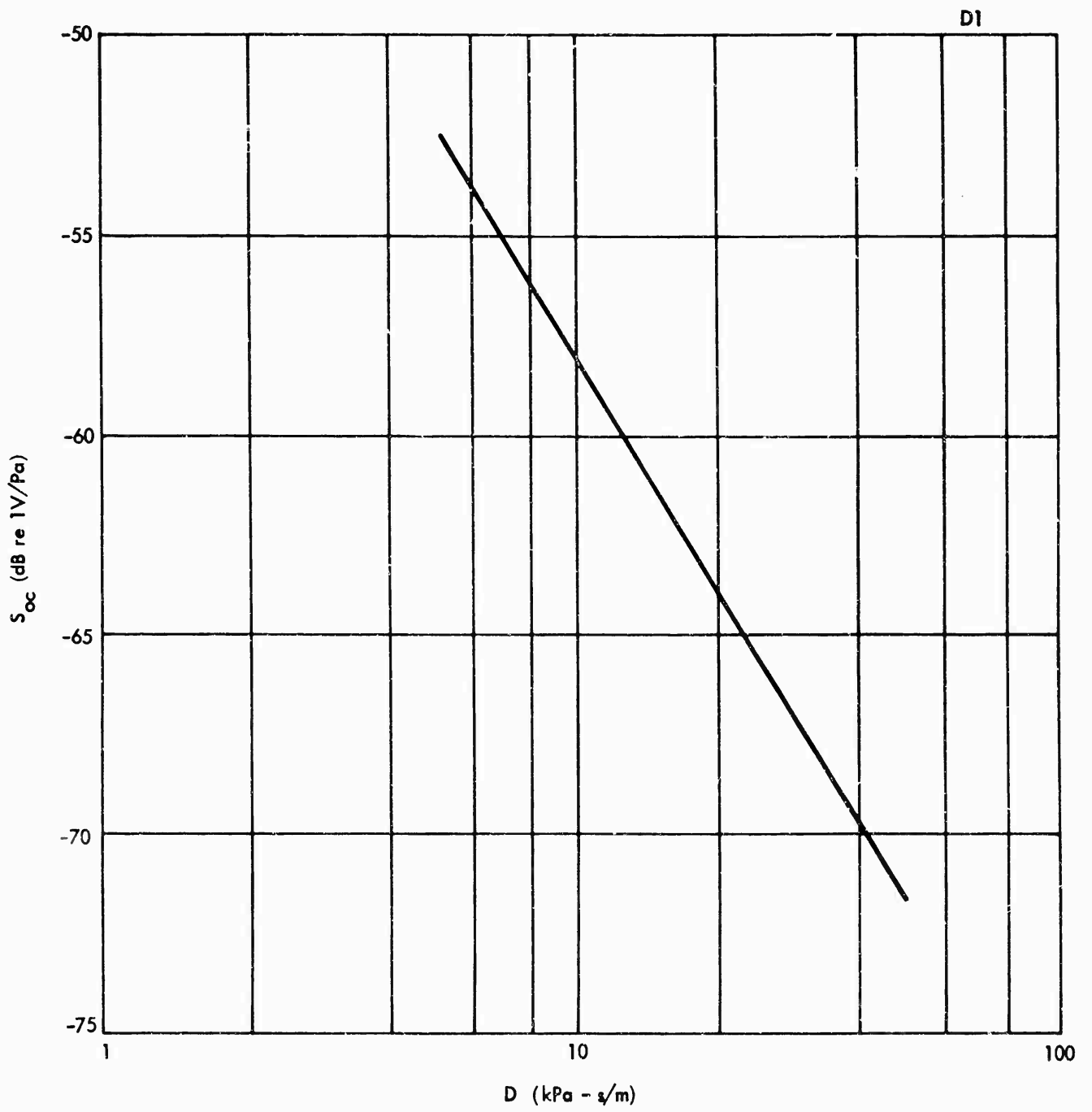


Figure 3-21. Open Circuit Sensitivity vs. Damping
3-36

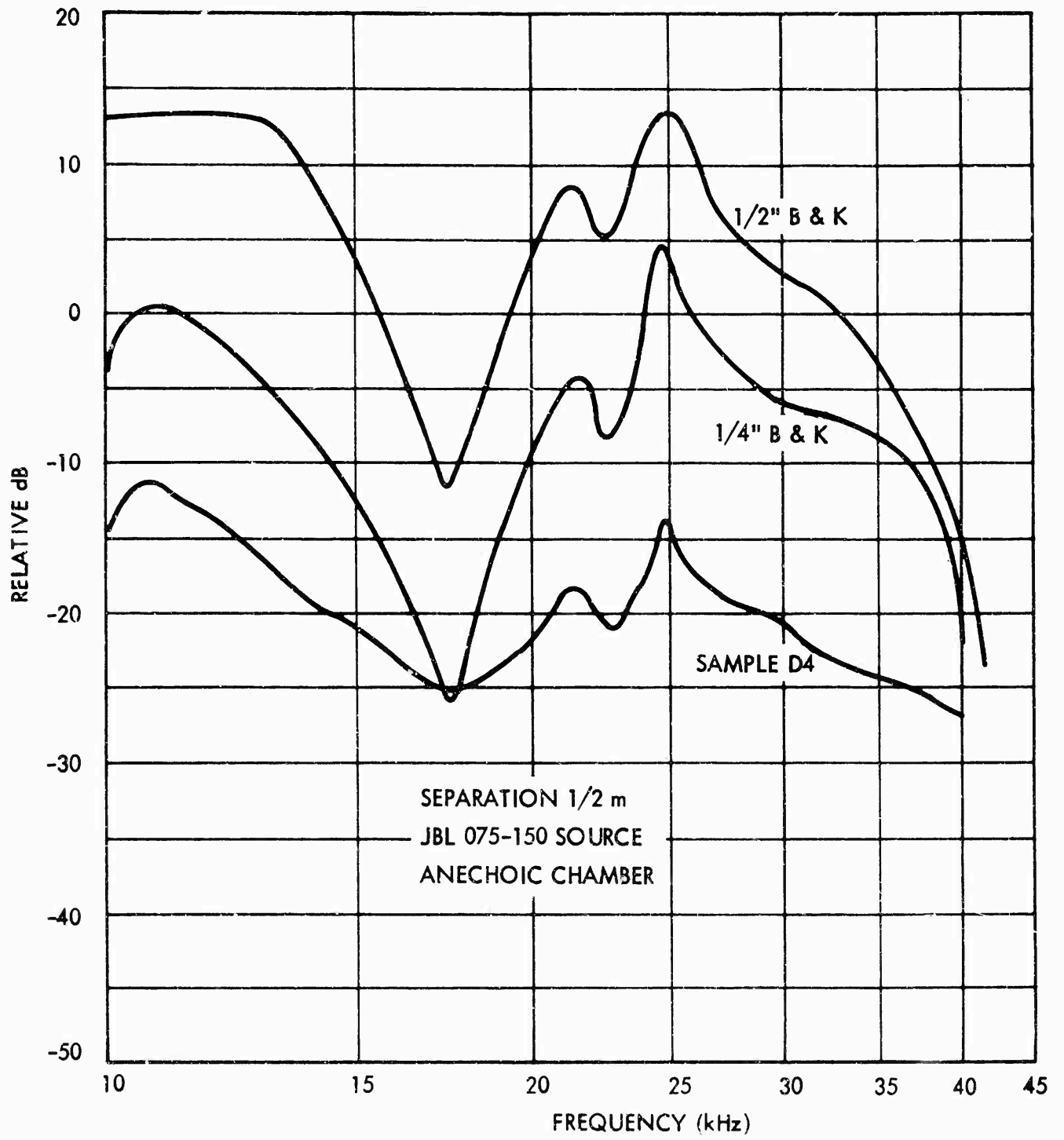


Figure 3-22. Standard Source Output as Measured by Three Receivers

3.5.3 Radiation

The bulk of the lab measurement effort was concerned with measuring the radiation characteristics of the samples. In addition to taking sufficient data to allow the calculation of radiation efficiency, we also measured several directivity patterns. The basic procedure is to drive the test sample with a known signal and to monitor the signal received by the standard microphone.

3.5.3.1 Instrumentation

The instrumentation is shown in the photographs of Fig. 3-23. The signal generator output is fed to the Crown DC-300 which in turn drives the test sample in series with a small precision resistor and a step controllable inductor (GR 1490B). The purpose of the inductor is to supply an inductive reactance exactly cancelling the capacitive reactance of the test sample so that the amplifier can work into a resistive load of fairly low value. The standard B & K 1/2" microphone is placed on the axis of the radiation. After its emergence from the B & K 2615 preamp and 2801 power supply, the signal is fed to an HP 20/40 dB voltage amplifier and the Krohnkite band pass filter. It is then monitored by an rms VTVM and a scope. In monitoring the input signal for purposes of calculating efficiency (especially for the case when one of the early samples [D1-D4] is being tested), it was found important to use low capacitance probes along with an AD-YU 406L phase angle meter (not shown). This was necessary to obtain the phase relationships among the various voltages and the currents.

The variable inductance has four decade inductances covering the range 1 mH to 10 H. The DC resistance of the inductor was fairly low, being roughly $42 L (\Omega)$, where L is the value of the inductance setting in henries. Unfortunately, the inductor is found to have an appreciable capacitance (on the order of 400 pF), so that at ultrasonic frequencies, its reactance cannot be depended upon to appear inductive.

Assuming that the real inductance can be represented as an ideal inductor, L in series with a resistor, R both of which are shunted by a capacitor, C , the effective inductance is given by

$$L_{\text{eff}} = \delta L$$

3-5

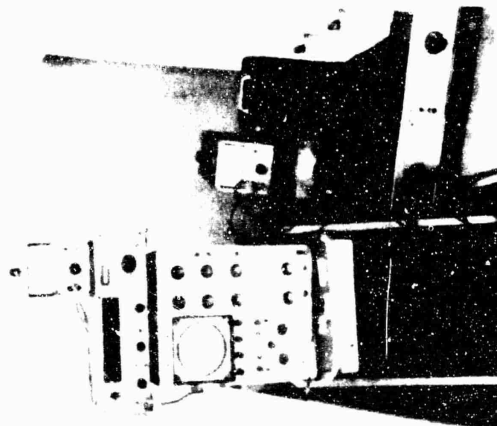
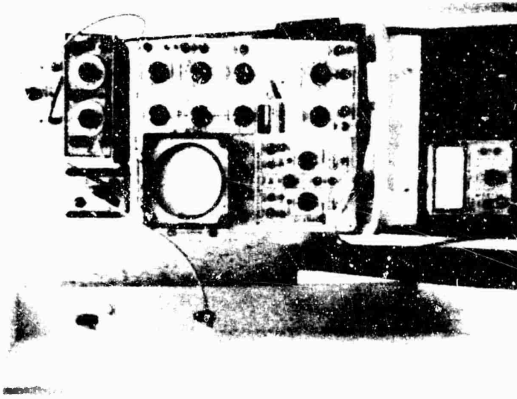
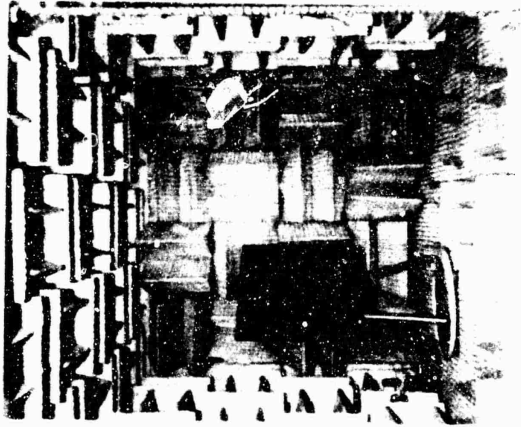


Figure 3 -23. Instrumentation Used in Determining Radiation Efficiency

3.5.3.1 (Continued)

where

$$\gamma = \frac{1 - Q^{-2} - f^2}{(1 - f^2)^2 + Q^{-2}f^2}$$

$$Q^2 = \frac{L}{R^2C} \quad \text{and} \quad f^2 = \omega^2 LC$$

Fig. 3-24 shows γ versus normalized frequency f , for $Q = 10, 100$, and 1000 . It is seen that near (but below) the frequency of self resonance, $\frac{1}{2\pi\sqrt{LC}}$, the effective

inductance increases and goes through a maximum. Above this frequency (not shown) the effective inductance is actually capacitive as is seen by the fact that γ goes negative in Eq. 3-5. This considerably complicates the radiation measurements because we cannot simply set the value of the variable inductor and know what its reactance is without also knowing the resistance, the frequency, and the associated capacitance.

3.5.3.2 Directivity

The directivity measurements were made in the anechoic chamber by rotating the sample about its axis (first the length then the width axis) while driving it electrically and monitoring its output 1/2 m away at a stationary microphone location as described in the previous section.

Fig. 3-25 shows the results of this procedure plotted in dB (relative to the maximum received signal) as a function of angle from the axis. The sample tested is D4, 30.8 kHz is the driving frequency, and this is the pattern in a plane perpendicular to the tape axis. The pattern shows a large major lobe centered about 10° off axis with half power points separated by 35.5° . From Fig. 3-13, it can be seen that for an infinitely long tape radiator this beam width would be expected to be associated with a kw of 4.5 (DI of 6.4 dB). However, for a long tape with an active width of 19 mm (such as D4), we would expect a kw of about 10.5 at this frequency (along with a DI of 10.2 dB from Fig. 3-14).

There are at least several plausible explanations for this lack of agreement. The obvious one is that the short length of sample D4 influences the result drastically.

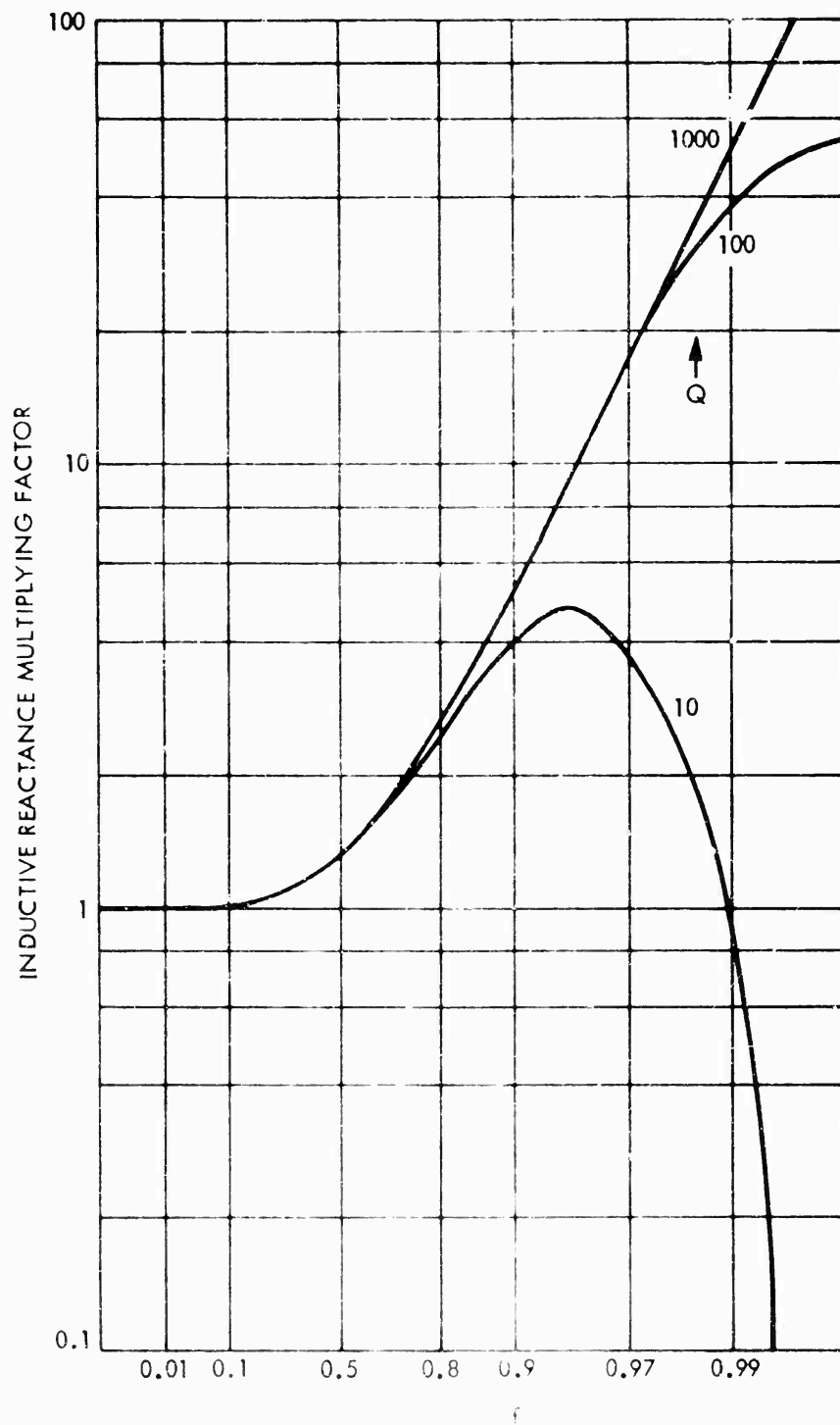


Figure 3-24. Effective Inductance Factor for Real Inductances

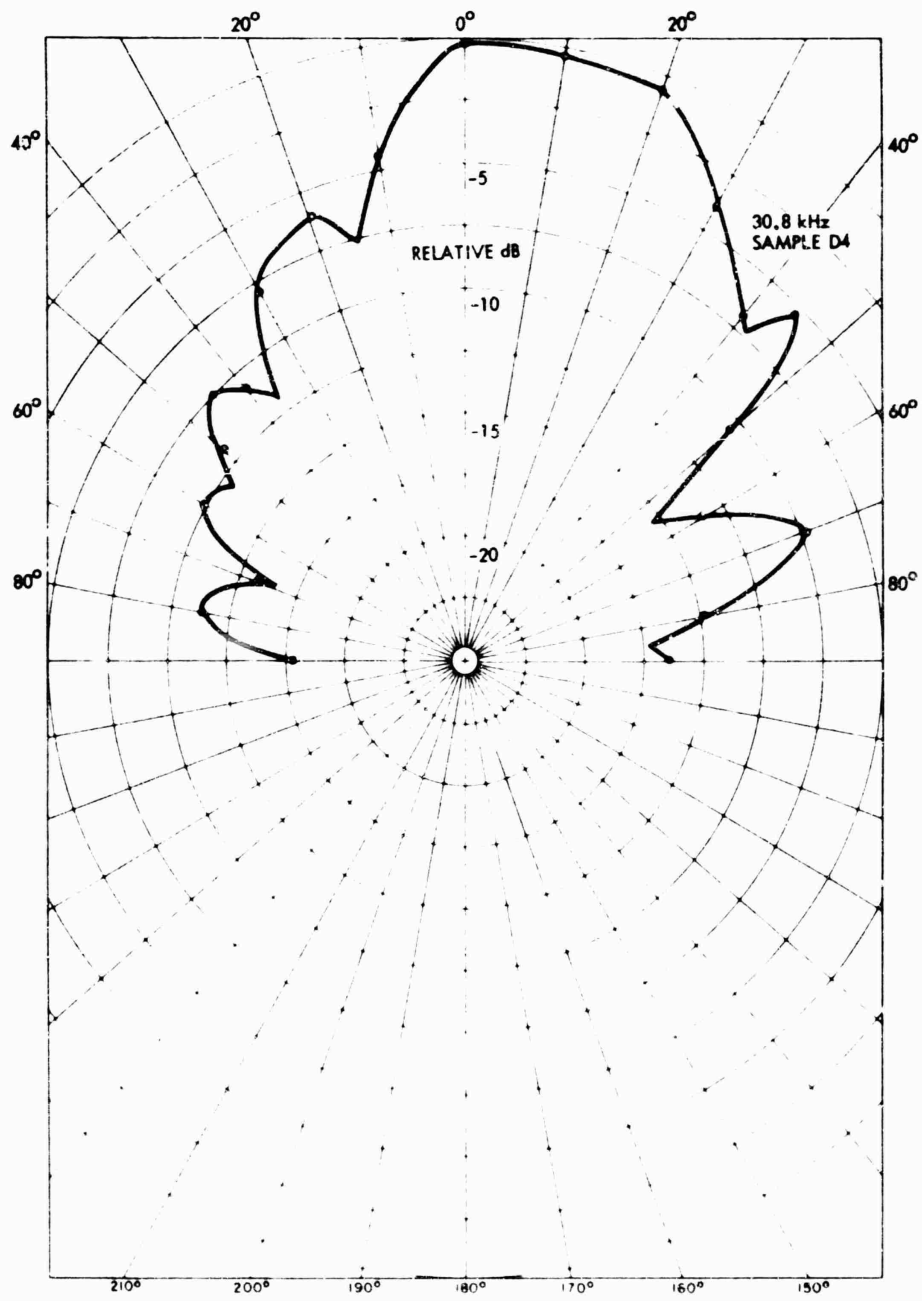


Figure 3-25. Measured Directivity Pattern for Sample D4

3.5.3.2 (Continued)

However, since a circular piston (diameter d) with $kd = 10$ has a DI of 14 dB^3 , we doubt if this effect would influence the results in the observed direction. More likely the effective radiating width is somewhat less than that not bonded with adhesive, or the entire moving surface is not moving uniformly (in phase and with equal amplitude). The 10° tilt of the pattern along with the raggedness of the side lobes seem to support the last explanation.

As expected, in the plane perpendicular to the width, the radiation pattern has a much sharper main lobe-- 16° . It is not tilted off axis more than a few degrees, but also has an irregular side lobe pattern. This indicates that in-phase radiation is occurring along a longer dimension (about twice as long as would be expected), but that again it is not uniform.

3.5.3.3 Efficiency

The acoustic power radiated is given for the very short baffled tape by

$$P = \frac{p_x^2 2\pi r^2}{\rho c Q} \quad 3-6$$

where Q is the directivity factor (>1 since $DI = 10 \log_{10} Q$)

p_x is the axial pressure

r is distance to measuring microphone

For the known sensitivity of the $1/2''$ B & K microphone and the known gain of the associated electronics and for $r = .5$, we find that the voltage E_m (in volts) of the microphone channel is related to the acoustic power by

$$P = \frac{3.74 \times 10^{-3}}{Q} E_m^2 \text{ watts} \quad 3-7$$

The electrical power delivered by the DC 300 is

$$P_E = E_o \frac{E_R}{R_1} \cos \angle E_o \quad 3-8$$

where E_o is the RMS output voltage of the DC 300

E_R is the RMS voltage across series resistance, R

$\angle E_o$ is the phase angle of E_o with respect to E_R

3.5.3.3 (Continued)

Of this, some is dissipated in R and in R_L (the DC resistance of the series inductor), so the power delivered to the transducer is

$$P_T = \frac{E_R}{R} \left[E_o \cos \angle E_o - \frac{E_R}{R} (R + R_L) \right] \quad 3-9$$

The efficiency is given by

$$\eta = \frac{P}{P_E}$$

and for $R = 10 \Omega$

$$\eta = \frac{.0374 E_m^2}{Q E_R E_o \cos \angle E_o} \quad 3-10$$

For sample D4 measurements were made of E_m , E_R , and $E_o \angle E_o$ at frequencies ranging from 15 to 35 kHz. Using $Q = 4$ (corresponding to the kw implied by the directivity measurements), the efficiencies ranged from 0.001 to .012%. The applied voltage was set at 8, 15 or 30 V and the resulting currents were found to be between 0.2 and 1.3 ma. The maximum electrical drive power used was under 40 mW and the maximum acoustic power radiated was less than half a microwatt. If the same power-to-area ratio were to hold for long lengths, then ~80 watts would be required for a 100 m length to produce at least as much acoustic intensity as the measured sample.

At this point it may well be asked why the efficiency is so much lower (factor of over 50) than that calculated by the model. This is especially apropos since Table 2-1 seems to indicate that the internal damping, D, is about the only parameter affecting efficiency, and we found that to be consistent with the sensitivity measurements, the D should produce an efficiency of about 0.7%. However, it should be remembered that the model results are calculated under the assumption that $Z_s = Z_{in}^*$ and that the layers are all uniform. In practice it is difficult to tell when we achieve $Z_s = Z_{in}^*$ and it is certain that considerable non-uniformity exists in the air gap thickness if not in the numerous adhesive layers. The electret's charge density is also known to be somewhat erratic in spatial distribution over the active surface. It is suggested that our inability to model these departures from the ideal is the basic cause of the large discrepancy in measured and modeled efficiencies.

4.0 Demonstration and Conclusions

4.1 Two-Tape Detection System Demonstration

As mentioned in the introduction, this study has been aimed primarily at the transducer portion of a new intrusion detection concept. We have measured the performance of the transducers both as radiators and receivers; however, we have not yet been able to develop the special electronics that would enable us to use a single transducer in both modes simultaneously (as envisioned in the detection system). Instead we developed the following two-tape detection concept to demonstrate the system as well as possible with the developed technology.

Fig. 4-1 shows the basic instrumentation and transducer placement. Two tape samples are placed side by side in the same horizontal plane as shown in Fig. 4-2. The samples used were 13 cm and 36 cm in length. One is driven as a radiator while the other acts as a receiver (the shorter, shielded one). If the received signal is connected to the vertical scope input and the driving signal to the horizontal scope input, the resulting trace will be a Lissajous figure that is very sensitive to relative phase (as well as amplitude) changes in the two signals. If an object is moved into the illuminated region above the transducers, a drastic wobbling of the Lissajous pattern is observed as the phase of reflected signal varies with respect to the steady drive signal. This display is very convenient for demonstration purposes since the skeptic can watch the effect of his own motions as he steps over or merely moves his hands over the transducers.

As expected, the detection is very easy for portions of targets (such as feet) passing within 0.5 m of the tape. Excellent detection was observed out to a height of 2 m for good reflectors (like books). The frequency used for the demonstration was about 25 kHz, but it was observed that detection was good over the entire range of frequencies from 20 kHz to 30 kHz. The demonstration shows that the electret tape transducer developed so far can function effectively as both source and receiver for an ultrasonic detection system based on phase shift or doppler.

4.2 Conclusions

This initial study has included theoretical analyses, computer models, electret charging method development, electret tape fabrication technique development, transducer

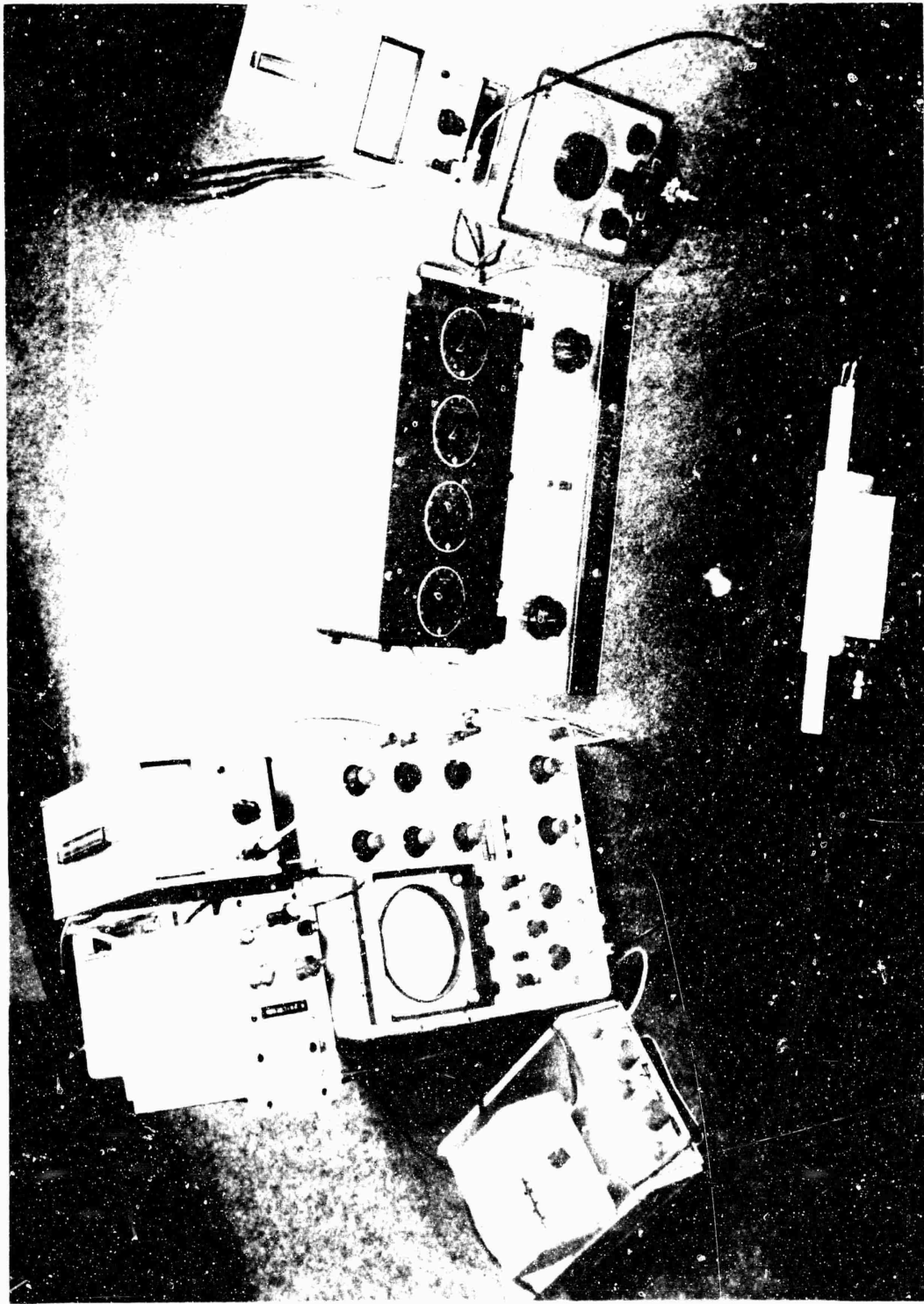


Figure 4-1. Instrumentation for Two Tape Detection Demonstration



Figure 4-2. Transducers for Two Tape Detection Demonstration

4.2 (Continued)

performance evaluation in the lab, and system detection demonstration. From this broad range of activities, we draw the following conclusions:

1. The ultrasonic doppler detection concept appears to be sound and the electret tape developed appears to be an adequate source and receiver for such a system.
2. Construction techniques are available for fabricating short tape transducers (0.5 m so far) that have open circuit sensitivities of at least -69 dB re 1 V/Pa and radiation efficiencies of at least 0.01% . Since this performance level was achieved on our fourth sample, it is felt that significant improvements will be made in subsequent samples.
3. A computer implemented model of the transducer has been developed for use in assessing its performance as a radiator, receiver and in a detection system. Discrepancies between the predictions of the model and the measurements in the lab appear to be due to non-uniformities in the hand-made transducers.
4. An adequate liquid contact charging technique has been developed that produces effective surface charge densities on 50 μm FEP of at least 0.1m C/m^2 even after four months. The typical decay rate is observed to be about 1 dB/time doubling after the first ten days.
5. The internal mechanical damping is very large in the current transducers (~ 50 to 70 times the characteristic impedance of air). This makes for lower efficiency but allows for fairly broad band operation so that the detection system can be operated over a frequency range of at least half an octave.

5.0 Recommendations

1. As noted in the text, the main shortcomings of the performance of the current transducers are believed due to imperfections in the construction techniques developed so far and not inherent in the system concepts. In particular a method for achieving a uniform air gap is considered very important, and a more nearly uniform surface charge density on the electret would also be desirable. Thus, we recommend that improved fabrication and charging procedures be developed for improving the quality of the tapes and for making them appreciably longer than current samples. The longer tapes are required for any realistic testing of the perimeter protection applications.
2. The computer model should be modified to take into account the effects of the inactive shielding layer and used to simulate the performance of potential or existing designs. In the current program the model was used primarily for studying the effects of transducer parameters. It is expected to be a useful tool in developing improved designs as well, and we recommend that it be so used. It can also answer important questions about operating frequency (with respect to the frequency of mechanical resonance) and about the effects of imperfect impedance matching.
3. The model will also be very important in providing inputs for the design of the hybrid electronics package required for the use of a single tape in both receiving and radiating modes in the desired detection system. It is recommended that this package be designed and fabricated for use with a long tape transducer. This will require a thorough knowledge of the transducer's input impedance.
4. Once both hybrid and long transducer are developed and checked out individually, they should be integrated into a detection system and evaluated as such.

References

1. Electroacoustics, F. V. Hunt, Harvard Monographs in Applied Science, No. 5, Harvard University Press, Cambridge, Mass., 1954.
2. "The Coupling of a Cylindrical Tube to a Half-Infinite Space", J. W. Miles, J. Acoust. Soc. Am. 20 No. 5, p. 652 (Sept. 1948).
3. Acoustics, L. L. Berauck, McGraw-Hill Book Co., 1954, New York.
4. "Charging of Polymer Foils using Liquid Contacts", P. W. Chadleigh, Appl. Phys. Lett. 21 No. 11, 547 (Dec. 1972).
5. "Stability of Liquid Charged Electrets", P. W. Chudleigh, R. E. Collins, G. D. Hancock, Appl. Phys. Lett. 23 No. 5, 211 (Sept. 1973).

APPENDIX A

Tape Transducer Analysis

1.0 Background

Consider the long tape transducer shown (in cross-section) in Fig. 2-1 of this report. Here we assume that the only layers in motion (in response to an applied voltage or an incident pressure field) are the jacket and outer conductor layers. This is assured in practice by making the stationary layers of much higher mechanical impedance than the moving layers. In addition, we assume that all charge distributions within the layers may be replaced by equivalent surface charge distributions. We also assume that the electrical signal propagates so rapidly that for the longest lengths to be considered the propagation delay can be neglected. Thus, we may use lumped electrical and mechanical elements to simulate the actual transducer's behavior. For this analysis, all time dependence will be assumed harmonic (steady state sinusoidal). The tape will be considered so long that end effects may safely be neglected.

2.0 Electrical Considerations

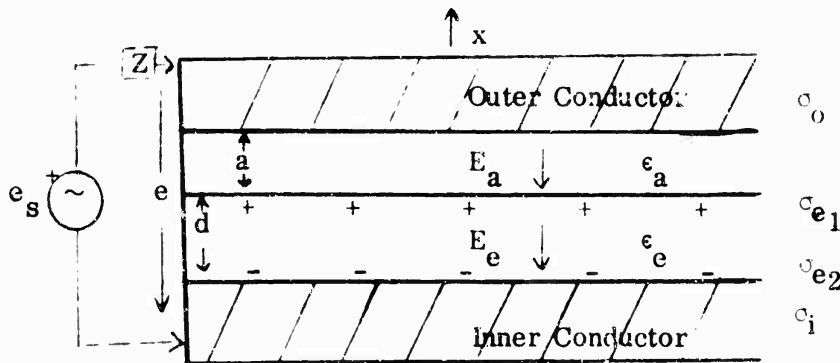


Fig. A-1 Electrically Important Cross Section

Fig. A-1 shows the electrically important parts of the transducer. The electret layer, thickness d , stores bound charges equivalent to surface charge densities σ_{e1} and σ_{e2} on its upper and lower boundaries respectively, and the internal electric field intensity in it is E_e . In the air/adhesive layer, thickness a , the electric field intensity is E_a . The free surface charges on the two conductors are σ_0 and σ_i for the outer and inner conductors respectively. An ideal voltage source, e_s , is applied to the conductors in series with a source impedance, Z_s , so that the interconductor voltage is e .

The interior of each layer is assumed to be charge-free, so that the electric flux is divergenceless there, i.e.,

$$\vec{\Delta} \cdot \vec{D} = 0.$$

2.0 Electrical Considerations (Continued)

Since we are neglecting fringing, the only non-zero field is in the x direction, and $D_x = D$ is the only non-zero component of \vec{D} . Thus $\vec{\nabla} \cdot \vec{D} = 0 \Rightarrow D = \text{constant}$, and within each layer we have $\epsilon E = \text{constant}$ where ϵ is the layer's electric permittivity. According to Gauss' Law, the electric flux out of a closed surface is numerically equal to the charge it encloses. Thus, at the inner surface of the outer conductor (where the surface charge is σ_o and no flux can enter the "perfect" conductor), we have

$$\epsilon_a E_a = \sigma_o \quad \text{A-1}$$

At the electret-air/adhesive interface applying Gauss' Law results in

$$\begin{aligned} \epsilon_e E_e - \epsilon_a E_a &= \sigma_{e1} \\ \text{or using A-1} \quad \epsilon_e E_e &= \sigma_o + \sigma_{e1} \end{aligned} \quad \text{A-2}$$

Similarly at the inner conductor surface of the electret we have

$$-\epsilon_e E_e = \sigma_i + \sigma_{e2}$$

Putting these expressions together to eliminate the electric field intensities, we find

$$\sigma_o + \sigma_i + \sigma_{e1} + \sigma_{e2} = 0 \quad \text{A-3}$$

The voltage e_1 dropped from outer to inner conductor is

$$\begin{aligned} e &= E_a a + E_e d \\ \text{or using A-1 and A-2} \quad e &= \frac{\sigma_o a}{\epsilon_a} + \frac{(\sigma_o + \sigma_{e1})}{\epsilon_e} d \end{aligned}$$

Let $\sigma_{e1} = -\sigma_{e2} = \sigma_e$ (equal and opposite charges on the electret's surface). Then

$\sigma_o - \sigma_i = 0$ from A-3. Defining the voltage across the electret due to its bound charges in the absence of any nearby conductor as

$$V_e = \frac{\sigma_e}{\epsilon_e} d = \frac{\sigma_e}{C_e} \quad \text{A-4}$$

2.0 Electrical Considerations (Continued)

where $C_e = \frac{\epsilon_e}{d}$ = per unit area capacitance of the electret and $C_a = \frac{\epsilon_a}{a}$ =

the per unit area capacitance of the air/adhesive layer, the voltage across the conductor becomes

$$e = \sigma \left(C_a^{-1} + C_e^{-1} \right) + V_e = \frac{\sigma}{C} + V_e \quad \text{A-5}$$

where C = capacitance/unit area between electrodes.

This says that at every instant the voltage across the conductors is the voltage of the electret due to its bound charge plus the induced surface charge density per unit total capacitance/unit area.

The current i into the outer conductor is simply

$$i = \dot{\sigma} S \quad \text{A-6}$$

where S is the total surface area of the electret and the dot denotes differentiation with respect to time.

The source voltage e_s and source impedance Z_s are related to the voltage across the device by (using Kirchoff's voltage law)

$$e_s = iZ_s + e$$

or in terms of the surface charge density using A-6 and A-5

$$e_s = Z_s \dot{\sigma} S + \frac{\sigma}{\epsilon_a} + \frac{\sigma}{C_e} = e_s = V_e \quad \text{A-7}$$

Both of the variables σ and a are functions of time in this first order linear differential equation with one non-constant coefficient. (While the impedance concept is normally reserved for steady-state analysis, we use it at this stage even though no specific time dependence has been assumed, anticipating the steady-state harmonic treatment to follow).

3.0 Mechanical Considerations

Now consider the mechanical situation. We wish to equate the applied and reaction pressures acting on the moving layers. First we define some of the constants required. If only the outer jacket (of density ρ_j and thickness d_j) and the outer conductor (of density ρ_c and thickness d_c) move in response to electrical or mechanical excitation, then the moving mass per unit area is $m_j = \rho_j d_j + \rho_c d_c$. However, the

3.0 Mechanical Considerations (Continued)

air/adhesive layer contacts the outer conducting layer and, therefore, must move to some extent also. If the density of the air adhesive layer is ρ_a and its thickness is a , the total moving mass per unit area is

$$M = m_j + \alpha \rho_a a$$

where α is the effective fraction of the air/adhesive layer which participates in the acceleration experienced by the adjacent conducting layer. We used $\alpha = 1/3$ for the numerical results.

The mechanical restoring force of the compliant layers (air/adhesive) is associated with a stiffness/unit area, K . If the compliant layers were entirely of air this constant would be

$$K_{\text{air}} = \frac{\delta P_0}{a}$$

where P_0 is the ambient air pressure and $\delta = 1.4$

If the compliant layer is a mixture of air and adhesive, the stiffness will be increased by some factor δ . So in general

$$K = \frac{\delta \delta P_0}{a}$$

We usually used $\delta = 1$ in this study since air is the controlling compliance source. The mechanical damping due to heat flow, friction, and viscous effects associated with the compliant and moving layers is lumped into the damping constant per unit area, D .

If x is considered positive in the outward direction (see Fig. A-1), then the reaction pressure is given by $M \ddot{x} + (D + Z_a) \dot{x} + Kx$, where Z_a is the specific acoustic impedance of an infinite baffled strip (see Appendix C for derivation) and $Z_a \dot{x}$ is the pressure on the outer moving layer resulting from its interaction with the external medium due to its velocity \dot{x} .

The applied pressures in the positive x direction are $-\frac{\sigma^2}{2\epsilon_a}$ caused by the free surface charge density on the outer conductor and $-p_i$ the pressure associated with the incident acoustic wave. Collecting all the pieces mentioned so far, we can write the equilibrium pressure equation as

$$M\ddot{x} + (D + Z_a) \dot{x} + \delta \gamma P_0 \frac{x}{a} = \frac{-\sigma^2}{2\epsilon_a} - p_i \quad \text{A-8}$$

3.0 Mechanical Considerations (Continued)

Note that this is a second order linear differential equation with non-constant coefficients.

Equation 7 and 8 in x and σ make a mildly non-linear set of differential equations. To make further progress, we expand these equations in the first few terms of a Fourier series. Thus

$$e_s = \frac{E}{2} e^{j\omega t}, \quad p_i = \frac{P}{2} e^{j\omega t}, \quad \sigma = \sigma_0 + \frac{\sigma_1}{2} e^{j\omega t}, \quad x = x_0 + \frac{x_1}{2} e^{j\omega t} \quad A-9$$

where the zero subscripts refer to constant, time-independent quantities. Thus, the air gap becomes $a = a_0 + x_0 + \frac{x_1}{2} e^{j\omega t}$.

Here a_0 is the basic air gap thickness (with an unchanged electret) and x_0 is the equilibrium displacement caused by all static pressures. Substituting relation A-9 into A-7 and A-8 and collecting terms containing no time dependence, we arrive at the zeroth order or static condition relations:

$$\frac{a_0 + x_0}{\epsilon_a} + \frac{1}{C_e} = \frac{-V_e}{\sigma_0}$$

A-10

$$\frac{\delta\gamma P_0 x_0}{x_0 + a_0} + \frac{\sigma_0^2}{2\epsilon_a} = 0$$

These can be combined to yield the cubic in σ_0 ,

$$\sigma_0^3 + \sigma_0^2 \left(\frac{\epsilon_a a_0}{d} \right) + 2\delta\gamma P_0 \frac{a_0}{d} \epsilon_e + \epsilon_a \sigma_0 + 2\delta\gamma P_0 \epsilon_e \epsilon_a = 0$$

Using $\sigma_0^{(1)} = \left(1 + \frac{\epsilon_e a_0}{\epsilon_a d} \right)^{-1}$ for the first guess, it was found very easy to solve for

σ_0 in the cubic using the Newton-Raphson iterative method. Then x_0 is found from substituting σ_0 back into A-10. These static solutions are required in the equations for the first order solution that result from substituting A-9 into A-7 and A-8. These are

3.0 Mechanical Considerations (Continued)

$$\left[j\omega Z_s S + \frac{a_o + x_o}{\epsilon_a} + \frac{d}{\epsilon_e} \right] \sigma_1 + \frac{\sigma_o}{\epsilon_a} x_1 = E$$

and

$$\frac{\sigma_o}{\epsilon_a} \sigma_1 + \left[-\omega^2 M - \omega X_a + j\omega(D+R_a) + \frac{\delta \gamma P_o a_o}{(a_o + x_o)^2} \right] x_1 = -P \quad A-11$$

By defining

$$T = \frac{\sigma_o}{\epsilon_a}$$

$$z_e = r_e + jx_e \equiv j\omega S Z_s + \frac{d}{\epsilon_e} + \frac{a_o + x_o}{\epsilon_a} = j\omega S Z_s + C_o^{-1}$$

$$z_m = r_m + jx_m \equiv -\omega^2 M - \omega X_a + j\omega(D+R_a) + \frac{\delta \gamma P_o a_o}{(a_o + x_o)^2}$$

A-12

and dropping the 1 subscripts from σ_1 and x_1 , we have simply

$$z_e \sigma + T x = E$$

$$T \sigma + z_m x = -P$$

A-13

The solutions are thus

$$\sigma = \frac{P T + E z_m}{z_e z_m - T^2} \quad x = \frac{-P z_e - E T}{z_e z_m - T^2}$$

A-14

The current and particle velocity, are then

$$i = j\omega S \sigma$$

$$v = j\omega x$$

A-15

4.0 Input Impedance and Mechanical Resonance

The input impedance at the electrical terminals of the tape transducer is given by

$$Z_{in} = \frac{E - i Z_s}{i}$$

Using the expression for i in A-15 together with the solution for the surface charge density σ in A-14 for the case of $P = 0$, the above becomes (after applying A-12 to eliminate Z_s)

$$Z_{in} = \frac{j}{\omega S} \left(\frac{T^2}{z_m} - \frac{1}{C_o} \right) \quad \text{A-16}$$

Using A-12 the real and imaginary parts are found to be

$$R_{in} = \frac{T^2(D+R_a)}{S[r_m^2 + \omega^2(D+R_a)^2]} \quad X_{in} = \frac{1}{\omega S} \left(\frac{T^2 r_m}{|z_m|^2} - \frac{1}{C_o} \right) \quad \text{A-17}$$

The input reactance is zero at $\omega = \omega_r$ satisfying

$$\omega_r^4 M^2 + \omega_r^3 2MX_A + \omega_r^2 [Z_A^2 + D(D+2R_A) + M(C_o T^2 - 2K)] + \omega_r X_A (C_o T^2 - 2K) + K(K - C_o T^2) = 0.$$

For the typical large internal damping, it was found that no real root exists (for typical values of the other parameters). It is certainly not satisfied by the frequency of mechanical resonance ($r_m = 0$) defined by

$$f_o = \frac{\sqrt{X_A^2 + 4KM} - X_A}{4\pi M} \quad \text{A-18}$$

5.0 Radiation Efficiency

The radiation efficiency is defined by

$$\eta = \frac{\text{acoustic power radiated}}{\text{total electrical power required}} \quad \text{A-19}$$

The acoustic power radiated

$$P_A = |v|^2 R_A S = \omega^2 |x|^2 R_A S$$

5.0 Radiation Efficiency (continued)

The electrical power required is $E \cdot \text{Re}(i)$

$$\eta = \frac{\omega R_A |x|^2}{E \text{Re}(j\sigma)}$$

By using A-14 to substitute for x and σ , performing the indicated operation and simplifying, we can derive the form

$$\eta = \frac{\omega R_A T^2}{X_e |z_m|^2 + X_m T^2} = \frac{R_A T^2}{SR_s |z_m|^2 + (D + R_A) T^2} \quad \text{A-20}$$

If the expression for R_{in} (A-17) is used along with A-12, we can simplify this to

$$\eta = \left(1 + \frac{F_s}{R_{in}}\right)^{-1} \left(1 + \frac{D}{R_A}\right)^{-1} \quad \text{A-21}$$

This form is quite reasonable. It says that to maximize efficiency one should try to make the source resistance much less than the input resistance of the device and try to make the internal mechanical damping constant much less than the acoustic radiation resistance.

If the source resistance matches the input resistance, the efficiency is simply

$$\eta_{R_s=R_{in}} = \frac{0.5}{1 + \frac{D}{R_A}} \quad \text{A-22}$$

6.0 Axial Pressure and Directivity Index

The far field radiated pressure field can be determined from a knowledge of the directivity pattern and the total radiated power. From Miles (Ref. 1 of main report) we know that in the far field

$$p(r, \theta) = p_x(r) \frac{\sin(kw \sin \theta)}{kw \sin \theta} = p_x(r) f(\theta) \quad \text{A-23}$$

where $p_x(r)$ is the axial pressure at a distance, r , (that on a line perpendicular to the plane of the tape and emanating from its width mid-point).

6.0 Axial Pressure and Directivity Index (Continued)

The total acoustic power radiated from length, ℓ , of tape is the integral of the normal component of intensity over a surface enclosing the source.

Thus,

$$P_A = 2 \int_0^{\ell} \int_0^{\pi/2} \frac{p^2(r, \theta) r}{\rho c} d\theta d\ell$$

Or using A-23 and solving for p_x we find:

$$p_x(r) = \sqrt{\frac{P_A \rho c}{2 \ell r \int_0^{\pi/2} f(\theta)^2 d\theta}} \quad \text{A-24}$$

A convenient method of performing this integral is

$$\int_0^{\pi/2} f^2 d\theta = \left[\frac{1}{2} (f_0^2 + f_n^2) + \sum_{i=1}^{n-1} f_i^2 \right] \frac{\pi}{2n} \quad \text{A-25}$$

where

$$f_j = f(\theta_j) \quad j = 0 \dots n \quad \text{for } n + 1 \text{ terms}$$

While A-23 may be used to generate far field directivity patterns for various values of $k\omega$, a single number measure of directivity is often adequate. This directivity index is defined as

$$DI = 10 \log_{10} \left[\frac{\text{Power that would be radiated if axial pressure were typical for entire semicylinder at given far-field range}}{\text{Actual power radiated}} \right]$$

Since the numerator is $\frac{\pi r \ell p_x^2}{\rho c}$ and the denominator is P_A , we can use A-24 to find

$$DI = -10 \log_{10} \left[\frac{2}{\pi} \int_0^{\pi/2} f(\theta)^2 d\theta \right] \quad \text{A-26}$$

which is easily evaluated using A-25.

7.0 Receiving Sensitivity

So far we have dealt with phenomena associated with the active transducer. Now we consider its passive operation where sensitivity to an incident pressure field is desired. We assume that the output voltage produced by an incident acoustic pressure field is developed across the impedance previously labeled Z_s . This will be considered the input impedance of the preamplifier for the received signal. For this situation $E = 0$ and we have (using A-13) for the magnitude of the output voltage, e_o

$$|e_o| = \omega S_p |c| |Z_s| = \frac{\omega S_p T |Z_s|}{|z_e z_m - T^2|}$$

where S_p is the area exposed to P

Using A-12 for z_e and letting $|Z_s| \rightarrow \infty$ for the open circuit case, the above can be reduced to

$$\frac{|e_o|}{P} \Big|_{oc} = \frac{S_p T}{S |z_m|} = \frac{T S_p / S}{\sqrt{(k - \omega^2 M - \omega X_A)^2 + \omega^2 (D + R_A)^2}} \quad A-27$$

At mechanical resonance where $r_m = 0$, this becomes simply

$$\frac{|e_o|}{P} \Big|_{oc} = \frac{S_p T}{\omega_r S (D + R_A)} \quad A-28$$

If Z_s is not very large, the sensitivity is not so simple and in general is

$$\frac{|e_o|}{P} = \omega S_p T \sqrt{\frac{R_s^2 + X_s^2}{T^4 + 2T^2(x_e x_m - r_e r_m) + |z_e|^2 |z_m|^2}} \quad A-29$$

8.0 Conjugate Impedance Matching

If $Z_s = Z_{in}^*$, which is desirable from the point of view of driving the device with a real amplifier, some simplifications result.

8.0 Conjugate Impedance Matching (continued)

In that case

$$R_s = R_{in} = \frac{x_m T^2}{\omega S |z_m|^2} \quad \text{and} \quad X_s = \frac{1}{\omega S C_o} - \frac{r_m T^2}{\omega S |z_m|^2}$$

Then from A-12 we can relate r_e and x_e to r_m and x_m .

$$r_e = \frac{r_m T^2}{|z_m|^2} \quad \text{and} \quad x_e = \frac{x_m T^2}{|z_m|^2}$$

From these it follows (for $Z_s = Z_{in}^*$)

$$|z_e| |z_m| = T^2$$

and

$$|z_e z_m - T^2| = \frac{2T^2 x_m}{|z_m|}$$

Putting these into A-29 we find the sensitivity for conjugate impedance matching to be:

$$\frac{|e_o|}{P} = \frac{S_p T}{2S x_m} \sqrt{\left(1 - \frac{r_m}{T^2 C_o}\right)^2 + \left(\frac{x_m}{T^2 C_o}\right)^2} \quad \text{A-30}$$

9.0 Beam Width

It is desirable to know the beam width of the major lobe of the radiation pattern implied by the current frequency and tape width. This is found from the expression of Miles¹ for the directivity pattern

$$D = 20 \log_{10} \frac{\sin(kw \sin \theta)}{kw \sin \theta} \quad \text{A-31}$$

The half power points occur at $D = -3.01$ or for

$$F(\theta) = \frac{kw}{\sqrt{2}} \sin \theta - \sin(kw \sin \theta) = 0$$

9.0 (Continued)

The Newton-Raphson iterative technique is then used:

$$\theta^{i+1} = \theta^i - F(\theta_i)/F'(\theta_i)$$

A-32

$$\theta^0 = 1.536 \text{ kw}^{-1.04}$$

The constants for the θ^0 expression were empirically derived. The method works well over the entire range of kw of interest.

APPENDIX B

Computer Program for Model of Electret-Tape Transducer Performance

In this appendix we include a listing of the Fortran coding that was developed for use in examining the effects of parameters on the performance of the transducer. A dictionary of the variables is included to assist the potential user in understanding the coding.

1.0 Fortran Coding

1.1.1 Ultrasonic Electret Tape Detector Model

```
COMPLEX ZE, ZM, QC, XC, DT, ZIN, ZL
REAL L, J, K, MO, KW, MOOM, LS
COMMON /TOUT/ LAB(6), TAPE(75)
DIMENSION I(5)
COMMON /DDIM/AO, OC, J, W, L, D /MAT/DM, DL, DA, DJ, DC, REA, REE
1 /ELC/QE, RS, LS /ZS/A, XO, QEZ /TGT/ TL, TR, TD
EQUIVALENCE (TAPE(1), ETOM), (TAPE(2), ETOF), (TAPE(3), ETOR), (TAPE(4), ETOX),
1(TAPE(5), EPM), (TAPE(6), EPF), (TAPE(7), EPR), (TAPE(8), EPX), (TAPE(9), SSM),
2(TAPE(10), SSF), (TAPE(11), SSR), (TAPE(12), SSX), (TAPE(33), DB), (TAPE(34), VE),
3(TAPE(35), CE), (TAPE(36), CAO1), (TAPE(37), COO1), (TAPE(38), GO),
4(TAPE(39), T), (TAPE(40), COI), (TAPE(41), K), (TAPE(42), MO), (TAPE(43), FDM),
5(TAPE(44), F2), (TAPE(45), F3), (TAPE(46), ZM), (TAPE(48), FK), (TAPE(49), KW),
6(TAPE(50), BW), (TAPE(51), X), (TAPE(52), CUR), (TAPE(53), PA), (TAPE(54), ETO),
7(TAPE(55), ZIN), (TAPE(57), ZL), (TAPE(59), PX), (TAPE(60), PS), (TAPE(61), P),
8(TAPE(62), CURR), (TAPE(63), EP), (TAPE(64), SS), (TAPE(65), RF),
9(TAPE(66), ZE), (TAPE(68), DT), (TAPE(70), CURM), (TAPE(71), CURF),
A(TAPE(72), QD), (TAPE(73), ZT), (TAPE(74), VG), (TAPE(75), OCS)
CALL BDATA
WRITE(12, 40)
40 FORMAT(' ULTRASONIC TAPE RADIATION
DB=3.
GAMMA=1.4
RCC=407.
EO=8.654E-12
PI= 3.141592654
PO=1.013E5
E=10.
WRITE(10, 85)
85 FORMAT(' ENTER FILE #, MONTH, DAY OF MONTH, YEAR')
READ(11) (LAB(N), N=1, 4)
MCT=75
LCT=0
1 ACCEPT I(1)
IF(I(1)) 99, 2, 3
3 ACCEPT (I(M), M=2, 4)
CALL DATIN(I)
IF(LCT.EQ.0) GO TO 2
MCT2=MCT*2+3
CALL FCMTD(1, 2, LAB(1), MCT2, IER)
TYPE MCT2, IER
WRITE(12, 75) LAB, (TAPE(N), N=1, MCT)
```

```

75     FORMAT(' **', 6I10, /, (6E20, 7, /))
      LCT=0
2     CONTINUE
      S=W*L
      WRITE(12, 55)
55    FORMAT(' AIR-GAP   COND. TH   JAC. TH   WIDTH   LENGTH   EL. TH   ST. PAR
1     AD. DEN   JAC. DEN   CO. DEN   AD. DC   EL. DC   EL. SUR. CHG')
65    FORMAT(// ' SOURCE RES. & INDUC.   MECH. DAMP   TAR. LGTH'
*, ' REFLECT.   TAR. RANG')
      WRITE(12, 56) AO, DC, J, W, L, D, DL, DA, DJ, DC, REA, REE, QE
56    FORMAT(1P3E10, 2, 0PF7, 4, F7, 0, F8, 5, F7, 2, F8, 2, 1X, 2F8, 0, F7, 2, F7, 2, 1PE11, 2)
      WRITE(12, 65)
      WRITE(12, 66) RS, LS, DM, TL, TR, TD
66    FORMAT(11X, 0PF8, 0, 1PE12, 3, 0PF10, 0, F10, 2, F11, 4, F11, 3, //)
      EE=EO*REE
      EA=EO*REA
      CE=EE/D
      CEI=1./CE
      VE=QE*CEI
      CAOI=AO/EA
      COOI=CEI+CAOI
      K=DL*PO
      XO=2.*EA*K
      A=XO*(1.+CE*CAOI)
      QO=-VE/COOI
      QEZ=QE
      CALL ZOSOL(QO, M)
      XO=- (AO/(1+XO/(QO*QO)))
      A=AO+XO
      T=QO/EA
      T2=T*T
      COI=CEI+A/EA
      K=K*GAMMA*AO/(A*A)
      MO=DJ*J+DC*OC+.333T*A*A
      WRITE(12, 57)
57    FORMAT(' VE, CE, CAOI, COOI, QO, A, T, COI, K, MO')
      WRITE(12) VE, CE, CAOI, COOI, QO, A, T, COI, K, MO
      WRITE(10, 50)
50    FORMAT(// ' ENTER FREQ SWEEP MODE(0=REPEAT, 1=LIN.) INTEGER, 1ST, LA
1ST, AND 1ST INCREMENT(KHZ)')
      ACCEPT JF, FL, FH, DF
      WRITE(12, 68)
68    FORMAT(1H0, 120(1H.))
      IF(JF.F'1.0) GO TO 8
      FL=1000.*FL
      FH=1000.*FH
      DF=1000.*DF
      NF=1.+(FH-FL)/DF
      F=FL-DF
      DO 4 N=1, NF
      F=F+DF

```



```

8   OM=2.*PI*F
    KW=OM*W/344.8
    OM2=OM*OM
    SOM=S*OM
    CALL STRIPZ(KW, RA, XA)
    RA=ROC*RA
    XA=ROC*XA
    RF=(SQRT(XA*XA+4.*K*MO)-XA)/(4.*MO*PI)
    RM=K-OM2*MO-OM*XA
    XM=OM*(RA+DM)
    T2=T2/(RM*RM+XM*X)
    COI=10.*ALOG10(T2)
    RIN=XM*T2/SOM
    XIN=(RM*T2-COI)/SOM
    ZIN=CMPLX(RIN, XIN)
    RL=RS
    XL=OM*LS
    IF(RS.GE.0.0) GO TO 12
    RL=RIN
    IF(RL.LT.2.) RL=2.
    XL=-XIN
    LS=XL/OM
CALCULATE F(DM) AND F2 AND F3
12  CT=T2/COI
    C2=CT-2*K
    RAD=RA+DM
    XARA=XA*XA+RAD*RA
    MOOM=OM*MO*(2.*XARA+OM*MO)
    F2=K*K+T*T*RAD/RL+OM*(-2.*K*XA+OM*(XARA-2.*K*MO+MOOM))
    FDM=K*(K-CT)+OM*(XA+C2+OM*(MO*C2+XARA+MOOM))
    F3=-K*XA+OM*(XARA-2.*K*MO+OM*MO*(3.*XA+OM*MO*2.))
    WRITE (12, 67) F, FDM, F2, F3, RM, XM
67  FORMAT(/, 1X, 'FREQ =', F9.1, ' F(DM) =', 1PE15.7, ' F2 =', E15.7,
*    F3 =', E15.7, ' ZM =', 2E15.3)
CALCULATE RADIATION PARAMETERS
    ZL=CMPLX(RL, XL)
    ZE=CMPLX((COI-SOM*XL), (SOM*RL))
    ZM=CMPLX(RM, XM)
    DT=ZE*ZM-T2
    XC=-E*T/DT
    QC=E*ZM/DT
    RI=-SOM*AIMAG(QC)
    CUR=SOM*CABS(QC)
    X=CABS(XC)
    V=OM*X
    PS=V*SQRT(RA*RA+XA*XA)
    PA=S*RA*V
    ETO=PA/(E*RI)
    FK=.001*F
CALCULATE BEAM WIDTH
    II=0
    B=1.5359*KW**(-1.04)
    C=KW/SQRT(2.)
14  II=II+1
    SB=SIN(B)
    FR=(C+SB-SIN(KW*SB))/(COS(B)*(C-KW*COS(KW*SB)))
    B=B-FR
    IF((ABS(FR/B).GT.1.E-8).AND.(II.LT.30)) GO TO 14
    BW=360.*B/PI

```

CALCULATE AXIAL PRESSURE AT DISTANCE TD METERS

```
SI=SIN(KW)/KW
SM=.5+.5*SI*SI
DLT=PI/180.
DO 15 II=1,89
SI=KW*SIN(II*DLT)
SI=SIN(SI)/SI
15 SM=SM+SI*SI
SM=2.*DLT*SM
QD=-10.*ALOG10(SM/PI)
PX=SQRT(PA*ROC./(L*TD*SM))
TLD=TL/TD
P=EXP(-TD*(.0000424*FK*FK+.144*ALOG(FK)-.3322))
P=P*TR*PX/SQRT(2.*SQRT(1+.0625*TLD*TLD))
XC=-P*ZE/DT
QC=P*T/DT
CURR=W*OM*CABS(QC)
EP=CURR*CABS(ZL)
SS=20.*ALOG10(EP/P)
EP=EP*TL
VG=20.*ALOG10(EP/E)
ZT=20.*ALOG10(EP/CUR)
WRITE(12,60)
60 FORMAT(//, ' FREQ(KHZ) KW BEAM-WIDTH DISPL(NM) I(AMPS) RAD. PWR(MW)
* TOTL-EFF. % INPUT-IMPED SOURCE-IMPED. ')
WRITE(12,61) FK, KW, BW, X, CUR, PA, ETO, ZIN, ZL
61 FORMAT(F8.2, F7.2, F9.2, 9PF11.2, 1PE12.3, 3PF9.4, 2PF13.4, 2X, 1P4E11.3, //)
WRITE(12,62)
62 FORMAT(' AXIAL-PRES SURF. PRES REC. PRES CUR(NA/M) V-OUT(-9)
*SENS(DB-V/(PA-M)) RES. F(KHZ)')
WRITE(12,63) PX, PS, P, CURR, EP, SS, RF
63 FORMAT(2X, 3F11.4, 9PF11.2, F11.3, 0PF15.3, 0PF16.1, //)
WRITE(12,77)
77 FORMAT(' ELECTRICAL IMPEDANCE DT
* DIRECT INDEX TRANS IMPED VOLT GAIN OPEN CIR SENS')
WRITE(12,78) ZE, DT, QD, ZT, VG, OCS
78 FORMAT(1X, 1PE15.5, 7E15.5)
WRITE(12,64)
64 FORMAT(1X, 120(1H-), //)
IF(CURM.LT.CUR.AND.LCT.NE.0) GO TO 88
CURM=CUR
CURF=FK
88 IF(ETOM.GE.ETO.AND.LCT.NE.0) GO TO 80
ETOM=ETO
ETOF=FK
ETOL=XL
ETOR=RL
80 IF(SSM.GE.SS.AND.LCT.NE.0) GO TO 90
SSM=SS
SSF=FK
SSX=XL
SSR=RL
90 IF(EPM.GE.EP.AND.LCT.NE.0) GO TO 4
EPM=EP
EPF=FK
EPX=XL
EPR=RL
LCT=1
4 CONTINUE
WRITE(12,69)
```

```

69  FORMAT(1X, 80(1H#), '( )
    TAPE(13)=AO
    TAPE(14)=OC
    TAPE(15)=J
    TAPE(16)=D
    TAPE(17)=REA
    TAPE(18)=REE
    TAPE(19)=QE
    TAPE(20)=W
    TAPE(21)=L
    TAPE(22)=DL
    TAPE(23)=DA
    TAPE(24)=DJ
    TAPE(25)=DC
    TAPE(26)=RS
    TAPE(27)=LS
    TAPE(28)=DM
    TAPE(29)=TL
    TAPE(30)=TR
    TAPE(31)=TD
    TAPE(32)=A
    TYPE 'TAPE:', (TAPE(N), N=1, MCT)
    GO TO 1
99  CONTINUE
    CALL FCMTD(1, 8, TAPE(1), 2, IER)
    TYPE IER
    WRITE(12, 100) (LAB(N), N=1, 4)
100  FORMAT(' END FILE #', I4, 10X, I2,
    END

```

```

SUBROUTINE DATIN(I)
COMMON /DDIM/ AO, OC, J, W, L, D
COMMON /MAT/ DM, DL, DA, DJ, DC, REA, REE
COMMON /ELC/ QE, RS, CL
COMMON /TGT/ TL, TR, TD
DIMENSION I(5), RTGT(3), RDIM(6), RMAT(7)
REAL L, J
EQUIVALENCE (RTGT(1), TL), (RDIM(1), AO), (RMAT(1), DM)
M=0
9 M=M+1
N=I(M)
IF((M.GT. 6). OR. (N.LT. 1))RETURN
GO TO (1, 2, 3, 4, 5, 6), N
1 WRITE(10, 51)
51 FORMAT(' ENTER NO. AND VALUES OF DIMENS OF AIR GAP, COND. TH.
1 JAC. TH., TAPE WIDTH, TP LNGTH. AND ELECT. TH. ')
ACCEPT N
ACCEPT (RDIM(K), K=1, N)
GO TO 9
2 WRITE(10, 52)
52 FORMAT(' ENTER NO. AND VALUES OF MECH. DAMPER, ADH. STIF. PARAM.
1 ADH. DEN., JAC. DEN., COND. DEN., ADH. REL. D. C.,
2 ELECT. REL. D. C. ')
ACCEPT N
ACCEPT (RMAT(K), K=1, N)
GO TO 9
3 WRITE(10, 53)
53 FORMAT(' ENTER ELEC. CHG. (C/M2) ')
ACCEPT QE
GO TO 9
4 WRITE(10, 54)
54 FORMAT(' ENTER SOURCE IMPENDANCE--RESIS(OHMS), PARALLEL
*CAPAC(PICO FD) ')
ACCEPT RS, CL
CL=CL*1. E-12
GO TO 9
5 WRITE(10, 55)
55 FORMAT(' ENTER NO. AND VALUES OF TARG. LENGTH, REFLECTIVITY, AND
* TARG. RANGE ')
ACCEPT N
ACCEPT (RTGT(K), K=1, N)
GO TO 9
6 CONTINUE
RETURN
END

```

```

C BLOCK DATA
SUBROUTINE BDATA
COMMON /ZS/A, B, C
COMMON /DDIM/ AO, OC, J, W, L, D /MAT/ DM, DL, DA, DJ, DC, REA, REE
1 /ELC/ QE, RS, CL /TGT/ TL, TR, TD
REAL J, L
DATA J/1. E-5, L/100., W/.015, OC/2. E-6, AO/2. E-4, D/5. E-4/
DATA DL/1. 0., DA/1. 18., DJ/2150., DC/8000., REA/1., REE/2. 1.,
10E/1. E-4, RS/-1., CL/1. E-10, DM/1000., TL/ 4., TR/ 5., TD/1. /
RETURN
END

```

```

SUBROUTINE ZOSOL(Q, I)
COMMON /ZS/A, B, C
I=0
1 I=I+1
Q2=Q*Q
FR=(Q*Q2+C*Q2+A*Q+B*C)/(3.*Q2+2*Q*C+A)
Q=Q-FR
IF((ABS(FR/Q).GT.1.E-8).AND.(I.LT.30)) GO TO 1
RETURN
END

```

```

SUBROUTINE STRIPZ(KW, R, X)
REAL KW
IF(KW) 1, 2, 3
1 WRITE(10, 20)
20 FORMAT(' KW NEGATIVE. SET TO ZERO!')
KW=0.
2 R=0.
X=0.
RETURN
3 IF(KW.GT.20.) GO TO 4
CALL POWERZ(KW, R, X)
RETURN
4 CALL ASYMPZ(KW, R, X)
RETURN
END

```

```

SUBROUTINE ASYMPZ(Z, R, X, I)
REAL J0, J1
CALL ABESIO(Z, 0, J0, Y0)
CALL ABESIO(Z, 1, J1, Y1)
CALL STRUMD(Z, S0, S1, I)
P=1.570796327
R=Z*(J1*(P*Y0+S0)-J0*(P*Y1+S1))
X=Z*(Y0*S1-Y1*S0)+1./(P*Z)
RETURN
END

```

```

SUBROUTINE POWERZ(KW, P, Q, I)
DOUBLE PRECISION R, X, A, B, C, D, E, G, S
REAL KW
  R=0.
  X=0.
  A=5. D-1*KW
  B=A*A
  G= .577215664901533D0 + DLOG(A)
  I=1
  K=0
  S=0.
  C=1.
1  K=K+1
  I=I+1
  KP=K+1
  K2=K+KP
  D=(2. D0*KP)/K2
  S=S+1. D0/K
  C=-C*B/(K*KP)
  E=C/K2
  R=R+E
  X=X+E*(S-G+D-1. /D)
  IF(DABS(E). GT. 1. D-8) GO TO 1
  P=A*(1. +R)
  Q=KW*. 3183098862*(1. 5-G+X)
  RETURN
  END

```

```

SUBROUTINE STRUMD(Z, S0, S1, I)
DOUBLE PRECISION A, B, C, D, X, XL
  I=1
  K=1
  A=1. D0/Z
  B=A*A
  C=-A*B
  X=C
1  K=K+2
  I=I+1
  XL=X*K+A
  B=B+XL
  X=-XL*K+A
  C=C+X
  D=DABS(X)
  IF((D. GT. 1. D-8). AND. (DABS(X). GT. D)) GO TO 1
  S0 =C
  S1=B
  RETURN
  END

```

```

SUBROUTINE ABESIO(Z, N, J, Y)
REAL J
DOUBLE PRECISION D, P, Q, X, XL, W
M=4*N*N
I=1
K=1
P=1. D0
W=DBLE(-.125/Z)
Q=W*(1-M)
X=-Q
1  I=I+1
   K=K+2
   X=X*(W+(K*K-M))/I
   XL=X
   P=P-X
   I=I+1
   K=K+2
   X=X*(W+(K*K-M))/I
   Q=Q-X
   D=DABS(X)
   IF((D. GE. 1. D-8). AND. (DABS(XL). GT. D)) GO TO 1
   X=DBLE(Z)-1. 5707963267949D0*(FLOAT(N)+. 5)
   W=DSIN(X)
   XL=DCOS(X)
   Y=SQRT(. 63661977237/Z)
   J=Y*(P*XL-Q*W)
   Y=Y*(P*W+Q*XL)
RETURN
END

```

2.0 Program Variable Dictionary

A	Actual air gap thickness (under electret influence)
AO	Original air gap thickness
B	Half Beam width (radian)
BW	Beam width (degrees)
C	$kw/\sqrt{2}$
CAOI	$AO/EA, C_a^{-1}$ where C_a is the capacitance of the air/adhesive layer per unit area (m^2/F)
CE	EE/D Cap/unit area of electret layer (F/m^2)
CEI	$1/CE$
COI	$C_o^{-1} = CEI + A/EA$, total inverse capacitance/unit area after static displ.
COOI	$C_{oo}^{-1} = CEI + CAOI$, total original inverse cap unit area
CT	$T^2 C_o$
CUR	$\omega S \sigma $, drive current
CURR	$w \omega \sigma $, receiver current per unit exposed length
C2	$T^2 C_o - 2K$
D	Electret layer thickness (m)
DA	Density of air/adhesive layer (Kg/m^3)
DB	No. dB down for beam-width calculation
DC	Density of the moving conductor (kg/m^3)
DF	Frequency sweep increment (kHz)
DJ	Density of jacket material (kg/m^3)
DL	δ , the factor by which the stiffness of the air adhesive layer exceeds that of air
DLT	$\pi/180$
DM	Mechanical damping ($Pa/m/s$) per unit area
DT	$Z_e Z_m - T^2$

2.0 (Continued)

E	Driving voltage of ideal source (V)
EA	ϵ_a Dielectric constant of air/adhesive layer (F/m)
EE	ϵ_e Dielectric constant of electret layer (F/m)
EO	$\epsilon_o = 8.854 \times 10^{-12}$ (F/m)
EP	Receiver output voltage across load (V)
EPM	Max. EP at frequency ETOF with source-imped. EPR + EP
ETO	Overall efficiency ETOM = Max. ETO at freq. ETOF with source-imped. ETOH + ETOX
F	Operating Frequency (Hertz)
FL	Lower frequency limite of scan (Hz)
FH	Upper frequency limit of scan (Hz)
F2	Function which vanishes at frequency of maximum radiation efficiency
F3	Rate of change of F_2 with respect to ω
FDR	Function which vanishes at frequency of zero input reactance
FK	.001 F frequency in kilohertz
FR	$F(\theta)/F'(\theta)$ used in Newton-Raphson iteration for beamwidth calculation
GAMMA	$\gamma = 1.4$ for air
I(5)	Control index vector
J	Jacket thickness (m)
JF	Frequency scan control integer
K	Mechanical stiffness of air/adhesive layer per unit area = $\delta \frac{\gamma P_o}{a}$; $\delta \gamma P_o$ for ZSOL
KW	$kw = \frac{\omega w}{c}$ acoustic size paramter
L	Tape length (m)
LS	Series inductance for matching conjugate input impedance
MO	M, Effective moving mass/unit area (kg/m^2)

2.0 (Continued)

MOOM	Temporary variable
OC	ρ_c , moving conductor density (kg/m ³)
OCS	Open circuit sensitivity (dB re 1 V/Pa)
OM	$\omega = 2\pi f$ = radian frequency
OM2	ω^2
P	Target related pressure at tape (Pa)
PA	Acoustic power radiated (W)
PI	$\pi = 3.14159265$
PO	Atmospheric pressure = 1.013×10^{-5} (Pa)
PS	Magnitude of pressure on tape due to radiation
Px	Maximum radiated pressure (on axis) Pa
QC	First order solution for charge (C)
QE	Electret charge density, given (C/m ²)
QEZ	QE for ZOSOL (C/m ²)
QO	$-V_e C_{00} =$ 1st guess for ZOSOL (C/m ²)
RA	Real part of acoustic radiation impedance
RAD	$R_A + D$ (Pa-s/m)
REA	Relative dielectric constant of air/adhesive layer
REE	Relative dielectric const. of electret material
RF	Mechanical resonance frequency at which RM=0 (Hz)
RI	Real part of drive current = $-\omega S \text{Im}(\sigma)(A)$
RIN	Real part of input impedance of tape
RL	Real part of source/electrical load impedance
RM	Real part of Z_m
ROC	Characteristic acoustic impedance of air = 407 (Pa/m/s)
RS	Resistance of source

2.0 (Continued)

S	Area of transducer, wl (m^2)
SB	$\sin(B)$
SI	Intermediate storage for axial pressure calculation
SM	Intermediate storage for axial pressure calculation
SOM	$S\omega$
SS	$20 \log_{10}$ [output voltage of receiver for reflected pressure on length l_p / reflected pressure]
SSM	Max. SS at freq. SSF with source imped. SSR + SSXi
T	Transduction coefficient, σ/ϵ_a (V/m)
TD	Target to tape separation (m)
TL	Target length (m)
TLD	TL/TD
TR	Target pressure reflectivity
TZ2	$T^2/ Z_m $
T2	T^2
V	Magnitude of partial velocity of diaphragm, $\omega x $ (m/s)
VE	QE * CEI The voltage across the electret required to maintain the surface charge in the absence of other layers
VG	Voltage transfer ratio, output voltage/input voltage (dB)
X	$ XC $
XA	Imaginary part of radiation impedance (Pa-s/m)
XARA	$XA^2 * RAD^2$
XC	Complex particle displacement of diaphragm
XIN	Reactive part of tape input impedance
XL	Electrical reactance of source/electrical load
XM	$\text{Im}(Z_m)$ (Pa-s/m)
XO	$2\epsilon_a k_a$ for ZOSOL, zeroth order diaphragm displacement (π)

2.0 (Continued)

- ZE Blocked frequency-and area multiplied electrical impedance ($\Omega\text{-m}^2/\text{s}$)
- ZIN Electrical input impedance of tape (Ω)
- ZL Source (load) impedance of drive (receiving) electronics
- ZM Open-circuited frequency-multiplied mechanical impedance/unit area
- ZT System transfer impedance = output voltage/input current (dB re 1 Ω)

APPENDIX C

Radiation Impedance of a Baffled Infinite Strip

Because of the importance of its effect on ultrasonic radiation, it was felt necessary to develop a good understanding of the impedance the medium presents to the strip (tape). Several authors¹⁻⁴ have published derivations for the radiation impedance of an infinite strip set flush into a rigid plane and radiating into a half space. J. W. Miles¹ (1948) appears to have been the first to publish. He uses a general variational method to solve for the acoustic field in the half space beyond a circular baffled aperture resulting from a plane axial wave (propagating along the cylinder terminated by the aperture). Although he confuses admittance with impedance, it is clear from the context that he is really talking about impedance. He goes on to apply the method to the infinite slot which is of interest here. His expression for the ratio of pressure to particle velocity (specific acoustic impedance) is (using $\nu = kw$, the dimensionless acoustic size parameter):

$$Z = \rho c \left[\int_0^{\nu} H_0^{(2)}(\nu) d\nu - H_1^{(2)}(\nu) + \frac{2j}{\pi \nu} \right] \quad (1)$$

where $H_0^{(2)}$ is the zeroth order Hankel function of the second kind. The other three references use different approaches to arrive at this same relation (though Reference 2 leaves out a term in its Eq. 25 for X). References 2 and 3 get rid of the integral by using the identities

$$H_0^{(2)}(\nu) = J_0(\nu) - jN_0(\nu)$$

$$\int_0^{\nu} H_0^{(2)}(\nu) d\nu = \nu \left\{ H_0^{(2)}(\nu) + \frac{\pi}{2} [H_1^{(2)}(\nu)S_0(\nu) - H_0^{(2)}(\nu)S_1(\nu)] \right\}$$

where S_0 and S_1 are the zeroth and first order Struve function. Thus, the real part of the normalized radiation impedance is given by

$$\frac{R}{\rho c} \equiv r = \nu J_0(\nu) \left[1 - \frac{\pi}{2} S_1(\nu) \right] + J_1(\nu) \left[\nu \frac{\pi}{2} S_0(\nu) - 1 \right] \quad (2)$$

and the normalized reactive part of the specific acoustic impedance is

$$\frac{X}{\rho c} \equiv \chi = \frac{2}{\pi \nu} + \nu N_0(\nu) \left[\frac{\pi}{2} S_1(\nu) - 1 \right] + N_1(\nu) \left[1 - \nu \frac{\pi}{2} S_0(\nu) \right] \quad (3)$$

Radiation Impedance of a Baffled Infinite Strip (Continued)

These can be evaluated for low values of ν by the power series expression for the Bessel and Struve function they contain. For large values the power series expressions require so many terms that round-off errors produce blow-up (rapid error increase).

First consider the real part of 1) The power series forms of J_0 and J_1 are well known. Performing the integration term by term and combining the series for the two functions in the real part of 1) we get

$$r = \sum_{k=0}^{\infty} \frac{(-1)^k (\nu/2)^{2k+1}}{k!(k+1)!(2k+1)} = \frac{\nu}{2} - \frac{\nu^3}{48} + \frac{\nu^5}{1920} - \frac{\nu^7}{129024} \quad (4)$$

Clearly this series converges rapidly for $\nu < 1$.

Similarly, we develop a small ν approximation for χ from 1) by using the identity

$$N_0(\nu) \equiv \frac{2}{\pi} \left\{ J_0(\nu) \left[\ln\left(\frac{\nu}{2}\right) + \delta \right] - \sum_{k=1}^{\infty} \frac{(-1)^k (\nu/2)^{2k}}{(k!)^2} s_k \right\}$$

$$\text{where } s_k \equiv \sum_{m=1}^k m^{-1}.$$

The integration is then performed term by term using the power series form of J_0 to yield

$$\int_0^{\nu} N_0(t) dt = \frac{2}{\pi} \nu \left\{ \left[\delta + \ln\left(\frac{\nu}{2}\right) - 1 \right] + \sum_{k=1}^{\infty} \frac{(-1)^k (\nu/2)^{2k}}{(k!)^2 (2k+1)} \left[\delta + \ln\left(\frac{\nu}{2}\right) - s_k - \frac{1}{2k+1} \right] \right\}$$

where δ is Euler's constant = .5772 ...

Using this in the imaginary part of 1) and combining terms we get finally:

$$\chi = \frac{\nu}{\pi} \left\{ \frac{3}{2} - \delta - \ln\left(\frac{\nu}{2}\right) + \sum_{k=1}^{\infty} \frac{(-1)^k (\nu/2)^{2k}}{k!(k+1)!(2k+1)} \left[s_k - \delta - \ln\left(\frac{\nu}{2}\right) + \frac{2(k+1)}{2k+1} - \frac{2k+1}{2(k+1)} \right] \right\} \quad (5)$$

Equations 4 and 5 are power series approximations for the resistive and reactive parts of the normalized radiation impedance of an infinite strip. Note that the terms in the summations in these equations have many common factors. This makes the computer generation of r and χ for small ν very simple compared to evaluating (2) and (3) by generating the Bessel and Struve functions. These expressions are believed to be derived here for the first time.

Radiation Impedance of a Baffled Infinite Strip (Continued)

However, we also need expressions valid for large ν . This is done in a straight-forward manner by using the well known asymptotic series expression (for large argument) for the Struve function in equation (2) and (3). This process is simplified by defining the auxillary functions:

$$Q_0(\nu) \equiv \sum_{k=1}^{\infty} \frac{(-1)^k \pi^k (2j-1)^2}{\nu^{2k+1}}$$

and

$$Q_1(\nu) \equiv \sum_{k=0}^{\infty} \frac{-(2k-1)^k \pi^k (2j-1)^2}{\nu^{2k+2}}$$

The large argument Struve function expressions are then:

$$S_0 = N_0 + \frac{2}{\pi} \left(\frac{1}{\nu} + Q_0 \right)$$

and

$$S_1 = N_1 + \frac{2}{\pi} (1 + Q_1)$$

and the real and imaginary parts of the large ν radiation impedance of a baffled infinite strip can be reduced to

$$r = \nu \left\{ J_1(\nu) \left[\frac{\pi}{2} N_0(\nu) + Q_0(\nu) \right] - J_0(\nu) \left[\frac{\pi}{2} N_1(\nu) + Q_1(\nu) \right] \right\} \quad (6)$$

$$x = \nu \left[N_0(\nu) Q_1(\nu) - N_1(\nu) Q_0(\nu) \right] + \frac{2}{\pi \nu} \quad (7)$$

The advantage of these expressions for large arguments is mainly that the asymptotic series forms of the Bessel function J_0, J_1, N_0 and N_1 (and also for Q_0 and Q_1) require few terms to achieve optimum accuracy.

Equations 4, 5 and 6, 7 represent the desired impedance for small and large arguments respectively. To find out when ν should be considered large, we coded and tested both sets of algorithms. We find that the crossover should occur for ν between 16 and 30. It takes 44 terms of the power series approximation to generate the impedance at $\nu = 30$ but only 4 terms for the asymptotic method to achieve the same accuracy. At $\nu = 16$, 9 terms is optimum for the asymptotic series but 26 terms are required for the power series. The power series produces the best accuracy for $\nu < 30$.

Radiation Impedance of a Baffled Infinite Strip (Continued)

If speed were much more important than accuracy, then we could crossover at $\nu = 2$ (and still achieve $< 0.1\%$ accuracy). We used $l = 20$ for the crossover.

Fig. C-1 shows the calculated real and imaginary parts of the normalized radiation impedance of an infinite baffled strip. It should be noted that at low ν the real part is proportional to ν . However, the imaginary part falls off with $-\nu \ln \nu$, i.e., more slowly. This means that the dominant acoustic load on the strip at low frequencies is the mass reactance of the surrounding fluid.

The accession to inertia (mass loading) per unit length is given by

$$m = \frac{w \rho c \lambda}{\omega}$$

where w = tape width

ω = radian frequency

ρ = medium density and

c = propagation velocity

At low frequencies we have (from 5)

$$m = \frac{\rho w^2}{\pi} \left[\frac{3}{2} - \gamma - \ln \left(\frac{kw}{2} \right) \right] \quad (8)$$

If we consider this much added mass/unit length to be contained within a layer of width w and thickness Δ on top of the tape, we see that the thickness is

$$\Delta = \frac{w}{\pi} \left[\frac{3}{2} - \gamma - \ln \left(\frac{kw}{2} \right) \right] \quad (9)$$

Interestingly, this thickness of the effective mass load/unit length increases as frequency decreases as is shown by Table C-1.

Table C-1
Thickness of Effective Mass Load at Low Frequencies

Dimensionless Frequency kw	10^{-5}	10^{-4}	10^{-3}	.01	.05	.1	.5
Dimensionless Thickness Δ/w	4.49	3.45	2.71	1.98	1.47	1.25	0.730

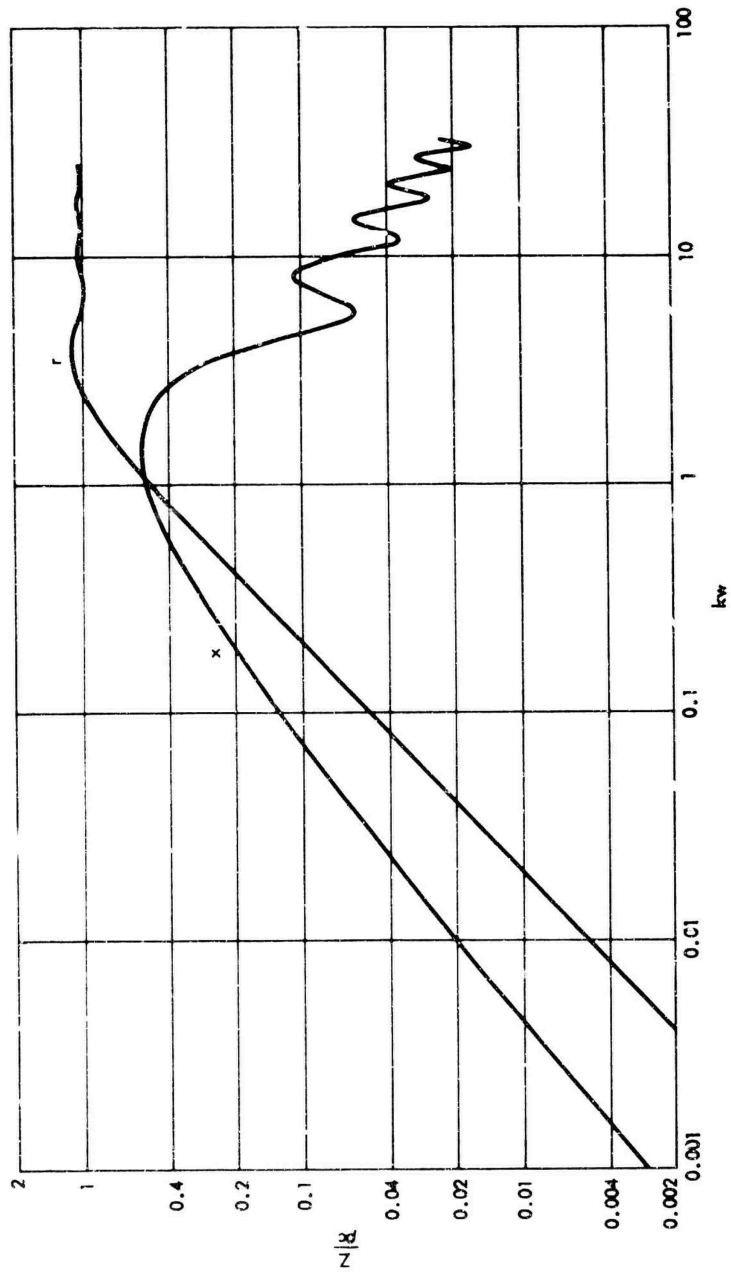


Figure C-1. Radiation Impedance of Baffled Vibrating Strip of Infinite Length

Appendix C: Radiation Impedance of a Baffled Infinite Strip (Continued)

As one would expect, the thickness of the entrained fluid for a strip and for a cylinder approach the same values at low frequencies if the width of the strip, $w = \pi a$, the semiperimeter of the cylinder.

References

- C1 "The Coupling of a Cylindrical Tube to a Half-Infinite Space", J. W. Miles, J. Acous. Soc. Am. 20 No. 5, 652-664 (Sept 1948).
- C2 "Radiation Impedance of Membranes and Plates: Their Acoustical Coupling with the Propagating Medium", S. Lowenthal, P. Tournois, J. Acous. Soc. Am. 35 No. 4, 1423-1428 (Sept 1963).
- C3 "Nearfield Pressure for a Steered Array of Strips", V. Mangulis, J. Acous. Soc. Am. 38 No. 1, 78-85 (July 1965).
- C4 "Radiation Impedance of a Long Narrow Rectangular Piston in a Plane Baffle", O. A. Lindemann, J. Acous. Soc. Am. 52 No. 3 Pt 2, 1045-1048 (March 1972).

APPENDIX D

Other Computer Model Plots

The computer model outputs include plots of a number of parameters not examined in detail in the main text. Some of these for sample D1 are included in this appendix.

The parameters defining design D1 are:

Length: 35 mm Width: 8 mm

Jacket Thickness: 16 μm , Material Mylar

Outer Conductor - Thickness: 9 μm , Material Aluminum

Air Gap - Thickness: 100 μm , Material Air

Electret - Thickness: 508 μm , Material FEP Teflon, Charge: 30 $\mu\text{C}/\text{m}^2$

Damping Constant: 5000 Pa-s/m

Target length: .4m, Height: 1 m, Pressure Reflectivity: 50%

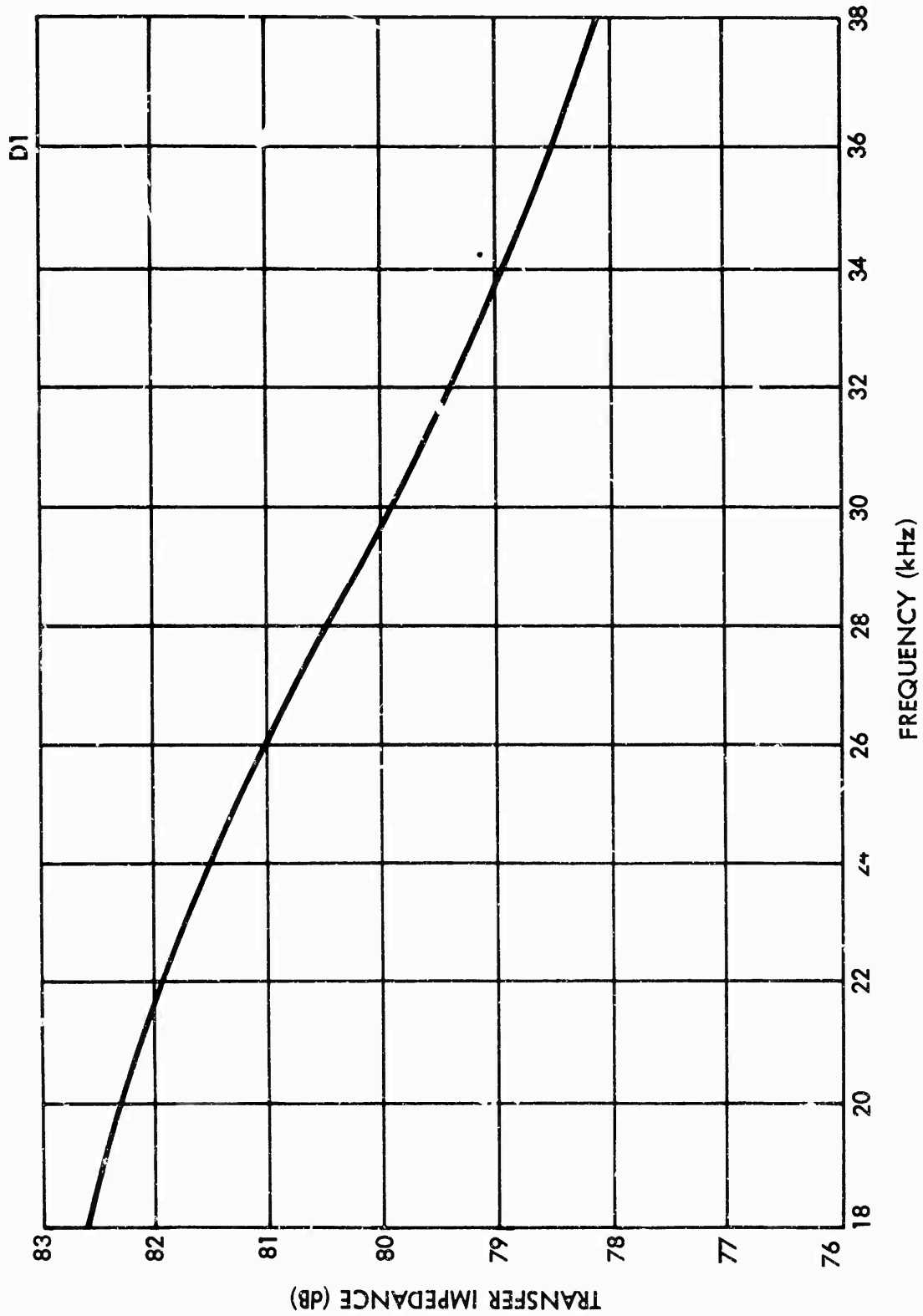


Figure D-1. Z_T vs. Frequency for Sample D1

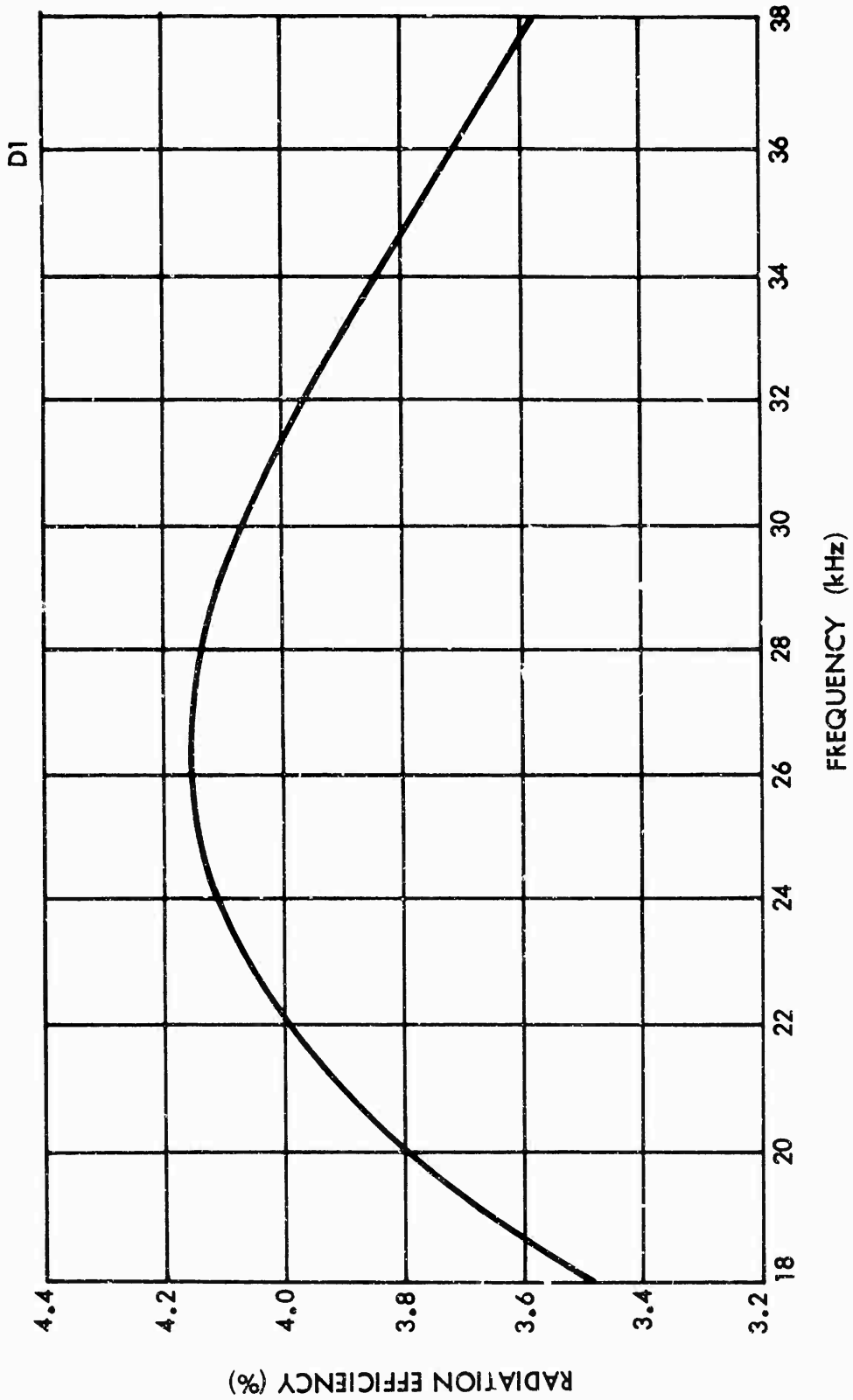


Figure D-2. Efficiency vs. Frequency for Sample D1

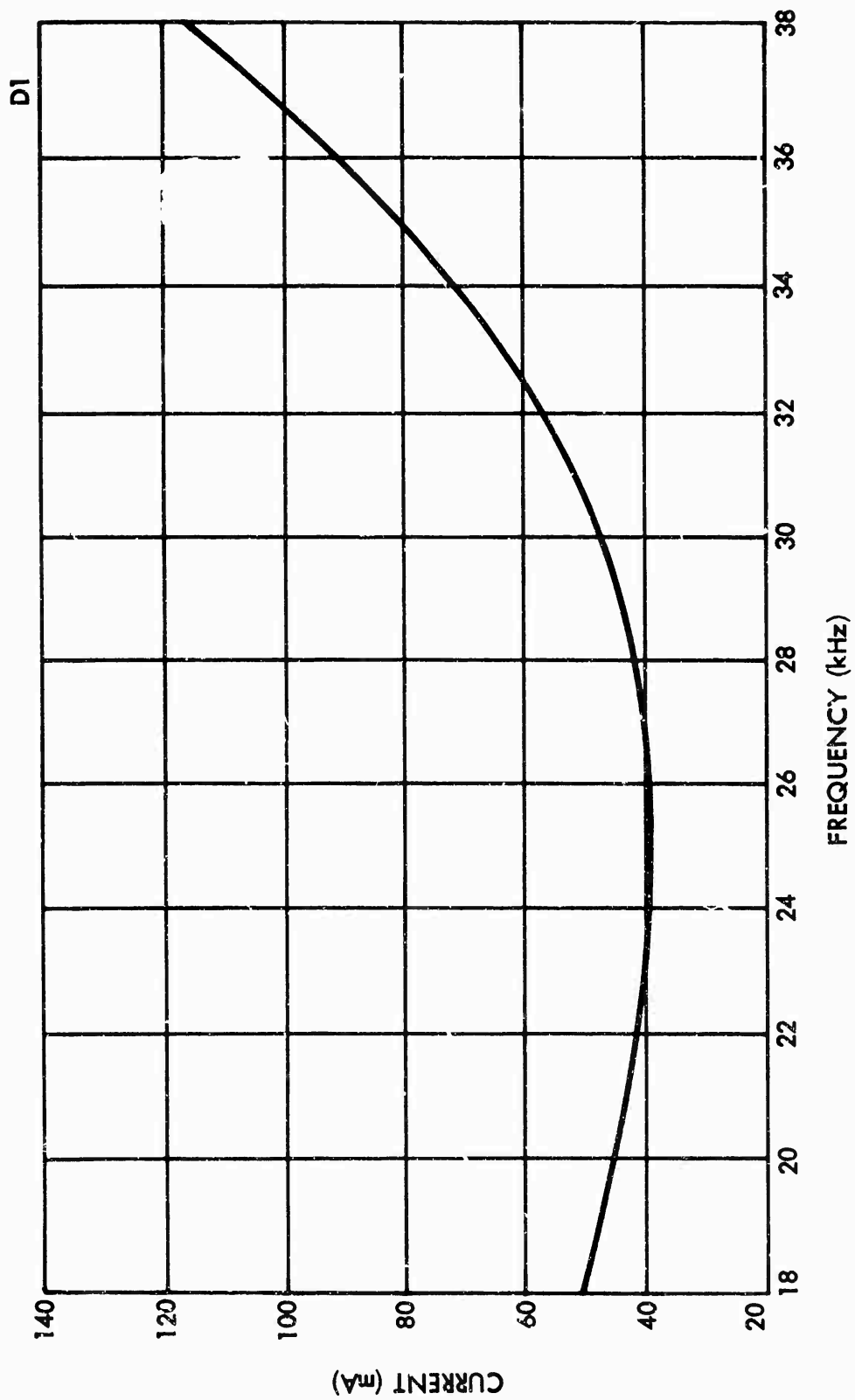


Figure D-3. Driving Current vs. Frequency

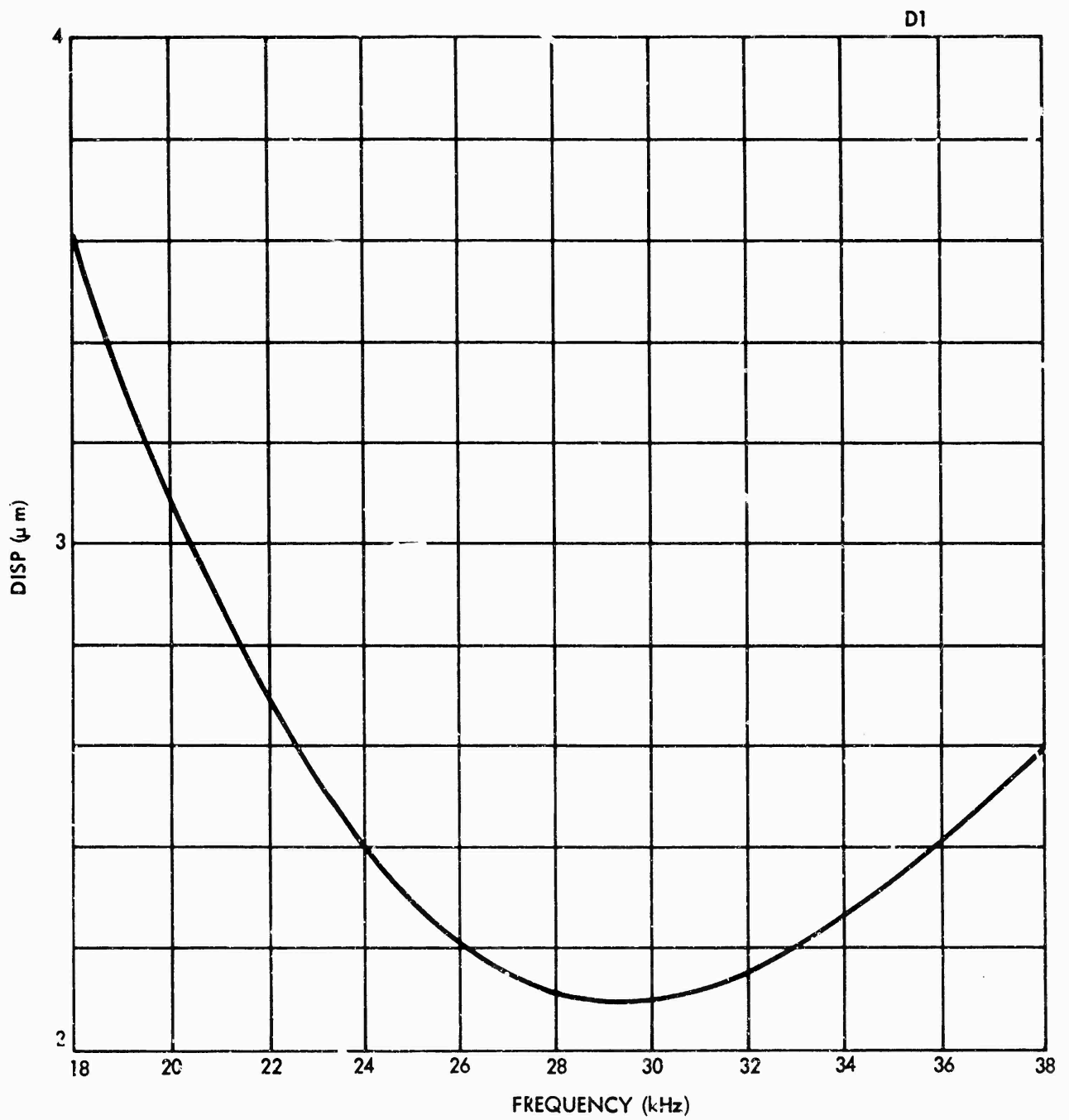


Figure D-4. Diaphragm Displacement vs. Frequency

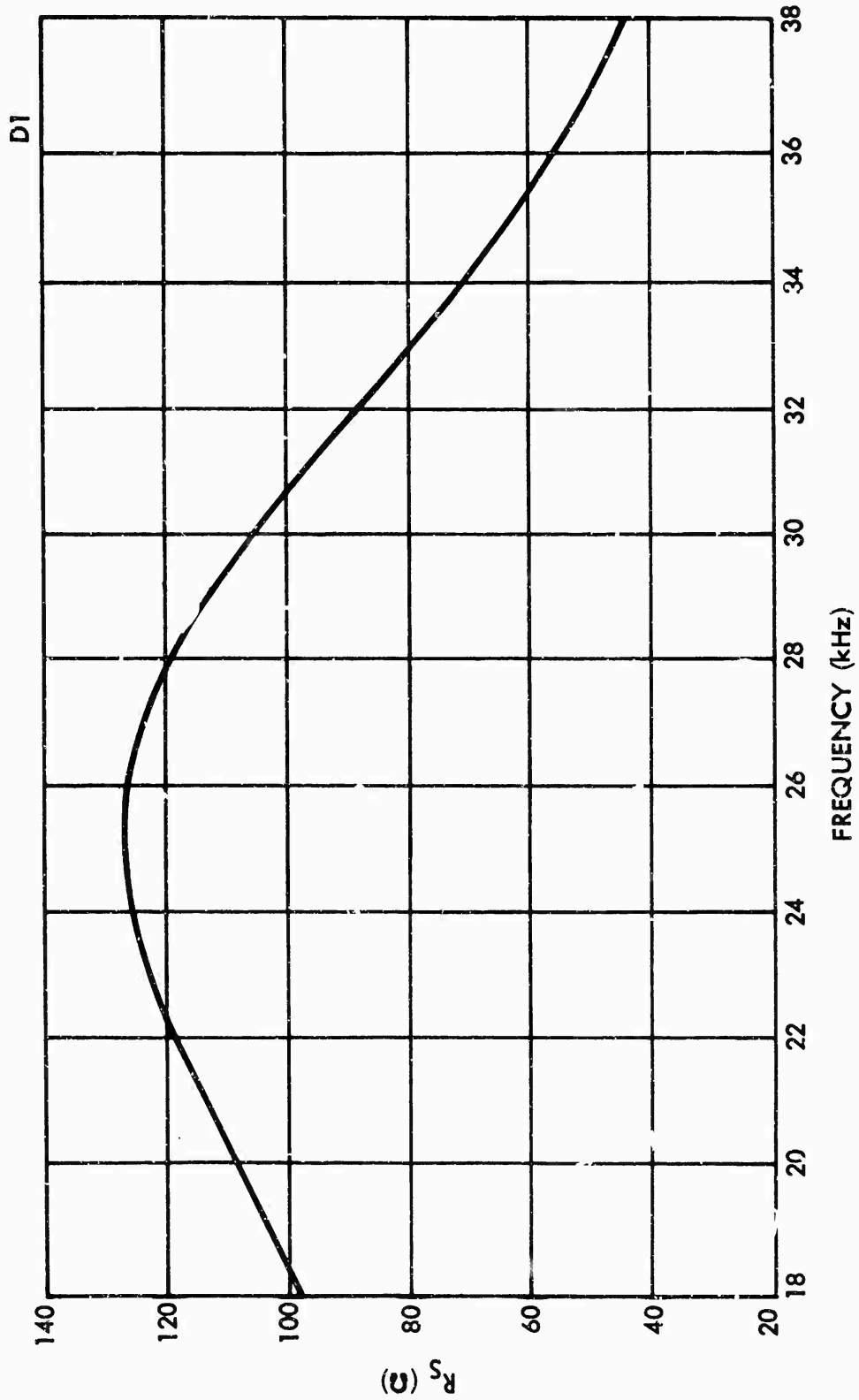


Figure D-5. Matching Source Resistance vs. Frequency

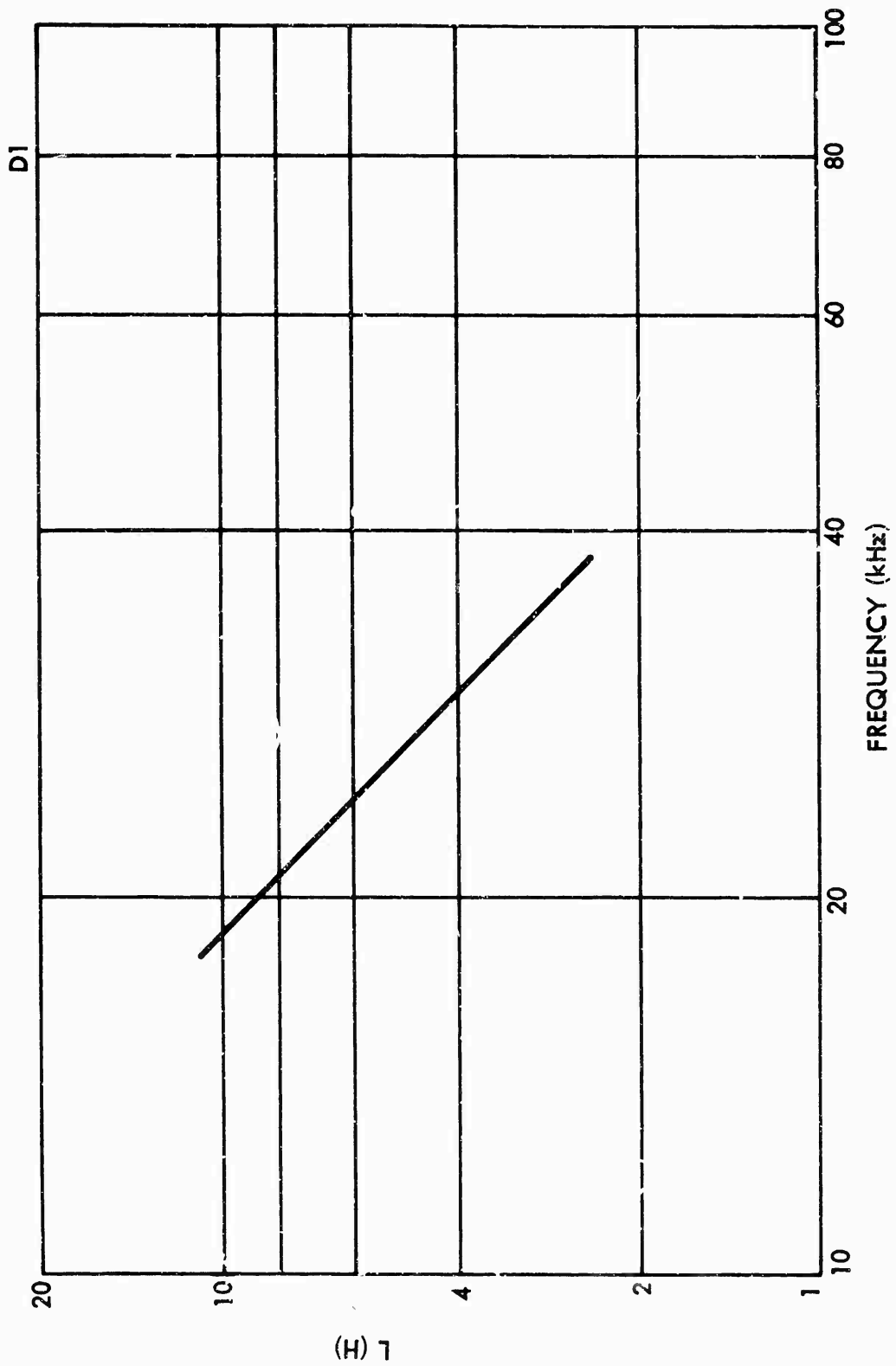


Figure D-6. Source Inductance for Conjugate Impedance Matching vs. Frequency

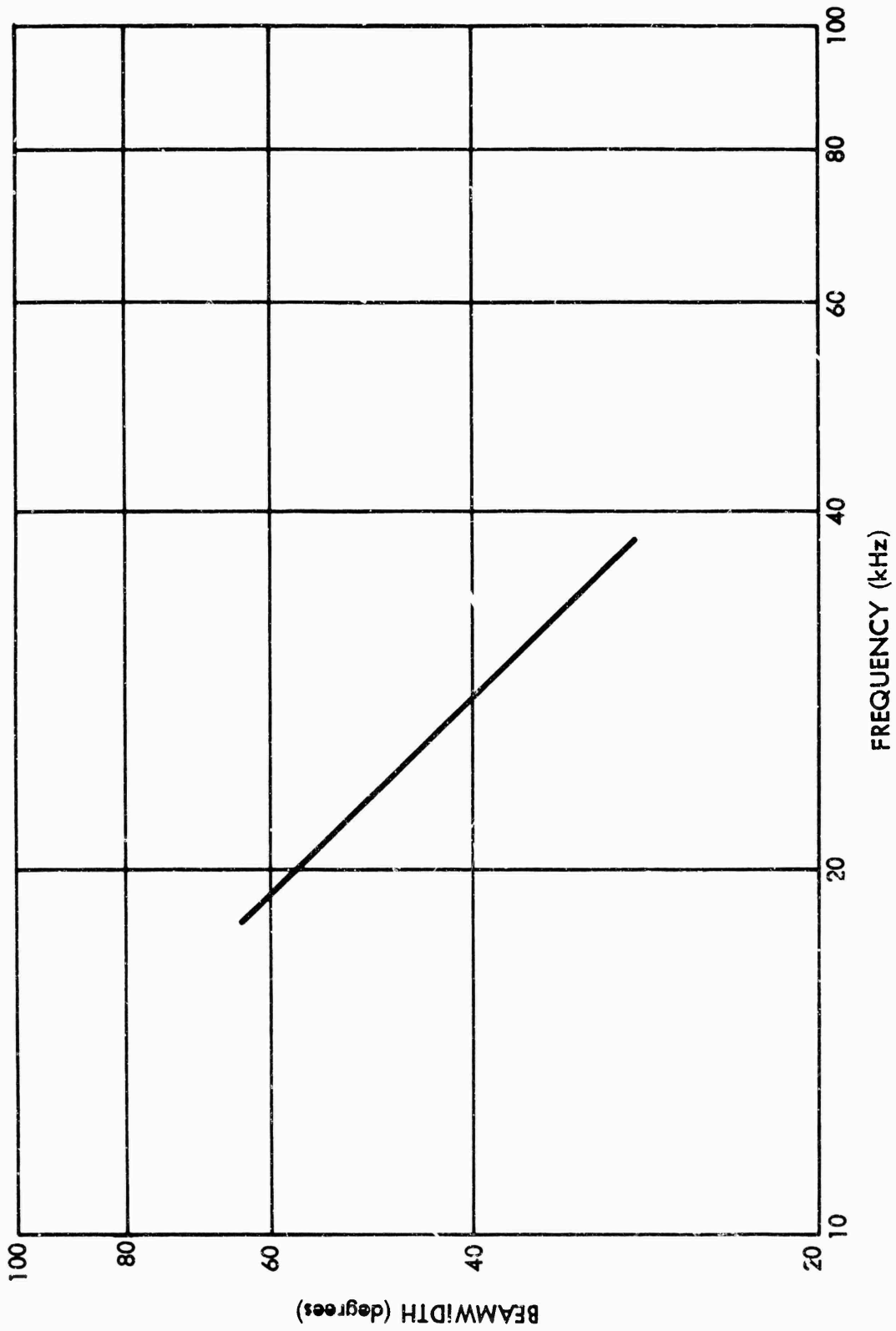


Figure D-7. Beamwidth vs. Frequency for Sample D1

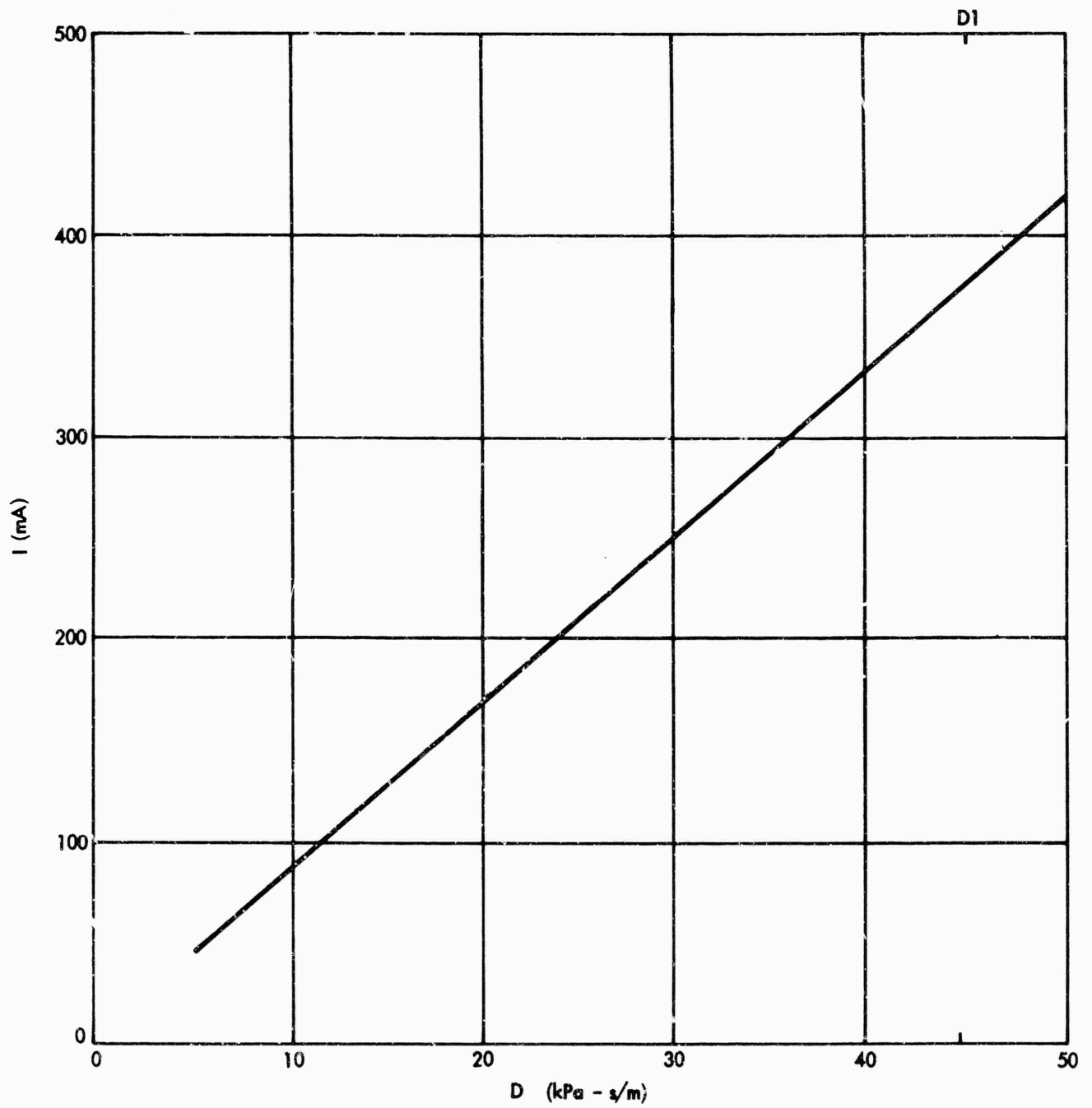


Figure D-8. Drive Current vs. Mechanical Damping Constant

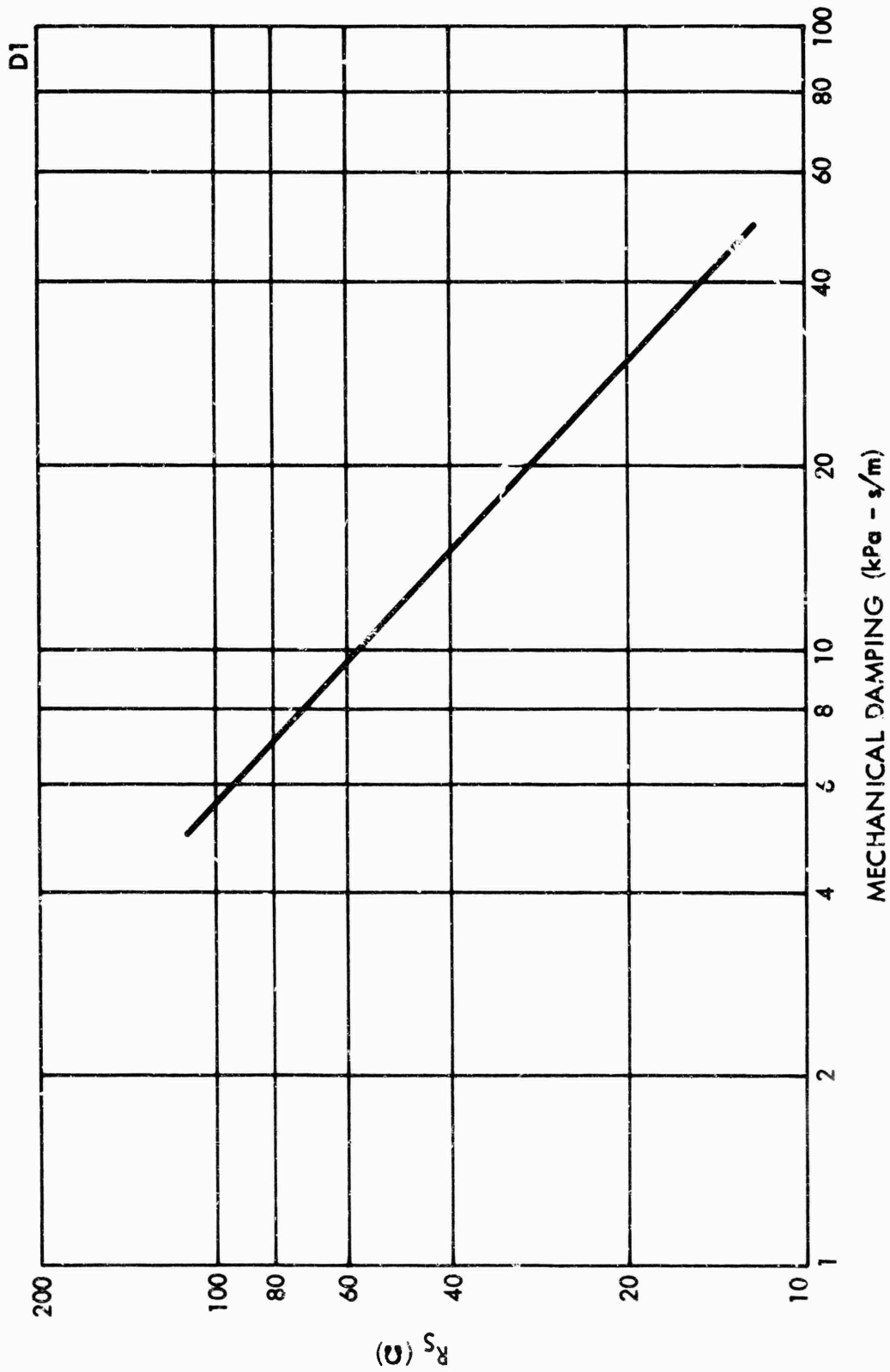


Figure D-9. Matching Source Resistance vs. Mechanical Damping Constant

(U) R_s

D-10